NASA Contractor Report 168334

Aviation-Fuel Property Effects on Combustion

T.J. Rosfjord

UNITED TECHNOLOGIES RESEARCH CENTER
East Hartford, CT 06108

February 1984

NASA

National Aeronautics and
Space Administration

Lewis Research Center
Cleveland, Ohio 44135

NASA Contractor Report 168334

Aviation-Fuel Property Effects on Combustion

T.J. Rosfjord

UNITED TECHNOLOGIES RESEARCH CENTER
East Hartford, CT 06108

February 1984

ACKNOWLEDGEMENTS

R84-915908-29

Aviation-Fuel Property Effects on Combustion

TABLE OF CONTENTS

LIST OF FIGURES

LIST OF TABLES

LIST OF SYMBOLS

A   Fuel aromatic content, vol. pct

B   Mass transfer number

CDA   Effective area of liner hole

CP   Gas specific heat

CPN2   Gaseous nitrogen specific heat

D   Soot particle characteristic diameter

DP   Fuel injector differential pressure

DPL   Combustor liner differential pressure

EINOx   Emission index for NOx

H   Fuel hydrogen content, wt pct

I   Scattered light intensity

I_0 Incident light intensity at sample volume

k   Gas thermal conductivity

L   Length of combustion zone

N   Fuel naphthalene content, vol pct

   Soot particulate number density

n   Complex refractive index

NN   Fuel injector nozzle number

PB   Barometric pressure

PF   Combustor exit temperature pattern factor

PHI   Complex light scattering function

R   Gas constant

R^2 Square of regression correlation

SMD   Fuel spray Sauter Mean Diameter

SMD_c Critical SMD

SN   SAE smoke number

SP	Fuel smoke point
TA	Air temperature in combustor calibration tests
U	Bulk gas velocity
u'	Turbulence intensity, pct
WA	Total airflow
WAL	Airflow associated with primary zone sample
WCO_2	Total metered carbon dioxide mass flow
We	Weber number
We,c	Critical Weber number
WF	Fuel mass flow
WN_2	Nitrogen mass flow
XCO_2	Fractional molar concentration of CO_2 in sample
x	Light scattering size parameter
θ	Light scattering angle
λ	Wavelength of scattered light
μ	Gas viscosity
ρ_F	Fuel density
ρ_g	Gas density
ϕ_p	Primary zone equivalence ratio

SUMMARY

The ASTM "Standard Specification for Aviation Turbine Fuels" (ASTM D-1655) defines acceptable limits for many properties of turbine engine fuel for civilian use. Fuels satisfying these limits will have characteristics acceptable to current gas turbine combustors. In particular, desirable combustion characteristics are assured by bounding the aromatic and naphthalenic hydrocarbon contents and the smoke point. Previous studies have been conducted in an attempt to identify which of these properties (or others) influence the performance, emissions and heat load of the combustor. Fuel hydrogen content, which is not a specification parameter, has been cited as a global indicator of fuel effects. These earlier studies, however, did not purposefully emphasize the fuel chemical properties; the combined influence of both physical and chemical properties was likely observed. Additionally, the burners were not always representative of current aircraft practice and the range of fuel properties studied was often limited.

In an attempt to rigorously study the fuel chemical property influence, UTRC, under contract to NASA Lewis Research Center, has conducted an experimental program using 25 test fuels. The burner was a 12.7-cm dia cylindrical device consisting of six sheet metal louvers. A single pressure-atomizing injector and air swirler were centrally mounted within the conical dome. Fuel physical properties were de-emphasized by using fuel injectors which produced highly-atomized, and hence rapidly-vaporizing sprays. A substantial fuel spray characterization effort was conducted to allow selection of nozzles which assured that such sprays were achieved for all fuels. The fuels were specified to cover the following wide ranges of chemical properties: hydrogen, 9.1 to 15 (wt) pct; total aromatics, 0 to 100 (vol) pct; and naphthalene, 0 to 30 (vol) pct. They included standard fuels (e.g., Jet A, JP4), specialty products (e.g., decalin, xylene tower bottoms) and special fuel blends. Included in this latter group were six, 4-component blends prepared to achieve parametric variations in fuel hydrogen, total aromatics and naphthalene contents.

Two test phases were conducted. First, fuel-effects tests were performed during which data were acquired for all 25 test fuels using a single burner configuration. Second, configuration-effects tests were performed using three fuels and two additional burner configurations which produced either higher or lower primary zone equivalence ratios than achieved with the fuel-effects configuration. Combustor heat load was documented by full-hemispherical-sensing radiometers mounted on the dome and by 39 liner thermocouples. Three narrow-angle radiometers mounted on the combustor case were used to sense shifts in the axial distribution of radiation. Arrays of thermocouples and sampling probes at the combustor exit were used to document the temperature pattern factor, and to acquire gaseous and particulate specie samples. The characteristic particle size and number density of the exhaust soot on the combustor centerline were determined by an optical technique which interpreted scattered light signals according to Mie theory. All data were acquired at a single airflow condition which simulated high-power operation of a gas turbine combustor--namely, combustor pressure = 1.3 MPa and inlet air temperature = 700K. Each test fuel was combusted at 3 fuel-air ratios which were specified to achieve combustor exit temperatures of 1246K, 1346K and 1473K.

Repetitive data points were acquired to determine the statistical consistency of the measurements.

The combustor operated in a consistent manner for all tests. Combustion efficiencies greater than 99.9 pct were always achieved; the exit temperature pattern factor was typically less than 0.15. The output from the case-mounted radiometers indicated that for each test condition, the reaction zone structure was not significantly altered by any of the test fuels. Hence all fuels were similarly atomized and distributed in the burner. For every fuel, both exhaust smoke number and particle number density decreased with increasing combustor fuel-air ratio (increasing exit temperature), while the characteristic particle size remained constant. Indeed, the particle size was also independent of fuel properties; the indicated size was always 0.22 $\pm$ 0.02 μm. The smoke number/number density trends indicated that the soot oxidation mechanism dominated the overall process of soot production. That is, despite an increasingly fuel-rich primary zone at higher overall fuel-air ratios, lower levels of exhaust soot were produced because of enhanced oxidation at higher exit temperatures. These consistent trends also revealed a correlation between smoke number and soot number density.

The principle influence of fuel chemical properties on the combustor behavior were reflected by the radiation, liner temperature and exhaust Smoke number (or equivalently, soot number density) data. The measured dome radiative heat transfer rates appear to correlate well with fuel hydrogen content. Used in this manner, however, the hydrogen content is a global indicator of the fuel property influence since it is accompanied by variations in total aromatics and naphthalenes. Results from tests with fuels which offered parametric variations in hydrogen, total aromatics and naphthalenes indicated that naphthalene content strongly influenced the radiative heat load while parametric variations in total aromatics did not. The hydrogen parametric test results indicated that, in a pure sense, hydrogen content does not influence radiation load; only in a global sense (i.e., with variations of hydrocarbon molecular structure) is a hydrogen influence observed. Regression analyses were performed on data from tests with all fuels in an attempt to identify the individual influences of the chemical properties. These analyses confirmed the importance of naphthalene content; a regression parameter containing both hydrogen and naphthalene content tracked the data significantly better than a parameter containing hydrogen content alone. For the range of chemical properties encompassed by Jet-A and ERBS, both the hydrogen and the naphthalene content variations would contribute similarly to a variation in radiative heat load. It was also observed that fuel smoke point correlated the data as well as the two-property parameter. Hence smoke point, an existing fuel specification parameter, appears to be an adequate global indicator of fuel chemical property influences. Similar fuel effects were also observed for liner temperature rise and exhaust smoke number.

The configuration-effects test results indicated that the fuel concentration pattern in the primary zone of the combustor strongly influenced the soot levels produced, and therefore also the radiative heat load. Since the fuel oxidiation is controlled by a turbulent diffusion flame structure, the global value of primary zone equivalence ratio (ϕ_p) does not always properly represent the important features of this region. Data indicated that particulate radiation heat loads on the combustor dome could

be constant despite c_p values ranging from 1.2 to 1.6 if fuel concentration patterns were invariant.

Aviation-Fuel Property Effects on Combustion

SECTION I - INTRODUCTIO·

Aviation gas turbine engines combust high quality fuel. The principle fuels for either commercial service, Jet A, or for military service, JP4 and JP5, were developed to possess excellent combustion characteristics while offering appropriate considerations for ease of ignition, safe handling and low-temperature fluidity. These fuels have attractive energy densities, atomize and vaporize readily, and burn completely in the time and temperature environment found in gas turbine combustors. The jet fuel specification assures obtaining this performance by controlling several key physical and chemical properties. The original specification was established to obtain these features while assuring adequate supplies of reasonably-priced fuel derived from domestic petroleum reserves. The availability of domestic crude oil has continuously decreased in recent time, however, forcing an increase in the quantity of petroleum imported to the U.S. In the last decade, the cost and availability of such imports has not been stable. The oil embargo of the early 1970's threatened adequate availability of petroleum in the U.S. and the subsequent production/ pricing practices of OPEC countries have caused dramatic increases in the cost of petroleum products. Gas turbine users have experienced more than a four-fold increase in unit fuel costs.

Substantial increases in gas turbine engine operating expenses have placed a premium on developing aircraft gas turbine systems which can offset the fuel cost burden. Two basic, although not mutually exclusive, approaches could be pursued: develop more fuel efficient systems or develop more fuel tolerant systems. The former approach is obvious and is likely a desirable goal for any level of fuel cost. The latter approach would attempt to use less costly fuel without sacrificing the performance or endurance of the gas turbine engine. It is possible that existing systems, with or without minor retrofit, could be qualified on less expensive fuels. Of course, the fuel cost is not represented by the fuel production cost alone. Fuel handling requirements, fuel system alterations, airframe modifications and gas turbine hot section (combustor and turbine) deterioration associated with the use of an alternative fuel represent costs which must also be considered.

One part of an overall evaluation of a fuel tolerant system is an investigation of the influence of fuel properties on the performance, emissions and heat rejection of a gas turbine combustor. Since 1975 numerous investigations have been conducted (Refs. 1 through 11) to quantify such influences. The studies have used laboratory model combustors, full engine hardware, actual fuel, hydrocarbon specialty products (i.e., solvents) and blends of these two material classes. Such efforts have identified areas which would likely be affected by changing fuel properties. For example, liner temperatures, exhaust smoke emissions and low power (idle) emissions are three parameters often cited as being influenced by fuel properties.

Unfortunately, the fuel variations studied have resulted in simultaneous changes in the physical and chemical properties. These two types of properties would be expected to influence different processes within a gas turbine combustor. Physical properties (specific gravity, viscosity and surface tension) would predominantly affect the fuel atomization process, and hence alter the distribution and rate of vaporization of the fuel. Chemical properties (hydrogen, aromatic or naphthalene content) would influence the fuel oxidation process, altering the type, concentration and rate of consumption of chemical species within and exiting the combustor. Depending on the dominant mechanisms within the burner, changes in the fuel, may or may not produce an interpretable change in a parameter of interest.

For example, if in an attempt to investigate high fuel aromatic content, the surface tension also significantly increased, it may not be possible to separate the multiple effects of these changes and correctly interpret the data. That is, high aromatic content alone may promote greater concentrations of carbon and hence higher liner temperatures because of increased flame radiation. Alternatively, the increased surface tension could degrade the fuel atomization and distribution, producing locally fuel-rich regions which could similarly could result in high liner temperatures. Clearly there was a need for an investigation which attempted to separate the influence of fuel physical property variations from those of chemical property variations.

United Technologies Research Center has conducted an experimental program under contract to NASA-Lewis Research Center (NAS3-23167) to investigate the influence of fuel chemical properties on the performance, emissions, and heat load on a gas turbine combustor. Fuel physical properties were de-emphasized by using injectors capable of achieving highly-atomized, and hence rapidly-vaporizing fuel sprays for each of twenty-five test fuels. The fuels were specified to cover wide ranges in fuel hydrogen, total aromatic and naphthalene content; a limited number of fuels were blended to achieve parametric variations of these properties. Two types of combustion tests were performed. First, fuel-effects combustion tests were performed with a constant burner design at a simulated high-power gas turbine operating condition using all 25 test fuels. Second, configuration-effects combustion tests were performed with burners designed to produce either higher or lower primary zone equivalence ratios than the baseline design. Combustor airflow calibration and fuel spray characterization studies supplemented the combustion tests.

This document reports the results of this investigation. Section II describes the selection and analysis of the test fuels, while the design and calibration of the combustor is detailed in Section III. The extensive fuel spray characterization effort is described in Section IV. Sections V and VI describe the combustor test facility and instrumentation, and the test condition, procedures and data handling, respectively. The results of the fuel-property-effects testing are presented and discussed in Section VII, with configuration-effects results contained in Section VIII. Conclusions and recommendations are listed in Section IX.

SECTION II   TEST FUELS

The ASTM standard specification (ASTM D-1655) defines acceptable
limits for many properties of turbine engine fuel for civilian use. Fuels
satisfying these limits will have fluidity, compatibility, cleanliness,
stability, volatility and combustability characteristics acceptable to cur-
rent gas turbine combustors. Fuel combustability is assured by bounding
the aromatic and naphthalene contents and the smoke point. Hydrogen
content is not a fuel specification paramter. However, many previous
studies have determined that the results of changing fuel chemical proper-
ties correlate with the fuel hydrogen content. Therefore, in this investi-
gation attention was focused on the fuel chemical composition as represen-
ted by the hydrogen, total aromatics and naphthalene contents. The smoke
point was not considered to be a fundamental parameter but rather resulted
from the hydrocarbon mix of the fuel. It may therefore be a desirable
global indicator of the fuel chemical properties. Indeed, the three
chemical property classes-hydrogen, total aromatics and naphthalenes--were
also gross parameters of the fuel. Obviously, hydrogen content alone does
not specify the type of hydrocarbon molecules contained in the fuel.
Similarly, "total aromatics" and "naphthalenes" do not pinpoint the type of
aromatics, etc. As reflected by the ASTM specification it has been assumed
that the three major property classifications selected dominate the
combustion characteristics and hence are the proper ones for evaluation.
The twenty-five test fuels were selected to provide wide ranges of
variation in these properites, with hydrogen contents from 9.1 to 15.0 (wt)
percent, total aromatics contents from 0.0 to 100.0 (vol) percent, and
naphthalene contents from 0.0 to 29.7 (vol) percent. Table I provides a
list of the fuels and these chemical properties as determined from analyses
described below. This section of the report describes the test fuels and
presents the results of extensive analyses performed on each.

Fuel Description

The test fuels could be divided into three general categories: common
fuels, specialty products and blends of these two categories. The common
fuels and speciality products were specified by NASA; UTRC collaborated
with NASA to specify the blends.

Common Fuels

Four of the test fuels were products commonly used in gas turbine
combustors: Jet A, JP4, JP5 and JP7. Each of these was a high-quality,
petroleum-derived fuel produced in accordance with ASTM and USAF specifica-
tions. Four additional fuels within this category were: ERBS, JP4-S,
JP4-A and DF2. ERBS (Experimental Referee Broad Specification) fuel
evolved from a NASA-directed workshop on alternative hydrocarbon fuels
(Ref. 11). Unlike most fuel specifications, which place upper limits on
certain chemical properties, a single level (and tolerance) of hydrogen
content is specified for ERBS. This approach minimizes the chemical
property variation of subsequent batches of ERBS production; it has become

a standard fuel for NASA-sponsored fuel effects investigations. JP4-S was a JP4 specification product derived from oil shale resources. JP4-A, like JP4, was a petroleum-derived fuel satisfying the USAF specification, but it had a high aromatic content. That is, while most JP4 fuel contains 16 to 18 (vol) percent aromatics, JP4-A contained 23 (vol) percent which is near the specification maximum of 25 (vol) percent. The DF2 fuel was a better quality No. 2 fuel oil.

Specialty Products

In order to extend the ranges of the chemical properties of interest, six of the test fuels were specialty products: decalin, tetralin, xylene tower bottoms (XTB), blending stock (BLS), Gulf Mineral Seal Oil (GMSO) and UTRC1. Many of these products have also been used in other combustor fuel effects evaluations. Both decalin and tetralin were pure, double ring hydrocarbon solvents procurred from E. I. duPont de Nemours. Decalin is a product of the complete hydrogenation of naphthalene to naphthene. Tetralin results from partial hydrogenation of naphthalene to result in a fused, double 6-carbon ring structure, with one ring being saturated and the other unsaturated. Hence while decalin retains no aromatic quality, chemical analysis would classify tetralin as fully aromatic. XTB consisted of various single-ring aromatic compounds (alkylbenzenes) while GMSO was a relatively high final boiling point oil consisting mostly of normal and monocyclic paraffins. BLS was a mixture of XTB and a gas oil that NASA had obtained to use for modification of fuel properties, and contained substantial single-ring and double-ring aromatic compounds. UTRC1 was a commercial solvent, EXXON Isopar M, chosen by UTRC to meet the NASA requirements for a high hydrogen content fuel void of aromatic compounds.

Fuel Blends

Eleven of the test fuels were blends of common fuels and specialty products. Of these, five were prepared to provide chemical property levels between those offered by other test fuels. For these, as for the common fuels and specialty products, simultaneous variation in hydrogen, total aromatics and naphthalene contents resulted. Six of the blends were specially prepared, however, to avoid this multiple variation. That is, two fuels were blended to achieve parametric variations in either hydrogen, total aromatics or naphthalene content.

The five fuels prepared to provide blends with additional chemical properties were: AFAPL2, AFAPL6, ERBLS1, ERBLS2, ERBLS3. The first two fuels were supplied by the Air Force Aero Propulsion Laboratory, WPAFB, and consisted of JP4, XTB and A-400 solvent and JP5, DF2 and A-400 solvent, respectively. (A400 is an aromatic solvent containing approximately 50 percent naphthalenes.) Both of these fuels have been used in fuel effects evaluations of gas turbine afterburners (Ref. 13). The latter three blends were diffent volume mixtures of ERBS and BLS; these fuels were blended by UTRC.

It was desired to evaluate test fuels which allowed parametric variations of fuel hydrogen, total aromatics and naphthalene contents. Such

variations were not easily achieved because alterations in any one property would normally affect one or both of the other chemical classes. Hence parametric variation of the properties of interest were obtained by substituting one type of compound for another from the same general class. For example, use of decalin in lieu of UTRC1 (i.e., EXXON Isopar M) would not change the total aromatics or naphthalene content of a blend, but would reduce the hydrogen content. The mix of saturated hydrocarbons would be altered, however, with a greater fraction of cycloparaffins being present with use of decalin, and a greater fraction of normal paraffins present with use of UTRC1. Only by careful selection of the fuel blend components were parametric variations achieved.

The specification for the parametric variation blends resulted from an extensive computer screening exercise. That is, recognizing that such fuels would result only from blends of several components, a computer program was written which, given the chemical properties of potential components, evaluated all possible combinations. Ten potential blending components were identified, with samples of each analyzed to provide consistent chemical property data, see Table 2. (Each of these components has been previously described except for the Methyl-naphthalene fraction. This solvent is a fully aromatic liquid with a very high naphthalene content.) The final blend was limited to four components. Goal levels for hydrogen, total aromatics and naphthalenes (and allowable tolerances) were input to the computer code which analyzed 4-component permutations of the ten candidates. The component volume fractions were incremented by 5 percent in successive evaluations, resulting in approximately 372,000 "computer blends".

Three-point parametric variations in hydrogen, total aromatics and naphthalenes contents were sought, based upon two fuel blends departing from a common fuel (e.g., ERBS). The results of the computer blending exercise indicated that meaningful three-point variations could not be achieved for hydrogen or aromatics, however, because the constraints imposed by the other two properties prohibited significant independent variation. As an alternative, a pair of 2-point variations in hydrogen and total aromatics (i.e., two base fuels) were determined. The compositions of the parametric blends are listed in Table 3 with the results of analyses to determine the blend chemical properties. The parametric variations achieved were identical to those predicted by the computer blending code (within the chemical analysis uncertainties) and represented the greatest variation that could be expected using the ten candidate components.

The three ERBS/BLS and six parametric blends were prepared by UTRC. The volume fraction specifications were translated to mass fractions and a shipping scale used to weigh the quantity of each component pumped into a 1000 liter mixing tank. The entire batch of each blend was mixed by pumping the fuel out of one end of the tank and into the other; the circulation time was sufficient to displace the blend volume at least ten times. The fuel was subsequently pumped from the mixing tank into drums; the mixing tank was then cleansed with the major constituent of the next blend to be prepared.

Fuel Analysis

A sample of each test fuel was analyzed by Southwest Research Institute in accordance with the properties and procedures indicated in Table 4. The results of these analyses are presented in Table 5. The levels of total aromatics and naphthalenes presented for any fuel (or blending component) were obtained from mass spectrometric analysis. All hydrocarbons contained in the aromatic fraction of the sample contributed to the "total aromatics" level. The naphthalene compounds were assumed to include the acenaphthenes (C_nH_{2n-14}) and acenaphthalene (C_pH_{2n-16}) hydrocarbons. The volume fraction values were determined from the reported mass fraction data and the following assigned specific gravity values:

Hydrocarbon Type	Specific Gravity
normal-paraffins	0.75
cyclo-paraffins	0.81
alkylbenzenes	0.87
indans and tetralins	0.93
indenes	1.00
naphthalenes	1.00
tricyclic aromatics	1.28

The type of hydrocarbon species in the fuel was independently determined from more than one analysis. The mass spectrometric analysis (ASTM D2425) separated the fuel into twelve classes while the fluorescent indicator adsorption (FIA, ASTM D1319) technique reported only on three general classes (saturates, olefins, total aromatics). The FIA was supplemented with the ultraviolet spectrophotometric technique (ASTM 1840) to determine naphthalene content. A comparison of the total aromatics and naphthalene contents obtained by two techniques is shown in Figs. 1 and 2, respectively. The mass spectrometry and FIA results for aromatics agreed remarkably well considering the wide range covered and the general acknowledgement that the FIA technique can be inaccurate for high aromatic levels. The two techniques did not correlate well only for BLS. The agreement with naphthalene analyses was poorer, with a substantial underprediction by the UV technique. This result was not surprising as this method is strictly applicable to fuels containing only up to 5 percent naphthalene; reasonable agreement was obtained to this level. The data in Fig. 2 again indicated that an analysis of BLS was questionable. In particular, it appeared that the mass spectrometric data were in error because the naphthalene content measured was less than obtained for the ERBLS3 blend (41 pct ERBS, 59 pct BLS).

The BLS analysis error was probably introduced by the the saturates-aromatics separation step of the mass spectrometric analysis. That is, the technqiue requires that the fuel sample be chemically separated into these two fractions, with each one being individually analyzed. The properties of the entire sample are determined by numerically weighting the fractional analysis by the percent of total mass represented by the fraction. After separation, the mass of the fractions ought to be equal to the original

6

sample mass. For most fuels, this conservation was obtained to over 98 percent. For BLS however the sum equaled only 85 percent. Clearly, the particular hydrocarbon mix of BLS did not separate into the saturates-aromatics fractions well and some compounds were lost to the separation solvent. This problem really stemmed from attempting to use analysis techniques beyond their intended range of applicability; however, efficient alternatives do not exist.

The levels of aromatics and napthalenes for BLS were determined from the values obtained for ERBS, and the three ERBS-BLS blends. Since the same fuels were used to prepare the blends, their properties ought to represent linear combinations of ERBS and BLS values. The property values for BLS were calculated from these blends, and it was concluded that the appropriate levels of aromatics and napthalenes for BLS were 76.0 and 29.7 (vol) percent, respectively. These levels, shown as corrected levels on Figs. 1 and 2, were used in test data analysis.

SECTION III - GENERIC GAS TURBINE COMBUSTOR

A model combustor was designed, fabricated and tested, which embodied the features of a gas turbine burner. This section of the report describes both the burner, specifying its geometry and expected performance, and calibration tests which were performed to document the burner airflow distribution.

Combustor Description

A combustor embodying the features of a gas turbine burner was designed and fabricated. That is, it was a high heat release device, with a strong swirling-recirculating flow structure at the front end (i.e., primary zone) followed by penetrating jets of air to gradually reduce the local fuel-air ratio, and hence gas temperature, to levels acceptable to a turbine. Design guidelines were established for both the geometry and performance of the burner. These were:

Geometry: (1) cylindrical burner with maximum axisymmetry
(2) burner diameter between 10 and 15 cm
(3) burner must permit meaningful changes in the primary zone fuel-air ratio

Performance: (1) combustion efficiency > 99 percent
(2) total pressure loss < 8 percent
(3) combustor exit pattern factor < 0.3
(4) liner temperatures consistent with current aircraft practice

The primary variable investigated in the program was fuel chemical properties; a single airflow test condition was used. Hence, the performance guidelines applied only to the following simulated high-power condition:

combustor upstream pressure: 1.3 MPa
combustor inlet temperature: 700K
combustor overall fuel-air ratio: 0.015, 0.018, 0.022

Strictly, the fuel-air ratios applied only for operation on Jet A fuel; for other fuels, the fuel-air ratios were to be specified at the levels required to produce ideal combustor exit temperatures equal to those for Jet A.

Considerations of these guidelines led to specifying a louver-cooled, cylindrical burner with an inside diameter of 12.7 cm (Fig. 3). It consisted of a dome constructed from a frustrum of a 90 deg cone and six, conventional sheet-metal louvers; the overall length was 41.1 cm. A flange on the dome was provided to mount a central fuel injector-swirler combination; the dome also had penetrations for a spark igniter and two transpiration radiometers (See Section V). The dome cooling air was admitted through four rows of equally-spaced holes, and each louver was fed by a

8

ring of equally-spaced holes. Four of the louvers contained six large holes to admit combustion air to the burner; these holes represented the greatest deviation from axisymmetry. The number and diameter of all combustor holes are listed in Table 6.

The combustor liner described above was the baseline configuration used in the fuel-effects combustion tests. A limited number of tests were conducted to determine the influence of a different primary zone equivalence ratio for a constant overall fuel-air ratio. These tests labeled "Configuration-Effects" tests, were accomplished by using either of two modifications to this baseline burner. For tests in which a leaner primary zone was desired, the combustion air holes in the first louver were opened to a diameter of 18.0 mm while the holes in louver 5 were blocked. This alteration kept the total open area constant while permitting additional air to be entrained into the primary zone. For tests in which a richer primary zone was desired, the diameter of the holes in the first louver was reduced to 6.4 mm while the holes in louver 5 were opened to 14.2 mm. Again, the total open area remained constant but a reduced airflow was available to the primary zone. The level of airflow associated with the primary zone was determined by a carbon dioxide tracer technique for the baseline configuration and extended to apply to the two modified burners. This technique and the results are described below in the subsection entitled Combustion Calibration.

The twenty five test fuels provided a wide range of both chemical and physical properties. In order to eliminate the influence of the physical properties on combustion, highly-atomized, and hence rapidly-vaporizing, fuel sprays had to be achieved. Recognizing that atomization quality deterioration can be offset by proper nozzle selection (i.e., capacity), a family of fuel injectors was sought. In particular, pressure atomizing injectors produced by Hago Manufacturing Inc. were used (Fig. 4a). All injectors produced hollow cone sprays with a rated included cone angle of 80 deg. The nozzle size used with each test fuel was determined from the spray characterization data described in Section IV.

An air swirler encircling the fuel nozzle provided the swirl necessary to assure stable combustor operation. The device enhanced fuel-air mixing and distribution and established the recirculating primary zone flowfield. The swirler used was a commercially available device developed by Pratt & Whitney Aircraft for the JT 12 combustor (Fig. 4b). It embodies both the primary air swirler and the nozzle nut. The swirler-injector combination mounted in a flange on the dome of the combustor; an annular clamp ring assured proper positioning and sealing.

The performance of the burner was evaluated to assure operation within the design guidelines. As originally planned, a combustor total airflow of 2.0 kg/s would be used, which would produce a liner pressure loss of 2.0 pct and a reference velocity (based on the combustor diameter and approach airflow density) of 25.4 m/s. (The actual airflow was reduced during shakedown testing to 1.8 m/s because of test facility limitations, which thereby reduced these levels to 1.6 percent and 23 m/s, respectively.) The stability and combustion efficiency characteristics were predicted

9

following the techniques of Odgers and Carrier (Ref. 14) with the efficiency re-affirmed by considering the carbon monoxide emissions according to Mellor (Ref. 15). In all cases, the burner was predicted to be very stable and to operate at combustion efficiencies greater than 99 percent. The level of penetration of the combustion air jets was also evaluated using the correlation presented by Abromovich (Ref. 16). Predicted penetration distances were similar to those achieved in a comparative commercial gas turbine combustor, indicating that a vigorous mixing of these jets and the bulk flow was likely; a low pattern factor was expected.

<h3 align="center">Combustor Calibration</h3>

Combustor calibration tests were performed to document the distribution of liner airflow. Data were acquired to calculate both the effective area (i.e., discharge coefficient * geometric area, CDA) of the holes at each axial station and the percentage of total airflow involved with the primary zone. This information was necessary to describe the gross variations in fuel-air ratio occurring within the burner. In particular, the primary-zone airflow split was necessary to calculate the equivalence ratio in this critical section of the combustor.

Effective Area Tests

As a first step in defining the combustor airflow distribution, the effective area of the liner holes at each axial section—i.e., dome, louver 1 cooling, louver 1 combustion air, etc—was determined. These data were obtained from tests performed in the UTRC Jet Burner Test Stand (JBTS) using the setup depicted in Fig. 5. All liner holes except those at the position of interest were taped closed. The liner was mounted in the test section, with this assembly mated to the normal upstream facility components (see Section V for a complete facility description). The liner exit was completely open to the test cell. High pressure, dry air was supplied to the JBTS and metered with a venturi sized to operate choked. The airflow pressure and temperature upstream and pressure at the throat of the venturi were measured. A board of water manometers was used to record the pressure drop across the liner. Three levels of airflow were used to acquire data at liner pressure losses of approximately 1, 2, and 3 percent. The effective area was calculated for each airflow according to:

$$CDA = \frac{WA}{[2*(PB+DPL)*DPL/R/TA]^{\frac{1}{2}}}$$

where WA = air mass flow
     DPL = measured liner differential pressure
     PB = barometric pressure
     TA = air temperature
     R = gas constant

The three values of CDA were plotted, with the value corresponding to a

combustor-equivalent flow parameter identified. In fact, since the combustor airflow Mach number was low for all tests, the effective area did not significantly vary with airflow rate. The selected effective areas are listed in Table 7. Also shown are levels obtained in separate tests for the swirler CDA and for the total liner. The sum of the individual station CDA matched the liner total to within the estimated uncertainty of $\pm$ 3 pct. The sectional values were adjusted to match the measured total liner CDA as indicated in the table.

Primary Airflow Study

The combustor primary zone is a region of high heat release which is largely responsible for burner stability, efficiency and exhaust emissions. The effectiveness of this zone is closely associated with the primary zone equivalence ratio, ϕ_p. However, calculation of ϕ_p is not straight-forward as the course of some airflows which penetrate the liner is unknown. That is, while the airflows admitted by the swirler and dome would clearly participate in this zone, it was not certain what percentage of the louver 1 combustion air would be entrained into the recirculating flow. In an attempt to clarify this situation, a carbon dioxide (CO_2) tracer gas was used to identify the primary zone flow.

The primary zone airflow tests used a test setup similar to that described above for CDA determination. That is, a metered airflow was delivered to a combustor liner mounted in the test section; the combustor exit was open to the test cell. All liner holes were open and a normal fuel nozzle-swirler combination was mounted on the dome. The fuel nozzle was a Hago device which had been modified by opening the internal flow passages and adding a 1-cm long, closed-end extension tube on its face. The tube had eight orifices distributed along its surface which permitted injection of CO_2 gas into the surrounding swirling airflow. During testing, the total airflow was set to match the flow parameter for the combustion tests, and a metered flow of CO_2 was injected into the primary zone. Gas samples were extracted using a multiple-point probe constructed from thirteen, 3.2 mm OD, equal length tubes (Fig. 6). The tubes were manifolded into two sets: Set one included the outer six and the central tube; set two contained the six tubes on the inner circle. The position of the probe assembly was identified by the axial and angular positions of the probe tip. Samples were obtained at axial intervals of 1.2 cm at the head end of the combustor, and for angular orientations which placed the sample tubes in line with or between the six, large combustion air holes in the first louver. Samples from either set were analyzed for CO_2 concentrations using a Beckman NDIR analyzer. Airflow splits (i.e., percent of the total airflow) were calculated from the local CO_2 concentration according to:

$$\frac{WAL}{WA} = K * \frac{WCO_2}{WA} * \left(\frac{1}{XCO_2} - 1\right)$$

where   WAL   = local air mass flow associated with sample
      WA   = total metered air massflow
      WCO_2 = total metered CO2 mass flow

XCO_2 = fractional molar concentration of CO_2 in sample
K = constant accounting for species molecular weights

Since only the total flowrate of air and CO_2 are metered, this tracer gas approach yielded quantitative information only if the region being investigated was well-mixed. A data consistency test was performed using a liner with all holes closed except those on the dome. The CO_2 concentration at the combustor exit was uniform, and its value corresponded to fully-mixed CO_2 and air at the metered flowrates.

The data acquired from tests of the total combustor are depicted in Fig. 7. Data for both probe sets and for probe orientations between and inline with the louver 1 combustion air holes are presented. The data indicated a relatively well-mixed primary zone (i.e., region upstream of the combustion air holes), with little distinction in data acquired for either probe set or azimuthal orientation. This homogeneous character permitted meaningful calcuation of the airflow split. Approximately 19.5 percent of the total airflow was determined to be involved in the primary flowfield.

Also shown in the figure are the cumulative effective open areas of the liner. The sum of the swirler and dome cooling CDA represented 16.3 percent of the liner total, indicating that airflow from another source had been recirculated upstream. It was assumed that all of this excess originated from the louver 1 combustion air holes; the calculated entrainment level was 26 percent of this flow.

The CO_2 tracer study indicated that 19.5 percent of the total airflow participated in the primary zone flowfield. Hence, the ϕ_p value would be 5.1 times the overall equivalence ratio, for the baseline combustor. Variations in ϕ_p applicable to the combustors used in the Configuration Effects Tests are depicted in Table 8 (the values are those associated with Jet A). For the baseline configuration, which was exclusively used in the fuel-effects tests, ϕ_p ranged between 1.2 and 1.7. For the configuration-effects tests, the combustion air holes in louver 1 and 5 were modified to produce leaner and richer primary zones (see Description of Combustor). Application of the above 26 percent entrainment level led to the airflow splits and ϕ_p variations presented in the table. As can be seen, the three configurations provided three levels of ϕ_p for a constant overall fuel-air ratio, and at least two levels of overall fuel-air ratio for the same ϕ_p.

SECTION IV -- FUEL SPRAY CHARACTERIZATION AND INJECTOR SELECTION

The principle objective of this program was to determine the influence of fuel _chemical_ properties on the operation of a gas turbine combustor. Fuel physical properties were de-emphasized by producing finely-atomized, and hence rapidly-vaporizing, sprays for all fuels. This section of the report describes the nozzle characterization effort necessary to select injectors which met the atomization goal.

Atomization Goal

The twenty-five test fuels provided wide ranges in both chemical and physical properties. Variations in either could influence the burner characteristics. Fuel chemical properties would primarily affect the type and concentration of hydrocarbon species within the burner. For example, hydrogen-deficient fuels might produce greater carbon concentrations, resulting in higher radiation heat loads (and subsequently higher liner temperatures). Fuel physical properties would primarily affect the level of atomization. That is, fuels with disadvantageous physical properties-- high levels of viscosity or surface tension--would tend to form coarse sprays, with these relatively larger droplets penetrating deeper into the airflow and surviving for significantly longer time periods. Clearly the size, location and intensity of the combustion zone would respond to such fuel distribution alterations, and consequently the combustor characteristics would also change. In order to isolate chemical property influences, the processes dependent on physical properties must be minimized. Only by achieving highly-atomized and hence rapidly-vaporizing sprays can this goal be satisfied.

Ballal and Lefebvre (Ref. 17) analytically considered the influence of fuel chemical and physical properties on the combustion efficiency of a gas turbine combustor. Limiting cases were identified where the heat release rate was dominated by either chemical reaction, mixing or fuel vaporization. Mixing-controlled situations were readily dismissed by the authors by stating that "there exists no evidence to suggest that mixing rates are ever limiting to the combustion efficiency of gas turbine combustors." Hence great attention was given to defining system characteristics which separated reaction-controlled and vaporization-controlled operation. In particular, a vaporizing fuel spray characterized by a Sauter Mean Diameter (SMD) droplet was analyzed. Convective heat and mass transfer was included by assuming that the droplets do not respond to the turbulent velocity fluctuations of the airflow. A critical SMD was identified (SMD_c); for $SMD > SMD_c$, fuel vaporization would control the heat release:

$$SMD_c = \left[2.4 * \frac{\rho_g^{0.5}}{\rho_f} * \frac{k}{C_p} * \ln (1+B) * L * \left(\frac{u'/U}{100\mu} \right)^{0.5} \right]^{2/3}$$

13

where ρ_g = gas density
       ρ_f = fuel density
       k = gas thermal conductivity
       CP = gas specific heat
       B = mass transfer number
       L = length of combustion zone
       u' = turbulence intensity, pct
       U = bulk gas velocity
       μ = gas kinematic viscosity

Large values of SMD_c would indicate that the fuel properties (fuel volatility through B) and flow condition (convective heat transfer through u') were favorable to vaporization--that is, a large SMD could be tolerated without becoming vaporization controlled. Longer combustion zones or greater residence times, L/U would also increase SMD_c.

The critical droplet size to avoid vaporization control was evaluated for the combustor used in this test program. In particular, the SMD_c value sought was to assure rapid vaporization within the combustor primary zone which, based upon the test conditions and flow splits, had a residence time of approximately 5 ms. Calculations indicated that for Jet A fuel, a 20 percent turbulence intensity, and a droplet lifetime half the primary zone residence time, SMD_c = 52 μm. That is, a Jet A spray with a SMD < 52 μm would vaporize sufficiently fast so as not to limit the heat release rate. The least volatile test fuel to be tested had distillation characteristics similar to a No. 2 oil. For the same conditions as described above, the critical diameter was calculated to be SMD_c = 45 μm.

A second analysis of fuel vaporization was conducted using the UTRC Spray Vaporization Computer Program. This code employs an axisymmetric stream tube calculation technique, with fuel vaporization and droplet-gas-phase mixing modeled through consideration of convective and diffusive exchange of mass, momentum and energy. Initial levels of the air pressure, temperature and velocity and fuel temperature, velocity and droplet size were specified. The multi-component nature of the fuel is treated following the technique of Cox (Ref. 18) by use of the fuel distillation curve. The governing equations are solved by a forward marching, finite-difference procedure to provide a streamwise evolution of the two-phase flow properties.

The calculated droplet lifetimes, i.e., complete vaporization, for specified initial droplet diameters of Jet A or No. 2 oil are presented in Fig. 8. The results were obtained for the same operating condition of the primary zone as for the Ballal analysis. Again the convective heat and mass transfer was represented by the inability of the droplet to respond to turbulent velocity fluctuations. To achieve complete vaporization within half the primary zone residence time, i.e., within 2.5 ms, the SMD of the Jet A spray could approach 65 μm while for No. 2 oil the spray must be limited to SMD < 56 μm. These results were similar to those achieved in the preceeding analysis and therefore confirmed the approximate level of atomization required to eliminate fuel physical property influences. In principle, the finest level of atomization, i.e., smallest droplets, ought

to be sought to truly minimize this influence. This extreme would have
imposed unacceptable demands on the test program—excessive fuel pressures
and/or nozzle substitution for every fuel, for each of three fuel flow-
rates, would have been required. These considerations and the results of
the vaporization analyses led to specifying a spray atomization goal of: 35
< SMD < 45 μm for all fuels at the median fuel flowrate. The selection of
fuel nozzles to achieve this goal was the objective of the injector
characterization effort.

Fuel Spray Characterization

In order to assure meeting the atomization goal, the fuel spray formed
by each of the 25 test fuels was experimentally characterized. Spray SMD
and cone angle were determined for all fuels with a single nozzle, with
additional tests performed to quantify the influence of nozzle size (capa-
city), fuel temperature and swirler airflow. As described in Section III
all fuel nozzles were pressure-atomizing devices produced by Hago Manufac-
turing Inc., which were rated to produce hollow cone sprays with included
cone angles of 80 deg.

Spray Characterization Facility

The characterization of the fuel sprays was performed in the UTRC
Ambient Pressure Fuel Spray Facility located in the Jet Burner Test Stand.
This facility, which is routinely used to determine spray patterns and
droplet size distributions, was designed to operate over wide ranges of
fuel and air flowrates. Fuel could be delivered from either a large capa-
city Jet A supply or a smaller (approximately 20 liter) batch supply. The
system also provides for fuel temperature conditioning (heating or
cooling). The pertinent components used for the present study are depicted
in Fig. 9. The fuel nozzle was mounted with the combustor air swirler on a
canister which acted as a plenum for swirler airflow; swirler airflow
was used only for a limited number of tests to document its influence on
the fuel spray. Either the Jet A or the batch fuel system could be
selected by activating a 3-way valve; each system contained the appropriate
components to pump the fuel and regulate its flowrate. The fuel delivered
to the nozzle was metered by a Micromotion mass flowmeter. Fuel pressure
and temperature were measured at the injector. A calibrated venturi was
used to meter the swirler airflow, with appropriate pressure and
temperatures at the venturi measured.

The fuel spray pattern and droplet distribution were documented.
Photographic records of the spray were obtained to determine the included
cone angle. A high power General Radio Strobolume illuminated the spray
with a 10 ms light pulse substantially freezing the droplet motion.
Polaroid film was used. A Malvern Model ST1800 Particle Size Analyzer was
used to measure the droplet size distribution in a plane 6.4 cm downstream
from the injector. This instrument is based on Fraunhofer diffraction of a
parallel beam of monochromatic light by moving or stationary particles. A
He-Ne laser beam traversed the spray diameter with the diffracted light
sensed on a 30-element photoelectric detector. The data were acquired

15

using a 300-mm focal length collecting lens which permitted detection of droplet sizes between 6 and 560 μm. The photocells were scanned 200 times (approximately 2.6 sec) to acquire a statistically meaningful average for each data point. A dedicated mini-computer stored the diffracted light data and, upon request, executed an analytical program to interpret these signals in terms of a Rosin-Rammler droplet distribution and calculate a spray SMD.

Test Plan and Procedures

Four sets of fuel spray characterization tests were performed:

(1) All fuels were sprayed at three fuel flowrates using one injector. The injector was a Hago No. 35 nozzle, where the nozzle number (NN) indicated the rated volume flow of No. 2 oil (gal/hr) at a dfferential pressure of 0.69 MPa (100 psid). The same fuel mass flowrates were used for all fuels, being 118, 133 and 162 kg/hr. These levels were approximately the flows required for Jet A at the combustor test condition.

(2) Two fuels were sprayed at three fuel temperature levels using one injector. The two fuels were Jet A and tetralin, at temperature levels of 290, 311 and 328K. A NN = 35 nozzle was used.

(3) Two fuels were sprayed at multiple flowrates through each of three injectors. The two fuels, Jet A and tetralin, represented a baseline and an extreme variation in physical properties. Nozzle sizes included NN = 20, 30 and 35. The five flowrates included the three above and, for the smallest nozzle, two lower rates of 83 and 96 kg/hr.

(4) Two fuels were sprayed using one injector and two levels of swirler airflow. The two fuels were Jet A and tetralin and the nozzle was a NN = 35 device. The two airflow levels were characterized by the differential air pressure established across the swirler (DPSW). Data were acquired for DPSW = 4.9 and 26.2 kPa, which corresponded to matching airflow velocity and momentum, respectfully, to those appropriate to actual combustor operation.

Th⁻ test procedures were similar for any of these tests. The instrumentation was checked each test day. Jet A flowrate was established at 133 kg/hr. If appropriate, the swirler air differential pressure and fuel temperature were set for the test condition. Two Malvern data points were acquired. The system was then switched to the test fuel by activating the three-way valve. The lowest fuel flowrate (118 kg/hr) was set and the airflow and fuel temperature condition re-established. Two Malvern data points were acquired; the spray was photographed. The test fuel flowrate was increased to the second and third levels, with similar care for holding The test condition and data acquisition. At the completion of this sequence, the system was momentarily switched back to the Jet A supply and then terminated. Another test fuel was loaded into the batch fuel system and the delivery lines purged of prior fuel. This sequence of acquiring

16

Jet A data and then test fuel data was followed during all four sets of testing.

Initial Results -- Weber Number Influence

Some preliminary tests were performed to verify that the nozzles were acting as expected. A single test was performed using a twenty-point patternator probe to confirm the hollow-cone spray quality. The probe spanned the spray diameter in a plane 7.6-cm downstream from the nozzle. The observed pattern is depicted in Fig. 10 where a clearly hollow cone behavior is evident.

The results from initial tests to determine a Jet A spray SMD were different than expected. Several investigators (Refs. 19 to 21) have characterized the sprays from pressure-atomizing nozzles and developed correlations for the dependence of SMD on fuel physical properties, fuel flowrate and nozzle size. For a given fuel, these studies have shown

$$SMD \sim WF^m \; DP^{-n}$$

where WF = fuel mass flowrate
       DP = injector pressure drop
       m,n = empirically-derived constants in the range:
            $0.20 < m < 0.25$
            $0.35 < n < 0.43$

The UTRC data did not fit this form. An investigation ensued, which included a comparative check of current and previous Malvern data for a standard nozzle and a review of the spray characterization literature. Valid data were being acquired; sufficient signal strengths were being received by the photodetectors. The normalized size distribution was mono-modal and well fit by the Rosin-Rammler distribution function. The Malvern data acquired with the standard nozzle duplicated previous results.

The literature review was fruitful in revealing the probable cause of the SMD discrepancy. Data presented by Simmons (Ref. 22) indicated a change in the dominant atomization mechanism as the flowrate through a pressure-atomizing nozzle was increased. This change was related to the nozzle Weber number (We) defined as the ratio of fuel inertia forces to surface tension forces. An expression for We as a function of the nozzle geometry, fuel properties and flowrate was derived and a critial Weber number, We_c, was identified at a value, $We \approx 1$. Below We_c, the SMD data did not match the above standard correlation while for $We^c > We_c$ agreement was achieved up to the maximum We investigated (We = 5).

Other investigators have also acknowledged the importance of We on atomization. In particular, Dickerson and Coultas (Ref. 23) noted changes in the droplet breakup mechanism near both We = 1 and We = 10. Their observation of "bag breakup" near We = 1 coincided with Simmons change in atomization behavior. Additionally they noted a change to a "shear breakup" mechanism at higher We. Therefore, just as Simmons observed that We = 1 was a lower bound to the range of applicability of the "standard

correlation", a We = 10 might represent an upper bound of application. Atomization correlations developed for 1 < We < 10 might not be applicable for high We cases. Indeed, applying the expression for We derived by Simmons to the investigations which developed the correlation revealed that they were generally restricted to 1 < We < 10 (Fig. 11). The investigations conducted by Jasuja at Cranfield (Ref. 21) did slightly exceed this upper limit. Review of these data indicated that the high We values showed the greatest deviation from the empirical correlation. Because of the sparceness of these points this phenomenon was probably overlooked. The range of Weber number covered by the nozzle size-fuel flow demands of the current program is also shown on the figure. Clearly, operation at We > 10 was to be experienced. These observations highlighted the need to recognize the application limits of empirical correlations. Use of the pressure-atomizing injector "standard correlation" would have been erroneous.

It is noted that a complete SMD correlation was not necessary for this program since spray characterization data were acquired for every test fuel. These data are being analyzed by UTRC to develop such a correlation; the results of this effort will be published in the future.

Characterization Results

Tests With All Fuels

Data which characterized the atomization of each fuel injected by a Hago No. 35 nozzle are listed in Table 9. The fuels are listed in generally decreasing order of atomization quality. As expected, the measured atomization levels for fuels with similar physical properties (e.g., Jet A and JP5 or JP4, JP4-S, JP4-A) were also similar. The dominant physical property appeared to be surface tension. Tetralin and decalin possessed the highest surface tension and atomized relatively poorly, while the JP4 fuels, with the lowest surface tension, atomized the best. An approximately linear influence of surface tension was apparent as indicated by the data plotted in Fig. 12. Viscosity did not systematically influence the spray atomization (Fig. 13) for the range of viscosity of these test fuels. These two influences were consistent with the identification of Weber number as a critical parameter as this variable was responsive to fuel surface tension but not fuel viscosity. Additionally, both of these physical property influences differed from dependences associated with the standard pressure-atomizer SMD correlation, again indicating a change in dominant atomization mechanism. The included cone angle did not significantly vary despite substantial changes in the spray SMD. Hence it was expected that fuel from all sprays would initally have the same direction.

Tests at Elevated Fuel Temperature

The data acquired from tests using a No. 35 Hago nozzle spraying Jet A and tetralin fuel at temperatures of 299, 311, 328K are listed in Table 10. These tests were scheduled in anticipation of reducing the spray SMD because of viscosity decreases at elevated temperatures. That is, the

18

standard correlation for pressure-atomizing injectors indicated a
significant dependence of SMD on fuel viscosity. Hence, it was originally
expected that a viscosity reduction would cause an SMD reduction; control
of fuel temperature (and thus fuel viscosity) was a proposed technique to
control spray SMD. The initial test results and the complete characteriza-
tion of all fuels showed that this approach was not applicable. As
demonstrated above, viscosity did not systematically influence SMD.
Therefore, despite viscosity decreases of 40 percent for tetralin, the
observed atomization level was insensitive to the fuel temperature. The
more dominant physical property, surface tension, decreased by less than 8
percent over the fuel temperature range invstigated and hence little
measurable influence would be expected.

Tests with Multiple Nozzles

The data acquired from tests with three Hago injectors with nozzle
numbers, NN = 20, 30, 35 are listed in Table 11. Five flowrates were
investigated—the three levels used above plus two lesser flows for the
smallest nozzle to permit acquisition of measurable (i.e., not too small)
SMD data. The expected significant dependence of spray SMD on nozzle size
was documented. The atomization level changed by up to a factor of five
for the range of nozzle numbers investigated. Cone angle variations were
small. Since SMD control by exercising fuel temperature control was not a
viable approach, the atomization goal could be met only by the proper
specification of nozzle size. The SMD data from these tests were analyzed
to quantify the SMD - NN relationship. For the medium fuel flowrate; it
was determined that:

$$SMD/NN^b = constant$$

with b = 4.0 for Jet A
     b = 3.1 for tetralin

The variation in "b" implied that a fuel property influenced the nozzle
scaling. This influence would be in addition to the surface tension effect
observed in tests with the same nozzle (Fig. 12).

Most of the atomization levels presented in Table 9 for a NN = 35
nozzle were above the goal of $35 < SMD < 45$ μm at a fuel flowrate of 133
kg/hr. Hence a smaller nozzle was often required. Since a value for "b"
was not available for all fuels, the value for tetralin was applied for all
nozzle scaling. Use of b = 3.1 was the conservative approach in selecting
the nozzle. That is, if a fuel would actually be represented by b > 3.1,
then using b = 3.1 would lead to a nozzle atomizing within or below the
goal range. Applying this scaling relationship to the SMD data obtained
with a NN = 35 device led to the specification of the fuel nozzles
indicated in Table 12. Calculated nozzle numbers were transformed to the
nearest available nozzle; four nozzle sizes were to be used. Also shown
are the predicted SMD values; they were within the atomization goal.

Tests with Swirler Airflow

Data acquired to document the influence of swirler airflow are listed in Table 13. The NN = 35 nozzle-air swirler combination was mounted on a 25-cm diameter canister which acted as a plenum for the airflow. The two levels of airflow, represented by the pressure drop across the swirler, corresponded to matching the airflow velocity or momentum of an operating combustor. Substantial decreases in SMD were observed indicating a strong secondary atomization process. Theoretically, it might be argued that the momentum-matched airflow represented the proper combustor simulation. UTRC experience has not substantiated this belief, however; velocity-matched airflows have been used with success to screen and select nozzle concepts. Indeed, data do not exist to clarify this issue. Therefore, while quantitative conclusions could not be drawn from these data, some reduction in spray SMD from the data presented in Table 12 was expected.

SECTION V - TEST FACILITY AND INSTRUMENTATION

The experimental program, including both the combustor calibration and the fuel-effects and configuration-effects combustion tests, were performed in the UTRC Jet Burner Test Stand (JBTS). This section of the report describes the specialized test facility assembled for these efforts. The instrumentation is detailed, with complete description given for two unique diagnostics--a transpiration radiometer and Mie-scattered light particle sizing apparatus.

Test Facility

The experimental program was conducted in the JBTS which is a self-contained facility with four test cells equipped for high-pressure combustion tests. The JBTS provides, in addition to the test cells with control rooms, assembly areas, automatic data acquisition systems, and air, fuel and gaseous nitrogen supply systems.

The test facility consisted of three sections: an air preparation section, a test and instrumentation section, and an exhaust section (Fig. 14). A specialized fuel delivery system supported the test facility.

The air preparation section provided airflow rates satisfying the requirements of the test conditions. Air was supplied to the JBTS through the system depicted in Fig. 15. The multi-staged receiprocating compressors, capable of pumping a combined flowrate of up to 4.5 kg/s, provided air at pressures up to 2.7 MPa. The airflow for the combustion tests was heated by an indirect-oil-fired burner prior to entering the JBTS; the typical preheat level was 420K. The heated airflow was regulated in the test cell and metered by a venturi, with appropriate measurement of air pressure and temperature performed upstream and at the throat of this device. The temperature of the venturi body was also measured to account for thermal expansion of the throat diameter. The metered airflow was heated further by use of an electrical resistance-type heater. A plenum at the heater exit assured that uniform airflow velocity and temperature profiles were delivered to the test section; arrays of four thermocouples and four total pressure probes documented this condition.

The test section housed the combustor liner, providing appropriate access for a spark ignitor, fuel injector support and other instrumentation. This section was fabricated from commercially-available pipe with an inside diameter of 15.2 cm. The 1.3-cm annular gap between the liner and housing permitted adequate backside convective cooling of the burner louvers. The combustor was supported by links on the dome with an aft sliding-seal to allow axial and radial growth. The position of the combustor in the housing and the layout of instrumentation on the liner and at the combustor exit are described below.

The exhaust section consisted of a water-cooled T-section and a backpressure valve. The T-section provide¹ a 7.6-cm diameter viewport to

permit direct observation of the combustor exit plane via closed-circuit, color television system. A remotely-operated butterfly valve was used to control the test section pressure. A high-pressure water quench reduced the gas temperature upstream of the valve to less than 700K to prevent damage to it.

The fuel delivery system consisted of three subsystems: a startup fuel subsystem, a test fuel subsystem and a nitrogen purge subsystem. Jet A was supplied to the test cell from underground storage tanks by positive displacement pumps. This fuel, referred to as Jet A-U was the startup fuel used prior to switching over to the test fuel. Data were acquired for the combustor operating on Jet A-U prior to operation on any test fuel. Jet A-U had properties identical to the Jet A test fuel; the drummed test fuel had been extracted from this source early in the program. The underground Jet A tank was isolated for this program; no additions were made to this tank once testing commenced. Drum quantities of the test fuel could be delivered by the test fuel subsystem which was capable of delivering 4.6 liter/min at a pressure of 6 MPa. Two solenoid valves, one in each fuel subsystem, were actuated by a common electrical circuit. A normally-open valve in the Jet A system and normally-closed valve in the test fuel system were switched in unison to provide a rapid, positive change in fuel. A Model C-12 Micromotion mass flowmeter was located in the common fuel delivery line at the test rig. This meter sensed the coriolis forces induced by fuel flowing through a curved tube to determine the mass flow. The meter contained no moving components (e.g., turbine vanes) and hence the rate measurement was independent of the viscosity. The nitrogen subsystem was available to purge the fuel nozzle and delivery lines inside the combustor rig and to cool these items during the setup of the test condition. The fuel system is depicted as part of Fig. 16.

Instrumentation

The test facility was instrumented as described below. The parameters measured are listed in Table 14 and schematically indicated in Fig. 16.

Measurements were made to document the airflow rate, pressure and temperature approaching the model combustor. The airflow rate was determined using a venturi with a 2.286-cm throat diameter; pressure and temperature upstream and pressure at the venturi throat were measured. The distribution of temperature and total pressure at the test section inlet were documented using arrays of four thermocouples and four total pressure probes. The test section housing contained four static pressure taps to document both the axial static pressure gradient in the airflow external to the burner and the pressure at the combustor exit.

The fuel supply contained provisions for acquiring pressure and temperature measurements necessary to control the flow. A thermocouple was inserted through the fuel tube to the nozzle vicinity to document the temperature of the injected fuel. As described above, a Micromotion mass flowmeter was used to determine the fuel flowrate. A dc voltage source,

interlocked with the fuel switchover valves, produced a signal for the data system to identify data points acquired when operating with the test fuel.

The model combustor was instrumented with thermocouples to document changes in the combustor metal temperatures. Three bundles of 13 type K thermocouples were mounted on the combustor liner--two thermocouples mounted on each louver and one on the dome for each bundle. The layout of these sensors formed axial arrays between alternative rows of the louver combustion air holes. The photograph of the combustor liner (Fig. 3) illustrates the liner thermocouple layout. The location of the thermocouples coincided with the end and 2.5 cm downstream of the inner louver lip.

Two types of radiometers were used to document the radiative heat loads--transpiration and thermopile devices. The thermopile unit was representative of a conventional approach to radiation measurement. Such a device requires a window to isolate the sensor from the combusting medium and thereby eliminate convective heat transfer. Windows are difficult to use adjacent to a sooting environment. Deposition on the surface can alter the transmission and hence the level of radiation sensed. A solution to this problem is to recess the window, but this practice narrows the view angle, prohibiting acquisition of full hemispherical fluxes. As explained below, a transpiration radiometer does not use a window and permits placement of the sensor at the combustor wall.

Two transpiration-type radiometers were mounted on the dome of the burner. Each radiometer was a probe-like device constructed from three concentric tubes; it had 1.6-cm OD and was approximately 25 cm long (Fig. 17a). The outer two tubes provided a delivery-return cooling loop to ensure survival of the probe, while the central tube ducted a metered flow of gaseous nitrogen to the probe tip. The tip was covered by a tightly-woven steel screen which permitted the nitrogen to seep out of the probe (Fig. 17b). It was mounted to place the screen flush with the combustor liner to acquire the full-hemispherical radiative flux.

The screen was the radiative load sensor. It was heated because of heat transfer from the combusting medium and cooled by the convective flow of nitrogen. At steady-state, the energy removed by the nitrogen must equal the input energy. Direct measurement of the energy gain of the nitrogen was not possible since it would have required measurment of the nitrogen temperature leaving the screen. However, if the screen was a perfect heat exchanger, the screen temperature would equal the exit gas temperature and therefore (ideally):

$$\text{Ideal Energy} = \text{WN2} * \text{CPN2} * (\text{TSCREEN} - \text{TN2UP})$$

where WN2   = nitrogen mass flow
      CPN2   = specific heat of nitrogen
      TSCREEN = temperature of probe screen
      TN2UP   = temperature of nitrogen upstream of screen

23

As shown by Moffat (Ref. 24), with sufficient nitrogen flow, the gas boundary layer will be blown-off the tip and only radiative transfer would heat the screen. The occurrence of blowoff depends on the flow of the inner, combusting flow; experiments with a flat plate suggest that the mass flux must exceed 8 percent of free stream value to achieve this condition. During this mode of operation, as the nitrogen flowrate is reduced, the probe temperature rise (screen minus upstream nitrogen temperatures) would increase while the energy input remains constant. Only at low nitrogen flow would the hot gas boundary layer re-attach, a situation to be avoided because the input energy would have destroyed the screen. Data were acquired at various nitrogen flowrates during combustor shakedown tests to confirm measurement of radiative heat transfer only (Fig. 18). As expected, the probe temperature rise did vary but the input energy remained constant. During combustor testing, a nitrogen mass flux of approximately 6 $gm/s/cm^2$ was used to assure operation in this mode. All probes were calibrated by the Pratt & Whitney Aircraft Commercial Engineering Heat-Transfer Laboratory at elevated pressures to account for the non-ideal heat exchanger behavior of the tip screen.

Three, water-cooled thermopile radiometers were acquired from Medtherm, Inc. to document the changing pattern of radiative heat transfer within the combustor. These devices were mounted on the test section housing to view the combusting medium through the 1.2-cm diameter combustion air holes located in louvers 1, 2, and 3. The radiometers were designed to have a narrow view-angle (effectively, 33.43 deg; form factor = 0.0215) to allow locating them on the case to view the combusting gas but not the metal liner. Since these devices accepted radiation over a relatively narrow angle, the indicated radiative load could be either higher or lower than the hemispherically-averaged level measured on the dome. However, the three case-mounted devices did provide an indication of the axial distribution of radiative heat transfer and how this distribution was influenced by fuel chemical properties or test condition. These radiometers used a thermopile sensor located behind a sapphire window. The narrow view angle derived from a significantly recessed window which, in turn, was continuously purged by nitrogen. The repeatability of Jet A-U data indicated that no window fouling occurred. Furthermore, the devices were re-calibrated by Medtherm after completion of the fuel-effects tests and found to deviate from the original calibration by less than 2 percent.

The combustor exhaust products were probed to determine the temperature distribution, average gaseous emission levels, smoke emission level, and particulate size and number density. The measurements utilized a serial buildup of intrumentation sections as depicted in Fig. 14. The combustor exit temperature distribution was determined by using six thermocouple rakes containing a total of 22 sensors. The thermoccuples were Type B (PT6RH/PT30RH) devices concentrically mounted in a vented radiation shield. The exposed portion of the thermocouple sheath and the radiation shield were fabricated from a platinum al'oy thereby allowing a thermocouple maximum use temperture of approximately 1850K. The average gaseous exhaust emissions were determined from examples extracted by four ganged sampling rakes containing a total of 20 sampling orifices. The samples were analyzed to determine unburned hydrocarbons, carbon monoxide, carbon

24

dioxide, oxygen, and total nitric oxides. Table 15 presents the types and ranges of the exhaust gas analyzers. Smoke emission levels were determined from samples extracted by three, ganged, steam-cooled probes. The probe orifice diameter (1.55 mm) was sized to achieve isokinetic sampling; the sampling procedures were those specified by SAE ARP 1179. The layout of these several combustor exit plane probes is shown in Fig. 19. The flow blockage was not as great as the figure might imply; the array did not measurably backpressure the combustor.

Particle size and number density were determined at the combustor exit from an in-situ, spatially precise technique--namely, from the scattered light emanating from an approximately 15 mm^3 sample volume on the combustor centerline. This non-intrusive approach was adopted because of the belief that probe sampling would alter the character of the soot; particulate agglomeration would be likely.

The scatered-light signals were interpreted according to Mie therory of light scattering. This technique has been detailed previously by several authors (Refs. 25, 26, 27) with a critical assessment of the accuracy of it given by Bonczyk (Ref. 28). In brief, this theory predicts the intensity of light scattered by particulates as a function of the scattering particle properties, the scattering geometry and the incident intensity:

$$I = K * I_0 * N * PHI$$

where I = light intensity scattered by particles
      I_0 = incident light intensity
      PHI = complex scattering function
      K   = constant including the scattering solid angle and the optical sample volume
      N   = particulate number density

The scattering function, PHI, is dependent upon the size parameter, x, the scattering angle, θ, and complex refractive index, n:

$$PHI = PHI (x, \theta, n)$$

where x = $\pi D/\lambda$, λ = the wavelength of the scattered light
      D = the particle diameter

PHI is also responsive to the polarization of the light. Strictly, this description is accurate only for spherical particles of uniform size. Extensions of the theory to permit definition of polydispersions result in greater analytical and experimental complexity. For combustion applications, where the particulate shape is non-spherical, it is difficult to determine all the parameters of the polydispersion. Therefore, for such appliations, it is common to assume a monodisperse particulate size distribution. This approximation (and the accompanying assumption of spherical particles) limits the accuracy of the D and N determinations.

25

The evaluation of particulate size and number density relied upon the angular disymmetry of the scattered light. From the above description, for a fixed polarization of the light (chosen to be perpendicular to the scattering plane), the ratio of light intensity at two different angles, $\theta 1$ and $\theta 2$ is:

$$I(\theta 1)/I(\theta 2) = PHI\ (D,\theta 1,n)/PHI(D,\theta 2,n)$$

This ratio is a function of D alone for given values of the complex refractive index and scattering angles. In this program, values of $\theta 1 = 45$ deg and $\theta 2 = 135$ deg were used; the scattered light had a wavelength of 514.5 nm. The dependence of the ratio of scattered light on D is depicted in Fig. 20 for two values of n. Note that the theory permits size determination for $D < 0.3$ μm; for larger diameters, the ratio is multivalued and are unambiguous size determination cannot be made. The proper value for the complex index of refraction of the combustor exhaust particles was not known; the value likely depended on the chemical composition of the particulates. The two values used to generate the curves in Fig. 20 were obtained from measurements either on graphite or on soot from an acetylene flame. For the valid range of diameter determination, the uncertainty introduced by these two n values was not great, however; the value for graphite (n = 1.94 - 0.66i) was used in the data reduction. Once D had been determined, the particulate number density, N, was calculated from the scattered light intensity meaured at $\theta 1$ and the known geometry of the scattering setup.

The particle sizing apparatus assembled for this program is shown in Fig. 21. The incident light was produced by an argon-ion laser with an output power level of approximately 1w at a wavelength of 514.5 nm. The polarization of the output beam was rotated to be perpendicular to the scattering-plane; the beam was chopped at a frequency of 2008 Hz. The beam was directed through a recessed sapphire window, across the combustor exhaust, through a second window and on to a laser powermeter. Two scattered light detector assemblies were rigidly attached to the test duct, one at 45 deg and one at 135 deg from forward scattering. The fabrication tolerances of the assembly mountings were specified to assure precise alignment of them; during installation of this apparatus it was observed that the beams from two He-Ne alignment lasers intersected on the test duct centerline. Each detector assembly contained a sapphire window, a polarizing disk, a narrow-pass filter (centered at 514.5 nm) and a fast linear focused (EMI type 980/B) photomultiplier tube (PMT). The solid angle of the scattered light was defined by two 3.1 mm dia appertures (separated by a distance of 20.0 cm) located along the detector centerline. The output from each PMT was input to a lock-in amplifier which was referenced to the chopper frequency. This setup enhanced the signal-to-noise ratio by providing an output voltage proportional to the difference between the laser-stimulated scattered light and any random light which might have been detected.

The laser beam path also contained two focusing lenses. Initially these lenses were not in the optical path. During combustor shakedown tests, the quality of the laser beam exiting the test duct was observed by

use of a television system. No significant beam steering was observed; however, substantial beam diameter growth was observed. That is, the 1.3-mm diameter laser beam had grown to fill the 12-mm diameter exit port. This growth was attributed to "thermal blooming" which occurs as light passes through gases which possess large temperature gradients. The thermal gradients produce gradients in the index of refraction which result in a lens-like expansion of the ray. It was suspected that the blooming occurred in the window recesses where cool nitrogen purge flow and hot combustion products were unavoidably mixed. The lenses were installed to focus the laser beam on the test duct centerline to minimize this problem. Once the lenses were added, the beam quality exiting the test duct substantially improved. The exit beam diameter was reduced to less than 2 mm; geometric considerations of the focusing implied that a 0.5-mm diameter beam passed through the measurement volume. An alternative solution, use of heated purge flow, was not compatible with the window seal design.

SECTION VI – COMBUSTOR TEST CONDITIONS, PROCEDURES, DATA ACQUISITION AND REDUCTION

The principle variable investigated in this program was fuel chemical properties. Only a single airflow condition was used, with fuel injected at three flowrates for each test fuel. The matrix also included test replications to permit determination of the statistical consistency of the data. This section of the report details the test conditions and procedures, and specifies the manner in which the data were acquired and statistically analyzed.

Test Conditions and Procedures

The single airflow condition used in this program simulated high-power operation of a gas turbine engine. Each fuel was tested at the three flowrates required to produce ideal combustor exhaust temperatures or 1247K, 1346K or 1473K. These three temperatures were the ideal temperature levels associated with combusting Jet A at fuel-air ratios of 0.015, 0.018 and 0.022, respectively. The actual flowrates for each fuel were determined from thermochemical calculations using the chemical properties determined from the fuel analyses. The combination of airflow parameters and combustor exit temperatures defined three test conditions indicated in Table 16.

These conditions were established in both of two phases of tests: fuel-effects tests and configuration-effects tests. In the fuel-effects phase, all twenty-five test fuels were evaluated in a single burner configuration. In the configuration-effects phase, three test fuels were evaluated in two modifications to the above baseline burner. These two configurations, described in Section III, provided either a higher or lower primary zone equivalence ratio than that of the baseline.

The test procedures were identical for all tests in both phases. The data acquisition system was set up each test day. Pressure transducer and thermocouple references were checked; flowmeter, analyzer and radiometer outputs were zeroed; signal amplifiers were calibrated. A drum of the test fuel was installed with approximately 12 liters pumped through the delivery and return lines to purge them of previously-used fuel. The appropriate JBTS support systems were activated; purge flows were established through the sample probes, radiometers and fuel delivery line. Combustor airflow was initiated and heated by both the indirect-fired and electrical heaters. The fuel purge was terminated and Jet A-U introduced. Because of the high inlet air temperature, the fuel ignited spontaneously at a minimal flow, avoiding a sudden increase in burner pressure. The fuel flowrate was increased and the airflow parameters (pressure, temperature, flowrate) adjusted to the Condition 1 setpoints. Probe purge flows were terminated and steady-state conditions verified by observation of the exhaust gas temperature and species concentrations.

Data were acquired for operation on Jet A-U prior to combusting test fuel. If the test fuel was the first to be investigated on the test

28

day (multiple fuels were evaluated in a day), data were acquired at all three conditions. For subsequent fuels in the test day, data were acquired only at Condition 1. For each condition, three data points were recorded on the data acquisition system and three smoke samples acquired. Key parameters displayed in the control room were hand-recorded to provide a reference of burner behavior. These readings were frequently reviewed during Jet A-U tests prior to test fuel operation to confirm that the combustor was firing in an expected and repeatable manner.

After obtaining data for Jet A-U fuel, the fuel supply was switched to operation on the test fuel previously loaded in the system. Switchover was always accomplished at nominal Condition 1 setpoints; the simultaneous activation of solenoid valves provided an uninterrupted flow of fuel and the burner never extinguished. Condition 1 operation was established for the test fuel and three data points and smoke samples acquired. The fuel flow was increased and airflow parameters adjusted to achieve Condition 2 and Condition 3 in sequence, with three data points and smoke samples acquired at each. Upon completion of this three condition sequence, the fuel flow was decreased and burner parameters adjusted to re-establish Condition 1. Similar data were acquired for this condition and subsequently again for Conditions 2 and 3. This sequence was repeated a third time to provide a total of nine data points for each test condition. These data were statistically analyzed as described below to determine whether consistent, repeatable data were being acquired.

After completion of these sequence tests, the fuel system was switched to the Jet A-U supply and then flow was terminated. Purge gas was established through the sampling probes prior to this process to avoid ingestion of unburned fuel; the fuel lines were purged immediately upon fuel termination. All systems were secured if the tests planned for the day were completed. Otherwise, the test fuel was changed, fuel lines purged and the Jet A-U/test fuel sequence described above was executed again.

Data Acquisition and Reduction

The complete set of test data was recorded by means of an automatic data acquisition system which stored the information on magnetic tape for subsequent computer processing. The data system accepted data on up to 25 channels, 10 provided with signal conditioners, and the remainder compatible with preconditioned input signals. The system was capable of controlling and accepting data from submultiplexers such as pressure and thermocouple scanning switches. The data channels were scanned sequentially at a rate of 12 channels per second and whenever a submultiplexer was connected to a channel, all ports were sampled before proceeding to the next channel. An analog-to-digital converter digitized the data and an incremental magnetic tape recorder stored it for subsequent computer processing. The format of the tape was structured for compatibility with the UTRC UNIVAC 1110 digital computer.

Data reduction was completed in the following three steps:

1. Data tape point-by-point reduction
2. Normalization to standard test conditions
3. Precision assessment

Data Tape Reduction

The data system magnetic tape was reduced by use of an existing computer program. This code applies the appropriate calibration factors to each signal to provide engineering units for pressures and temperatures for calculation of parameters of interest. Among those selected for this program were: airflow rate, fuel mass flowrate, combustor reference velocity, radiative heat flux, exhaust emission indices, fuel-air ratio from either metered flows or exhaust species, particulate size and number density (using look-up tables generated by a code for Mie-scattered light), primary zone equivalence ratio, ideal combustion temperatures for either the primary zone or overall combustor, and combustion efficiency. Averages of pressures and temperatures which characterized the inlet airflow or combustor exhaust were also calculated. The output from this data reduction code was a Summary Table which displayed all measured and calculated parameters for every data point. This Table was reviewed for spurious measurements (e.g., open thermocouples) with hand-recorded data input if available. Also items not acquired by the data system (e.g., SAE smoke number) were entered into the Summary Table.

Test Condition Normalization

In any test program, attaining the precise values of the test condition parameters is difficult. The conditions achieved in this program generally matched the desired parameters to within 0.5 percent. In an attempt to minimize the influence of even these small deviations, relationships were derived to normalize the performance parameters to the exact test conditions. These relationships were either analytical expressions, correlations or complex relationships expressed by analytical models (e.g., influence of pressure on ideal combustion temperature). A listing of the test parameters and the calculated and measured performance parameters is given in Table 17. The parameters designated by the asterisk under the Parameter Type column were those which established the test conditions and were set according to the values specified by the test matrix. The parameters which were not test parameters were designated either as measured parameters or calculated parameters. Measured parameters included those that were directly measured or those which required only a straight-forward arithmetical manipulation (such as obtaining the averages of four combustor entrance air temperatures to obtain the average entrance temperature). Calculated parameters were those which were derived from the measurements and in general were dependent on more than one test parameter.

The methods for normalizing the parameters to the standard test values and an indication of which parameters were subjected to a precision analysis are also indicated in Table 17. In the case of the test parameters themselves, the normalized value was that specified in the test matrix. Most measured parameters were normalized by use of influence coefficients (IC). An influence coefficient is a weighting factor which specifies the

percentage change in the measured parameter for a 1 percent change in an independent (test) parameter. This approach is equivalent to correcting the parameter by mathematically forming a first-order expansion about the measured value (i.e., a single term Taylor series) and hence was an adequate technique for small departures from the desired test conditions. The influence coefficients were obtained either from derivatives of simple equations relating measured and test parameters (e.g., fuel pressure-fuel flowrate dependence) or from the response of computer model calculations from perturbations of the test conditions (e.g., influence of pressure on the combustion temperature). In particular, the radiation measurements were normalized by the quotient of ideal radiative loads predicted for the desired and actual test conditions. In these calculations, the emissivity was computed from the model of Lefebvre (Ref. 29). An existing computer code tc predict liner temperatures was used to develop their IC from results obtained from parametric perturbations of the test parameters (airflow, fuel flow, etc.) The trace exhaust emission species (UHC, CO, NOx) were normalized by use of correlations developed by Sarli (Ref. 30). Calculated parameters were normalized by performing the calculation with the normalized parameter values.

Precision Asssessment

For each of the performance parameters subjected to a precision analysis (see Table 17), the following statistical properties were calculated:

1. The mean value
2. The standard error of estimate
3. The interval about the mean within which the true means lies to a confidence level of 90 percent
4. The interval about the standard error estimate within which the standard deviation lies to a confidence level of 90 percent.

Precision is a measure of the repeatability of data. It is customary to express precision in a quantitative manner by using the standard error of estimate. This statistic is often erroneously referred to as the standard deviation. However, the standard deviation is a measure of precision for an infinite set of data while the standard error of estimate is a measure of precision for a set of S (finite) data. In practice, for reasonable values of S, the two statistics have essentially equal values. The use of properties of the standard error curve to describe the precision of a set of S data is based upon the assumption that the data are randomly distributed about the mean of the data. It can be shown that for reasonable values of S (> 30), this assumption is valid. However, for small values of S, there is a non-zero probability that the data are not randomly distributed about the mean value so that the calculated standard error of estimate will differ from the true standard deviation value.

In this program nine values were obtained for each parameter at each test condition. Therefore, there was a reasonable probability that each set of data was not randomly distributed about its mean value and the mean value differed from the true mean (assuming that the data were otherwise

31

free of bias). To assure that the statistics describing the precision of the data were reliable, it was necessary to use statistical techniques applicable to small data sets. No inference procedure was capable of producing an exact result. Instead, a statistic was calcualted that had a specific probability of being correct. One technique applicable to the present case is Student's t-test. This procedure assumes the standard deviation calculated for a small set is reliable (i.e., the data are randomly distributed about the mean value of the set) and estimates the degree to which the true mean for the data differs from the calculated mean. The determination of the confidence interval for the mean value requires that the confidence interval for the standard deviation be specified. It also is not precisely known for small sample sizes, and therefore, a "Chi-square" method was applied to establish the confidence interval for the standard deviation.

A computer program was written which accessed all data contained in Summary Tables and grouped the points common to a test condition for each fuel. These groups were normalized and analyzed for precision. A publication-quality printout was produced and bound to represent one part of the Comprehensive Data Report for this program.

SECTION VII - COMBUSTOR TEST RESULTS: FUEL-EFFECTS

The principle objective of the program was to quantify the influence
of fuel chemical properties on gas turbine combustor operation, emissions
and heat load. As described in previous sections of this report, fuel
physical properties were de-emphasized by achieving highly-atomized, and
hence rapidly-vaporizing, fuel sprays. Test fuels were specified to
present wide ranges of fuel hydrogen, total aromatic and naphthalene
contents. This section of the report presents and discusses the data
acquired from combustion tests with these fuels to determine the chemical
property influences on the burner.

General Combustor Operation and Data Quality

The baseline combustor configuration, which was used in all of the
fuel-effects tests, operated in a consistent manner. The combustion effi-
ciency (determined from exhaust gas analyses) was always 99.9 pct or
greater. Often the unburned hydrocarbons and carbon monoxide were below
the threshold detection level of the analyzers. The NOx emissions were
relatively constant at a level EINOX = 12 to 14. The combustor exit
temperature pattern factor was typically 0.12 $\pm$ 0.01 at Test Condition 1,
increasing slightly to 0.14 $\pm$ 0.02 at Test Condition 3. On the last test
day, the indicated pattern factor for conditions 2 and 3 rose to 0.18 $\pm$
0.02. One fuel tested this day was Jet A which had been tested several
other days as the startup fuel, Jet A-U. All other Jet A data (radiation
load, emissions, liner temperatures) were in agreement with values
previously obtained with Jet A-U. Hence, it was concluded that these
higher pattern factors were anomalous; inspection of the exit thermocouple
rakes indicated that, because of coolant leaks, some temperature
measurements were affected. Since the Jet A-U radiation load, liner tem-
perature and emission data were similar to the levels obtained in previous
tests, the associated test fuel data were considered valid and included in
the analyses. These constant and relatively low levels of pattern factor
indicated that all fuels were injected and distributed similarly. While
gross mixing patterns in the combustor would tend to smooth variations in
fuel concentration, experiences with other burners would indicate that the
low pattern factor values would not be achieved if significant maldistribu-
tions were present.

The combustion test data were acquired from a repetitive test cycle as
described in Section VI. Each test condition was established three times,
with three data points obtained for each setup to develop a set of nine
data points available for statistical analysis. A high degree of test con-
dition repeatability was achieved That is, the standard error for the
nine data point set was typically less than 0.8 pct of the mean value of
inlet air pressure and temperature, air flow and fuel flow. Furthermore,
the conditions achieved very nearly matched the desired conditions,
assuring that the data normalization process would impose small changes to
the measured data. Typically, the actual conditions deviated from the
target values by less than 0.9 pct. As a result of the care exercised in

33

repeating test conditions, the combustor performance parameters were also very consistent, with the following typical values of data set standard error: radiation heat transfer, 2 pct; liner temperature, 0.3 pct; smoke number, 1.5 units; exhaust particle size, 5 pct; and particle number density, 25 pct.

The fuel effects data were acquired from tests performed on several test days with multiple fuels evaluated each day. The day-to-day variation and the variation during a test day of the combustor operation were small. Figure 22 presents the dome radiation data acquired from combusting Jet A-U fuel each test day prior to each test fuel. The abscissa has been scaled to reflect the relative atomization of the fuel according to the SMD $\sim NN^b$ (b = 4.0) relationship developed in Section IV. During each test day (each day is represented by a different symbol), the variation in the data was within 2 pct of the mean value. In general a day-to-day comparison cannot be made since differing levels of atomization would be expected; as indicated on the figure, over the range of nozzles used, more than a three-fold increase in the SMD for Jet A-U was predicted. Since an SMD = 60 μm was measured for the fuel flowrate associated with Test Condition 1 and NN = 35 (Table 9), the SMD predicted for NN = 40 was 100 μm. This droplet size was substantially larger than the calculated critical diameter required to avoid fuel physical property influences. The rather slight change in radiation level suggests that such large changes in SMD did not occur. This could be true if airflow-induced secondary atomization processes existed which resulted in high levels of atomization always being achieved. Data were acquired for operation with the same nozzle (NN = 32) on three test days. The daily mean values were within 5 pct of the mean for all data with this nozzle.

Three case-mounted, narrow-angle radiometers were used to sense changes in the axial distribution of the combusting gas radiation. One device was aligned with a large combustion air hole in each of louvers 1, 2, and 3 (hence referred to as a liner radiation measurements). It is important to note that these devices did not measure the total radiation to the liner at the measurement point. The narrow view-angle (33.4 deg included effective angle) limited the accepted radiation to only 2.2 pct of the potential hemispherical solid angle source. Hence, assuming that the radiative heat transfer was uniform over this view angle, the liner radiation data were expressed as a liner radiance (radiation flux density per solid angle, kW/m^2/sr). Figure 23 presents data typically obtained for all test fuels. As indicated, the radiance increased in switching from Jet A-U to ERBS and the radiance distribution shifted with changes in test condition. The former behavior was expected because of the generally poorer fuel chemical properties of ERBS--lower hydrogen, higher total aromatics and naphthalene contents. The shift in radiance distribution resulted from changing local fuel-air ratios as fuel flow was increased. Table 18 presents a calculated equivalence ratio in the vicinity of each of the first three louvers. These values are based upon the airflow distribution determined from the combustor calibration activity assuming that the stoichiometry is established by airflow from the upstream louver; the air entering a combustion air hole was assumed to deflect downstream and thus not dilute the mixture at that port. For Condition 1, the

stoichiometry in the vicinity of louvers 2 and 3 was very fuel-lean providing a rather non-luminous flow, while at louver 1 the equivalence ratio was transitioning from the fuel-rich primary to a fuel-lean condition. Hence, high radiance levels would be expected at louver 1 with low levels for louvers 2 and 3. For Conditions 2 and 3, the extent of the fuel-rich region and its average equivalence ratio grew; an increase in the quantity of soot produced in the primary zone would be expected. The high radiance levels measured at in louvers 2 and 3 indicate the presence of carbon in these regions despite a local flow characterized by overall fuel-lean stoichiometries. Apparently the higher levels of soot produced in the richer primary zones persisted further in these regions before being completely oxidized.

The liner radiance levels obtained for all test fuels are compared in Figs. 24 and 25 for Test Conditions 1 and 3, respectively. The second ordinate represents the equivalent, uniform full-hemispherical, radiation flux required to produce the associated liner radiance. These values are not the true liner radiation load since significant spatial variation of the radiation source would be expected. Clear trends in the radiance levels are evident. Importantly, these data confirm that the combusting flow structure was not significantly altered by any of the test fuels. That is, for Condition 1 (Fig. 24) the radiance in louver 1 was always greater than in louvers 2 and 3. Furthermore, the variation imposed by changing chemical properties was small compared to the difference between louver 1 and louvers 2 and 3. Similar distinctive trends were evident for Test Condition 3 (Fig. 25). Such trends could not be easily identified for Test Condition 2 since the radiance levels were nearly constant (as indicated in Fig. 23). However, it was plausible to conclude that since the flow structures were not significantly affected by fuel properties for Conditions 1 and 3 they also would not be affected for Test Condition 2. This independence also affirmed that for each condition, every fuel was similarly atomized and distributed within the burner.

Chemical Property Influences

The influences of fuel chemical properties on the combustor behavior were reflected by the dome radiation, liner temperature rise, exhaust smoke number, and particle size and number density data. All of these data indicated that the principle result of variation of the chemical properties was to alter the quantity of soot formed in the front end of the combustor. That is, fuels with a high indicated propensity to soot (i.e., lower smoke point) produced high radiation heat loads and exhaust soot concentrations, with correspondingly high levels of liner temperature rise and smoke number, respectively. Data analysis indicated that the chemical property influences on each of these operational parameters were similar. Further, the influences determined at one test condition were similar to those determined at the other two conditions. Therefore the following detailed discussions of data will focus on one parameter, dome radiation, as documented at Test Condition 2; the general results for all three parameters at all conditions are presented in a summary at the end of this section.

35

Soot Formation in Combustors

Soot formation processes have been studied by many researchers; several, comprehensive reviews of these efforts exist in the literature (e.g., Refs. 31-33). All of these affirm that the detailed chemistry of soot formation is not fully established. The general trends of sooting propensity were established nearly three decades ago. For premixed flames the increasing tendency to soot is (Ref. 34):

acetylenes < olefins < paraffins < benzenes < naphthalenes

while for diffusion flames the trend is (Ref. 35):

paraffins < olefins < acetylenes < benzenes < naphthalenes

It has been argued (Ref. 36) that these sequences do not reflect the true influences of hydrocarbon structure alone, but rather are dictated by a temperature-sensitive controlling mechanism. That is, the soot produced by a flame is a result of two competing mechanisms--formation of soot precursors during fuel pyrolysis and oxidation of the precursors in the flame. For premixed flames, both mechanisms exist, with the oxidation mechanism increasing more rapidly than the formation mechanism as the temperature increases. Hence soot production decreases with increasing temperature. The order of increasing sooting tendency indicated above for premixed systems corresponds to decreasing flame temperature, or equivalently, decreasing oxidation. In contrast, for diffusion flames, soot is formed in the fuel-rich regions where the oxidation mechanism does not exist. Increasing temperatures enhance the pyrolysis rates and result in higher soot levels. The above sequence for diffusion flames follows a higher flame temperature--higher sooting tendency trend. While this separation of controlling mechanisms may be correct (and hence the true influence of hydrocarbon structure not represented by the above sequences), for systems in which flame temperature is not controlled, the sooting tendency of these hydrocarbon groups would correspond to the above trends.

Detailed studies of soot formation indicate that for the many types of hydrocarbon molecules contained in avaition fuels, two principle soot formation mechanisms are active [Fig. 26 (Ref. 37)]. For aliphatic hydrocarbons (i.e., paraffins, olefins, acetylenes) oxidative and thermal pyrolysis of the parent molecule leads to acetylenic-type compounds. It has been suggested (Ref. 36) that these species undergo radical reactions to form conjugated structures, stabilized by chemical resonance, which can survive the high temperature regions of a flame. Such precursors subsequently proceed through nucleation and growth stages leading to soot particles. For aromatic hydrocarbons, fragmentations can occur at high temperatures (above 1600-1800K) leading to precursor formation and reaction as above. At lower temperatures, parent aromatic molecules can be pyrolyzed to radicals which undergo condensation reactions. The resulting polynuclear, cyclic structures would be favorable nucleation sites, with subsequent growth to soot particles. Multi-ring aromatic molecules could also follow these paths, either fragmenting to provide soot precursors or pyrolyzing to lead to nucleation sites. For multi-ring structures, it

would be expected that the nucleation sites would be larger than those from benzene-type molecules, representing an advanced step in the growth process. In diffusion flames, where the fuel heating rate is slower than the chemical reaction rates, pyrolysis would precede fragmentation and hence the sooting tendency of aromatics would favor the condensation route. This is considered to be the dominant route in the combustion tests performed in this program.

Data Analysis Methodology

The data acquired in this program were analyzed to determine the influence of fuel chemical properties on the combustor, with the resulting trends compared to those indicated by the sooting tendencies and mechanisms presented above. The chemical property influences were discerned from analysis of two sets of data--data from limited tests which provided parametric variations in fuel properties, and data from all tests to include the widest range of chemical properties.

Tests were performed with fuels offering parametric variation of chemical properties in an attempt to isolate the influence of hydrogen, total aromatics and naphthalene content. It is appropriate to recognize which chemical constituents were actually varied as indicated by the details of the fuel analyses (Table 5). The hydrogen content variation, at constant total aromatics and naphthalenes, was principly achieved by substitution of cyclo-paraffinic hydrocarbons for normal-paraffins. The total aromatic content variation, at constant hydrogen and naphthalene content, was achieved by substitution of various paraffinic hydrocarbons for benzene-type molecules. The mix of paraffinic hydrocarbons in the fuel with lower total aromatic content was also shifted toward multi-cycle saturates in an effort to retain a constant hydrogen content. The naphthalene content variation, at constant hydrogen and total aromatics, resulted from exchange of benzene- and naphthalene-type molecules.

The data acquired from tests with all fuels were analyzed to discern chemical property dependence of the combustor parameters for the wide ranges of chemical properties offered by the twenty-five fuels. Multi-variable regression analyses were performed. The limits of this approach were recognized. That is, in performing regression analyses, one attempts to determine the best functional relationship between the dependent variables (combustor performance parameters such as dome radiation, smoke number, etc.) and the independent variables (fuel properties such as hydrogen content, smoke point, etc.). Often several relationships are formulated and evaluated. Unfortunately, since regression analyses do not derive from first-principle considerations, no general guide is available for their formulation, and poor representations of the data can result solely from assuming improper functions. The quality of the data representation by a function was evaluated by using the square of the correlation coefficient, R^2. This term indicates the fraction of the total variation in the data that is represented by the function; $R^2 = 1$ would denote a relation which perfectly tracks the observed data. The functional expressions developed during this effort were good-to-excellent representations of the data with $R^2 > 0.7$ always

37

achieved and values greater than 0.9 often encountered. Hence, reasonable functional forms were evaluated, especially for cases which achieved $R^2 >$ 0.9. Furthermore, because of these R^2 values and the large number of test fuels, the correlation coefficients were statistically significant, with distinct correlations obtained to a confidence level exceeding 0.99. The fuel property regression equation was limited to include exponential functions of fuel properties such as:

$$\text{combustor parameter} \sim H^{C1} A^{C2} N^{C3}$$

where: H, A, N represented the percent hydrogen, total aromatics and naphthalene contents, respectively, and C1, C2, C3 were constants optimized during the regression process. Several fuels had total aromatic or naphthalene contents near or equal to zero. The above exponential form could not be used in regression analyses for fuels with zero concentration and, for fuels with low concentrations, was susceptible to large error because of the uncertainties in the property analyses. For such instances, the fuel property was expressed as the difference from total concentration (e.g., 100-N). Among the several fuel property functions evaluated were:

(1) H^{C1}

(2) SP^{C2}

(3) $H^{C1} A^{C2} (100-N)^{C3}$

with H, A, N as above, and SP denoting fuel smoke point. These forms were evaluated in an attempt to both globally represent the combustor parameter response to chemical property variations and to discern particular fuel property influences.

Detailed Analysis of Dome Radiation Data

The radiation on the dome of the combustor was determined by use of two transpiration radiometers. These devices (described in Section V) were mounted to place their sensing element flush with the combustor liner and hence received the total (i.e., full hemispherical) radiation to that location of the dome. One of these two radiometers performed consistently throughout the test effort, providing repeatable values for tests with Jet A-U fuel and duplicating the initial calibration. The data acquired with this device (referred to as QDOME1 in Table 14, the Appendix Data Tables, and Comprehensive Data Report) were used to determine the fuel chemical property influences on radiation. The second radiometer was not consistent, with values either higher or lower than QDOME1 obtained; the calibration was not repeatable. Hence these data were not analyzed.

The variations of dome radiation for the several test fuels are represented in Figs. 27 to 29 which display the data in terms of fuel hydrogen, total aromatics or naphthalene content, respectively. Clear and expected trends are observable in each figure, with increased radiation levels obtained with lower chemical quality fuel. Used in this manner, each of these properties is treated as a global indicator of the fuel

38

property influence. That is, the depicted hydrogen content dependence (Fig. 27) also reflects variations in both total aromatics and naphthalenes; it does not represent the influence of hydrogen content alone. Similarly the total aromatics and naphthalene representations include the influence of all other chemical property variations. As noted earlier, aromatic hydrocarbons (benzenes and naphthalenes) display a high propensity to soot. Hence it would be expected that increasing concentrations of these species would promote greater soot concentrations, raising the emissivity of (and consequently radiative heat transfer from) the combusting medium. The range of the hydrogen content variation principally resulted from the range of the of benzene and naphthalene content variations. Since these hydrocarbons have relatively low hydrogen content, increasing concentrations of them reduced the fuel hydrogen content; hence increased aromatics increased the radiation heat load while reducing the reduced hydrogen. Of these three, the hydrogen content representation correlated the data better than either total aromatics or naphthalene content. Significant scatter is observed in Fig. 28 indicating that total aromatic content does not properly represent the chemical property influences. Naphthalene content correlated the data well except for two, low naphthalene fuels--tetralin and xylene tower bottoms (XTB). Tetralin is a double-ring molecule produced by saturating one ring of naphthalene. A principle pyrolysis product of tetralin is naphthalene (Ref. 38) and therefore in the diffusive burning environment of the combustor, tetralin likely behaves as a high naphthalene content fuel. Indeed, the radiation level measured for tetralin was slightly greater than obtained for BLS, a fuel with a naphthalene content of 30 pct. The XTB fuel consisted of 100 pct benzene-type hydrocarbons. High sooting rates would be expected, and based on acquired data, were achieved. Hence naphthalene content alone could not be expected to fully correlate all data.

It is noted, however, that the chemical properties of tetralin and XTB were exceptional. Both were from the specialty products class of fuels, with each composed entirely of a single hydrocarbon-type molecule. Further, each of these hydrocarbons had a high propensity for sooting. Twenty-one test fuels had compositions which included mixtures of single ring and multi-ring aromatics (two other specialty product fuels were purely paraffinic, decalin and UTRC1) which spanned the ranges: total aromatics, 2.5 to 76 (vol) pct and naphthalenes, 0 to 29.7 (vol) pct. Data from tests with these fuels dominate the trends depicted in Figs. 27 to 29. It is apparent that for these 21 fuels the naphthalene content was a stronger influence on the radiative heat load (and hence on the soot formation) than the total aromatic (or by difference, the single-ring aromatic) content of the fuel. Furthermore, the dominance of naphthalene content was established despite its content being a minor portion of the total aromatics. Again, radiation levels for ERBLS3 with 30-pct naphthalene content (76-pct total aromatics) were comparable to a 100 pct single-ring aromatic fuel (XTB).

As stated above, considering all fuels tested, hydrogen content was a better global indicator of the chemical property influence than total aromatics or naphthalene content alone. Figure 30 depicts the variation in dome radiation with an acknowledged global fuel specification parameter,

39

smoke point. The data were well correlated by this parameter. In fact, regression analyses indicated that smoke point correlated the data better than hydrogen content:

$$\text{radiation} \sim H^{-1.65}, \quad R^2 = 0.87$$
$$\text{radiation} \sim SP^{-0.6}, \quad R^2 = 0.93$$

The latter regression is depicted in Fig. 31.

As discussed by others (e.g., Ref. 39) the smoke point is a good indicator of the sooting tendency of a fuel. Hence the quality of the data fit is consistent with the premise of changing chemical properties principally affecting soot formation.

The influence of specific chemical properties was pursued by examining the results of the parametric variation tests and of further regression analyses of all data. Results from the parametric variation tests are presented in Fig. 32 (which is an enlarged section of Fig. 27). Mean values of the nine-point data set are depicted with brackets indicating the extent of the data set standard error. The values in parentheses are the hydrogen, total aromatics and naphthalene contents, respectively. The following fuel combinations comprised the property variations: hydrogen--ERBS and 7A; total aromatics--ERBS and 8A; napthalene--ERBS, 9A and 9B.

A relatively minor change in dome radiation was attained for the hydrogen content variation. The mean value did increase with reduced hydrogen content, but the overlapping limits of standard error prohibit precise definition of the influence. Indeed, the error limits allow the possibility of no influence of hydrogen content on radiation. While the variation of hydrogen content might appear to be small (0.75 pct point), it does represent 70 pct of the difference in hydrogen contents of Jet A and ERBS. Hence these results indicate that despite a significant variation of hydogen content (at constant single- and multi-ring aromatic content), no statistically significant change in radiation would be expected. This result is consistent with the actual fuel composition variation achieved in these tests. As indicated above, the hydrogen variation arose from exchange of normal- and cyclo-paraffins. Both of these saturates have low sooting tendencies and hence no significant combustor influence would be expected. This observed independence of radiation on purely hydrogen content emphasizes the global character of representations like that depicted in Fig. 27. Used in this manner, hydrogen content variation represents a variation of species more fundamental to the sooting process.

The dome radiation level also did not significantly vary for tests performed with fuels offering a parametric variation of total aromatic hydrocarbons. That is, despite a substantial reduction in this property, the mean value of radiation reduced only slightly, with the limits of standard error overlapping. The total aromatic variation was achieved by exchanging saturated hydrocarbons for single-ring aromatics. Hence the data indicate that benzene-like structures did not strongly contribute to the radiation load. This result is in contrast to the high radiation levels indicated earlier (Fig. 29) for XTB, and the well established

sooting propensity of benzene-type molecules. The difference in these results may be due to the naphthalene content in the fuels. That is, the variation in total aromatics was achieved at a constant naphthalene content of 13.5 pct. As discussed previously it appears that naphthalenic hydrocarbons present a dominant influence on the sooting process. At the 13.5 pct level, these structures may have overridden the single-ring variation. Another total aromatic parametric variation was achieved in tests performed with fuels ERBLS1 and UTRC3B, both of which possessed a naphthalene content of approximately 15 pct. Again, no significant influence of total aromatics was observed. Further definition of the influence of these hydrocarbons was sought via regression analyses of data acquired for all fuels; these results are discussed below.

Substantial increases in the dome radiation were observed for parametric increases in the fuel naphthalene content over a range comparable to the difference in this property for Jet A and ERBS. Since total aromatic content was held constant, reductions of naphthalene content resulted from substitution of single-ring aromatics for double-ring naphthalenes. Thus, the lowest naphthalene content fuel, UTRC 9A, had the highest concentration of benzenes in this fuel sequence, while ERBS had the highest naphathelenes and lowest benzenes. The radiation level followed the naphthalene trend, and hence decreased for increasing single-ring aromatics. This behavior again demonstrated the importance of naphthalene content, reaffirming them to be more influential than the benzenes. These data also indicate that the naphthalene influence was non-linear. That is, most of the total increase in radiation occurred for the first half of the total naphthalene content change. Therefore slight increases in a low naphthalene content fuel could result in disproportionate increases in sooting tendency, and consequently in the radiation load.

Regression analyses were performed to discern specific chemical property influences. Generally, data from tests with all fuels were used to cover the wides range of fuel property variation. Results from analyses using a three property parameter [i.e., $H^{C1} A^{C2} (100-N)^{C3}$] indicated that total aromatic content was not a significant correlating term; the data were tracked equally well with or without its inclusion. The following two-property parameter, which embodied both hydrogen and naphthalene content was the best representation of the data (See also Fig. 33):

$$\text{radiation} \sim H^{-1.2}(100-N)^{-0.4}, \quad R^2 = 0.93$$

Four important features of this correlation were noted. First, both fuel property terms contribute significantly to the predicted change of radiation. For example, for the property changes associated with Jet A and ERBS fuels, half of the predicted radiation increase is attributed to the hydrogen content decrease and half to naphthalene content increase. Second, this correlation does not fully prescribe the influence of specific chemical properties. As previously discussed, the change in hydrogen content is a global indication of a more fundamental hydrocarbon-type change. Its presence in this correltion compensates for many unknown chemical features such as the apparent interactive influence of benzenes and naphthalenes. The regression analyses did, however, discern the

41

important influence of naphthalenic hydrocarbons. Third, the quality of this correlation was equal to that for a smoke point correlation, both of which were superior to a solely hydrogen content correlation. Hence, while naphthalenes are recognized as an important chemical property class, smoke point--an existing fuel specification parameter--appears to properly prescribe the influence of fuel chemical properties. Fourth, none of the correlations was a perfect fit to the data. Hence, for any two fuels the three functional relationships--hydrogen, smoke point, hydrogen and naphthalene--may overpredict, underpredict or perfectly-predict the changes evidenced by data. For example, the parametric property variation test results indicated that naphthalene content variation was principly responsible for the difference in radiation for Jet A and ERBS. None of these three correlations reflects such a strong influence and hence all underpredict the change in radiation. A user of regression analysis results ought to recognize the implicit assumption that the trends established by a large data set (e.g., twenty-five fuels) are more reliable than trends indicated by a subset (e.g., two fuels) of the data. For a perfect correlation ($R^2 = 1$), this issue is academic; for non-perfect (i.e., realistic correlations) this issue magnifies as the departure from $R^2 = 1$ grows.

As asserted above, the chemical property influence on dome radiation was similar to the influence discerned for exhaust soot. It was concluded that the unifying influence on both was the level of soot produced in the dome region of the combustor--increased soot producing higher emissivities and hence greater radiation heat loads, and increased soot providing a higher source concentration prior to its oxidation down to combustor exhaust levels. In general, radiation heat transfer depends on both the medium emissivity and its temperature. Since the calculated combustion temperature of a fuel depends on its composition, with generally increasing levels obtained for decreasing hydrogen content, a significant variation in radiation might be expected only because of a temperature variation. However in the test combustor, continuous radiation from soot particles represented a major portion of the total radiative load and the temperature of these particles may not be equal to the combusted gas temperture. That is, the combustion of these particles will be controlled by diffusion of oxygen to the surface, with the particle temperatures dominated by stoichiometric carbon oxidation, modulated by the concentration of oxidizer in and radiation exchange with the neighboring media. Temperature measurements in the primary zone of another model combustor (Ref. 40) using the Kurlbaum technique indicated only a very small temperature change of the radiating source despite significant changes in fuel chemical composition. Further, the temperature levels measured were essentially independent of the combustor fuel-air ratio. These observations support the concept of soot forming in a diffusion flame zone, and hence always in near-stoichiometric fuel-air mixtures, and that the particles radiate at temperature levels associated with soot oxidation. If it is assumed in the present program that the radiation source temperature also did not vary with fuel composition or overall fuel-air ratio, then the observed changes in radiation level must be attributed to changes in emissivity, and hence from changes in chemical property induced soot production. This situation is consistent with the observed similarity of chemical property dependences

42

for the dome radiation and exhaust soot data. The emissivity levels can be determined only if a temperature of the soot particles is assumed. The measurements of Ref. 40, adjusted to the combustor inlet air temperature of the current effort, indicate this temperature to be 2250K. Using this value, and a Stefan- Boltzmann relationship, the black body radiation level would be 1450 kW/m^2 and the emissivity for any measured radiation level:

$$emissivity = dome\ radiation/1450$$

The data acquired spanned the general range of 300 to 700 kW/m^2 indicating a corresponding emissivity range of 0.2 to 0.5.

Summary of Chemical Property Influence

Liner Temperature Rise and Smoke Number

Influences of fuel chemical properties were also evident in the liner temperature rise and exhaust smoke number data.

The liner temperature rise parameter analyzed was the difference between the combustor inlet air temperature and an average of ten liner thermocouples. The data obtained from the case-mounted radiometers indicated that the chemical property effects were concentrated in the dome and first three louver regions of the burner. During the test program, several of the original 39 liner thermocouples failed because of thermal or mechanical stress. Therefore, the ten measurements used in the analyses were confined to the dome and first three louver regions, and used thermocouples which existed for all tests. Eight of these were located either on the dome or at the first axial position (slightly downstream from the louver lip) on louvers 1, 2, or 3. The metal temperatures for these eight locations would be influenced more by changes in the radiation heat transfer than by changes in convective heat transfer. Hence the temperature rise parameter used reflected changes in the radiation heat load.

The smoke number data were obtained from three, ganged, smoke probes at the combustor exist. Data acquired for any fuel indicated that the oxidation mechanisms within the secondary zone of the combustor dominated the soot production mechanisms in the dome. As shown for ERBS fuel in Fig. 34, as the combustor exit temperature increased (because of increased overall fuel-air ratio) the smoke level decreased, despite an increasingly fuel-rich primary zone. As observed for the radiation data, there was not a significant influence of fuel nozzle size (for the range of nozzle numbers used in this program) as smoke numbers for Jet A-U fuel were similar for all injectors, except for smoke numbers acquired on a second test day using a NN=32 nozzle. That is, data were acquired with this nozzle on two test days. On one day the Jet A-U smoke numbers were consistent with values obtained on other test days (with other nozzles) while values acquired on the other test day were lower. This difference was believed to result from a bias on samples acquired the second test day. Since other combustor parameters were similar for both days, it appears

43

that the bias was associated with the sampling process. The smoke numbers acquired for the six fuels on the second day were adjusted by use of data acquired for Jet A-U. In particular, the test fuel smoke numbers were scaled in proportion to the ratio of the Jet A-U data acquired the second test day to the Jet A-U data normally acquired.

The influence of chemical properties on the liner temperature rise and exhaust smoke number were similar to those observed for the dome radiation. (Figures A-1 to A-8 in the Appendix present the variation of these parameters for Test Condition 2.) The variations of each were globally represented by the fuel smoke point which was again found to be a better correlating parameter than fuel hydrogen content alone. Plots of the combustion parameters indicated that total aromatic content did not properly represent the chemical property influence while naphthalene content was an important influence. As discussed for the dome radiation, the liner temperature rise and smoke number data for tetralin and xylene tower bottoms were not correlated by fuel naphthalene content. Results from tests with fuels offering parametric variations of chemical properties indicated that changes in either hydrogen and total aromatic contents did not significantly affect either the liner temperature rise or smoke number. The former result reflected the pure influence of hydrogen content, and not an apparent influence because of changes in sooting hydrocarbon structures. The insensitivity of the combustor parameters to total aromatic content is believed to be associatd with the level of naph-thalenes present in the fuels, as discussed in the presentation of the dome radiation data. Regression analyses of data from all fuels again indicated that total aromatic content was not a sta.istically-significant term in the correlation parameters investigated. The best correlating parameters embodied two fuel properties, hydrogen content and naphthalene content, and hence were improved global representations. This feature is depicted in Fig. 35 which displays the excellent correlation between liner temperature rise and the two property parameter. That the best correlation parameter included fuel naphthalene content re-affirmed the importance of this property.

Table 19 presents results from regression analyses of the dome radiation, liner temperature rise and smoke number data for all three test conditions. These results were obtained from regressions performed in the logarithm plane [i.e., log (dome radiation)] and hence differ slightly from results presented previously which were optimized in the real plane. For each variable, each regression parameter tracked the data similarly for all three test conditions; only a small variation in the exponents (C1, C2) and quality (R^2) was observed. The similarity of the chemical property influence on the radiation, liner temperature rise and smoke number data discussed above were also reflected in these regression analyses by the exponent quotient, C1/C2. The small variation indicated that hydrogen and naphthalene contents had the same relative influence on these three combustor parameters.

Particulate Size and Number Density

A characteristic size and number density of the soot exiting the

44

burner on its centerline were determined from light scattering measurements. Data typically obtained for these measurements are depicted in Figs. 36 and 37. As indicated, the particle size was invariant to operating condition, with an 0.22 $\pm$ 0.02 μm particle size being indicated. Indeed, the particle size determined for tests with any fuel, at any condition, was within these limits. This interesting result was not dictated by the measurement technique as its sizing sensitivity has been demonstrated in a laboratory set up over a particle size range of 0.09 to 0.50 μm. As used, the measurement technique identified a single particle size assumed to be representative of a size distribution. However, light scattering signals are greatest for large particles, implying that the characteristic size is biased toward the larger particles of the distribution. Hence, the data indicate that a significant quantity of 0.22 μm particles existed for all fuels, for all conditions. The sizing sensitivity of the scattering arrangement used would not be strongly responsive to variations of the smaller particle sizes. Characteristic sizes similar to those observed in this program have been determined using optical techniques for a variety of other burners ranging from a ramjet-type dump combustor (Ref. 41) to a laboratory mono-disperse spray flame (Ref. 42). In those instances (as well as in the present study) the particles were far removed from the soot generation region and therefore, as discussed in Ref. 42, likely were mature agglomerates of large numbers (600-3000) of primary soot spheroids. The constancy of the particle size indiated that it results from fundamental soot growth mechanisms in times short compared to those offered by a wide variety of burners with little (if any) regard for fuel-type.

The soot particle number density decreased witn increasing combustor exit temperature, again indicating a vigorous oxidation mechanism in the burner secondary zone. As observed for smoke number, the number density responded to the fuel chemical properties, increasing for fuels with greater propensity to soot (i.e., decreased smoke point). The constancy of particulate size implied that a relation existed between soot number density and smoke number. Regression analyses for these data, for all fuels at all test conditions, resulted in the correlation depicted in Fig. 38:

$$\log_{10} N = 4.9 \ SN^{0.082} \ , \ R^2 = 0.83$$

where N = Number density and SN = Smoke Number

While the quality of the correlation is only fair, the standard error of the number density data indicated that further improvement was not warranted. While a clear trend is indicated for the smoke number range evaluated, it ought to be recognized that the trend must change for very high smoke numbers. That is, by definition, the maximum smoke number is 100. Therefore, in the coordinates of Fig. 38, the number density must approach this limit with a vertical asymptotic character.

Soot was clearly being oxidized within the burner. Direct observations within the burner using a fiber optic probe [activity conducted under a NASA contract immediately subsequent to the experiments

45

of this program (Ref. 43)] documented that the highly luminous, strongly
radiating media in the dome became transparent by the burner exit. The
axial distribution of radiation (Fig. 23) also documented this feature.
Soot formation and growth were limited to regions near the dome as farther
downstream the global equivalence ratio rapidly became fuel-lean. The
particle size and number density trends would indicate that the initial
soot number density was responsive to the fuel sooting tendency, with
decreasing concentrations along the burner because of oxidation. Data do
not exist to determine how the particle size varied. It would be expected
that small particles would be rapidly oxidized in accordance with the
"d-squared" law, with larger particle sizes reducing more slowly.
Combined, these processes could result in significant reduction in soot
while retaining sufficient numbers of larger particles to be interpreted as
a nearly constant particle size. Additional investigations are required to
acquire data on changing soot physical properties within a practical
combustor.

A limited number of combustion tests were performed in an attempt to
determine changes in fuel chemical property influences because of changes
in the combustor airflow distribution. Two combustor configurations were
evaluated, one providing a reduced primary zone airflow and another
providing a greater airflow than the baseline burner used for the
fuel-effects tests. These two burners are described in Section III. At
the same overall fuel-air ratio, these combustors provided a leaner or
richer primary zone equivalence ratio (ϕ_p), respectively, than the
baseline because of the altered airflow distribution. Tests were performed
at the three conditions defined in Table 16, resulting in the ϕ_p variation
indicated in Table 8. Note that the adjectives "lean" and "rich" are used
in a relative sense. The primary zone was fuel-rich for all tests. Data
were acquired in tests with three fuels (in addition to Jet A-U): ERBS,
ERBLS2 and xylene tower bottoms (XTB). Because of the relatively few
variations (two configurations, four fuels) regression analyses were not
performed. Instead, general data trends were sought which permitted
interpretation of the configuration influences.

General Combustor Operation and Airflow Interaction

Both combustor configurations performed consistently, attaining a 99.9
percent combustion efficiency for all tests. Data acquired with Jet A-U
prior to combusting each test fuel were repeatable. The combustor exit
temperature pattern factor (PF) was nearly constant for each configuration,
but varied between configurations. For the baseline burner values for Test
Conditions 1, 2, and 3 were nominally 0.12, 0.13 and 0.14, respectively.
For the lean configuration, values higher than the baseline were achieved
(PF = 0.17, 0.19, 0.23) while lower values (PF = 0.09, 0.09 and 0.10) were
observed for the rich configuration. This trend was a result of the
technique used to alter the airflow distribution. The lean configuration
was achieved by opening each of the six combustion air holes in louver 1
while closing the corresponding holes in louver 5. Hole diameter changes
were specified to maintain a constant liner open area, or equivalently,
constant liner pressure loss. Therefore, while additional airflow was
admitted to the primary zone, lesser airflow was available for tertiary
zone injection. Furthermore, the smaller diameter downstream holes reduced
the penetration of this airflow into the core flow. These two effects
reduced the mixing level and resulted in the observed increase in pattern
factor. The opposite trends held for the rich combustor configuration.
Less primary zone airflow provided greater tertiary zone flow, resulting in
greater mixing and reduced pattern factors. This interaction of primary
zone airflow and tertiary zone mixing was unavoidable for the simple
combustor configurations used.

The changing tertiary zone mixing behavior could significantly alter
the chemical property influences discerned in the fuel-effects tests. For
example, Fig. 39 depicts the smoke number data acquired for Test Condition
2 for each configuration. The fuel property variation is represented by
the smoke point. For this condition ϕ_p varied from 1.2 to 1.55. While the
expected trend of decreasing smoke number for lower sooting tendency fuels
(i.e., higher smoke point) is observed, the ϕ_p influence is opposite the

expected trend. That is, richer primary zones did not produce greater exhaust soot. This contradiction is apparently the result of the tertiary zone mixing behavior described above. Data for the highest ϕ_p were acquired from use of the rich burner configuration, the device with the greatest tertiary zone mixing, while data for the lowest ϕ_p were obtained with the lean combustor. The low smoke number values from the rich combustor indicate that the vigorous mixing enhanced soot burnout, a behavior consistent with the strong oxidizing tendency noted in the fuel-effects test phase. In those tests, it was observed that exhaust smoke levels decreased with increasing overall fuel-air ratio despite corresponding increases in the rich primary zone equivalence ratio. In that case, the higher combustor exit temperatures promoted oxidation processes which overcame the enhanced soot production in the primary zone. For these configuration-effects data, the average combustor exit temperature was equal for all three burners. The improved (i.e., lowered) pattern factor indicated that fewer low temperature (and hence weaker oxidizing) regions existed, resulting in greater soot burnout. The opposite trend was true for the lean combustor. Despite primary zone soot production levels lower than expected for the baseline, the lean burner produced equivalent or greater exhaust soot concentrations. The degraded mixing of this device rendered it inefficient at consuming the soot.

These data indicate that the rapid increase in soot emissions from use of poor chemical quality fuel can be offset by enhanced particle burnout. Uniformly high tertiary zone tempertures are optimal. If this condition is achieved, a reduced chemical property influence can be experienced as evidenced by the relatively small smoke number variation over the range of sooting propensities offered by XTB to Jet A.

Configuration Influences in the Primary Zone

The influence of changes in the combustor configuration on the primary zone were represented by the dome radiation data. Two types of influence were investigated: influence of variations of primary zone equivalence ratio (ϕ_p) at a constant test condition, and influences of variations of test condition for constant ϕ_p. Data for the former case were obtained from tests with each configuration operated to provide identical combustor exit temperatures for each fuel (i.e., nearly identical fuel flowrates). In the latter case, data were acquired in tests with the three configurations operating at compensating conditions to achieve a nearly constant ϕ_p. Hence, both the configuration and the test condition varied in this sequence. These two variations can be viewed as variations along a column or along a positively-sloped diagonal, respectively, of the ϕ_p values contained in Table 8.

Data representing the influence of ϕ_p on the dome radiation level for Test Condition 2 are presented in Fig. 40. The open symbols denote the normalized data acquired for the fuel variation represented by smoke point values. Radiation levels for the lean burner were consistently higher than for the baseline, while lower values were obtained for the rich configuration. Identical trends were observed for data obtained at Test Conditions 1 and 3. If all of the radiation heat load was produced by soot formed in the primary zone, the opposite trend could be expected. That is, as discussed previously, the soot appears to radiate at a relatively con-

48

stant temperature because it is oxidized in a diffusion flame structure. Richer ϕ_P could be expected to produce higher soot concentrations, resulting in higher emissivities and heat loads.

The observed trend in dome radiation suggested that a temperature responsive effect was present. In particular, while the soot temperature was insensitive to the equivalence ratio, the gas temperature was not. A UTRC exponential wide-band model was used to calculate the radiation level for the equilibrium gaseous species concentration which would exist for each primary zone equivalence ratio. These gaseous radiation levels were used to adjust the data to the values shown as solid symbols in Fig. 40, which represent the variation of particulate radiation for differing ϕ_P and fuel properties. The expected radiation increase for increased fuel sooting tendency is apparent. Of more interest, however, is the indicated insensitivity of this radiation to equivalence ratio. This feature is attributed to the constancy of the fuel distribution resulting from use of the same fuel flowrate (for any fuel) with each configuration. The primary airflow was varied for each configuration to produce the ϕ_P change. However the swirler surrounding the injector was not altered and the liner pressure loss was held constant by specifying compensating hole diameter changes in louvers 1 and 5. Therefore, the airflow expected to impose the principle influence on the fuel spray was invariant. It appears that while the global equivalence ratio did vary, the fuel pattern (or equivalently the fuel concentration) did not. Hence the diffusion flame structure in the primary zone would remain constant producing similar soot levels for these configurations. Gaseous combustion products apparently did mix with the primary airflow, with greater radiation loads produced in the higher temperature, lean burner ($\phi_P = 1.2$) than for the baseline configuration. Differing levels of dome radiation were observed for equivalence ratio variations in the fuel-effects tests. In those instances, however, the variation was achieved by altering the fuel flowrate. These configuration-effects results indicate that the fuel-effects ϕ_P influence likely resulted from a differing fuel distribution in the primary zone. Unfortunately, data do not exist to specify this alteration. Such a change is a real effect, however, that could be experienced in other burners using pressure-atomizing injectors. Combustors using air-blast nozzles would be expected to show less sensitivity to his phenomenon as the fuel distribution would be dominated by the airflow patterns. It is restated that at any one condition, the combusting zone structure was similar for all fuels. Therefore data acquired at any condition could be consistently compared for fuel-effects or configuration-effects. The alterations imposed by changing fuel flow invalidate similar analyses of data from multiple conditions.

These configuration-effect test results also indicate that the global value, ϕ_P, does not always adequately represent the important features of the primary zone. For the configuration-effect tests, radiation levels decreased with increasing ϕ_P; in the fuel-effects tests, radiation levels increased with increasing ϕ_P. The manner in which the variation was achieved dictated the result. This feature is further illustrated in the data presented in Fig. 41, which depicts the variation in dome radiation for changes in test condition but at an approximately constant primary zone equivalence ratio. Differing levels of radiation were observed, re-affirming that ϕ_P does not fully describe the primary zone behvior. The data were acquired from tests with the three configurations. However, each was operating at a different test condition and, consequently, at a

different fuel flowrate. Fuel distribution differences likely existed, resulting in the observed spread in radiation heatload. Note that the highest radiation levels were consistently achieved for the lean burner which operated at Test Condition 3. The highest dome radiation levels in the fuel-effects tests were also obtained at this condition but with a global value of ϕ_p = 1.7. Indeed, the levels obtained for the ϕ_p = 1.4 tests were higher (as indicated by the comparison on Fig. 41) because of greater gaseous radiation. This influence is identical to that demonstrated in Fig. 40, and indicates that the concentration of any individual fuel is a strong influence in determining the combustor radiative heat load. For each configuration (or equivalently at each condition), the data for all fuels follow nearly identical trends. That is, the fuel chemical property influence for each configuration was similar, the same result observed in the fuel-effects tests.

SECTION IX CONCLUSIONS AND RECOMMENDATIONS

Based upon the data acquired in the combustion test program the following conclusions have been made:

1. The influence of changes in fuel chemical properties on a gas turbine combustor are properly represented by changes in the fuel smoke point, a specification parameter.

2. Fuel naphthalene content is a strong contributor to gas turbine combustor radiative heat load and exhaust soot emissions.

3. The size distribution of the agglomerated soot particles exiting a gas turbine combustor is adequately represented by a characteristic size of 0.2 μm. This size does not depend on fuel chemical properties.

4. The strong oxidizing character of a gas turbine combustor can be used to offset potentially increased soot emissions from use of a lower chemical quality fuel if high mixing rates are achieved in the secondary and tertiary zones.

5. Fuel concentration patterns in a gas turbine combustor primary zone strongly influence the quantity of soot produced, and therefore also the radiative heat load.

6. Fuel oxidiation in the primary zone of a gas turbine combustor is controlled by diffusional processes and is therefore not always well represented by a global equivalence ratio.

It is recommended that investigations be conducted to address the following technology needs as indicated in this program:

1. Development of fundamental mechanisms and models of soot production from aviation-type fuels.

2. Data to document the soot particle size, size distribution and number density within a gas turbine combustor.

3. Data to quantify the contribution of single-ring aromatic structures to fuel chemical property influences on a gas turbine combustor.

4. Data to separately define the fuel chemical and physical property influences on a gas turbine combustor at low-power operation.

5. Data to identify changes in chemical property influences associated with the use of air-blast fuel injectors in gas turbine combustors.

6. Development of models and acquisition of data to determine the atomization and distribution of fuel sprayed into a gas turbine combustor operating at a high-power condition.

REFERENCES

1. Butze, H. F. and R. C. Ehlers: Effect of Fuel Properties on Performance of a Single Aircraft Turbojet Combustor. NASA TM X-71789. October 1975.

2. Blazowski, W. S. and T. A. Jackson: Evaluation of Future Jet Fuel Combustion Characteristics. AFAPL TR-77-93. July 1978.

3. Jackson, T. A. and W. S. Blazowski: Fuel Hydrogen Content as an Indicator of Radiative Heat Transfer in an Aircraft Gas Turbine Combustor. AFAPL TR-79-2014. February 1979.

4. Moses, C. A. and D. W. Naegeli: Fuel Property Effects on Combustor Performance. ASME Paper 79-GT-178. March 1979.

5. Gleason, C. C. et al.: Evaluation of Fuel Character Effects on F101 Engine Combustion System. AFAPL TR 79-2018. June 1979.

6. Szetela, E. J. et al.: Analysis of the Impact of the Use of Broad Specification Fuels on Combustors for Commercial Aircraft Gas Turbine Engines. AIAA Paper 79-1195. June 1979.

7. Naegeli, D. W. and C. A. Moses: Effect of Fuel Molecular Structure on Soot Formation in Gas Turbine Engines. ASME Paper 80-GT-62. March 1980.

8. Gleason, C. C. et al.: Evaluation of Fuel Character Effects on J79 Smokeless Combustor. AFWAL TR 80-2092. November 1980.

9. Vogel, R. E. and D. L. Troth: Fuel Character Effects on the TF41 Engine Combustion System. AIAA Paper 81-1391. July 1981.

10. Naegeli, D. W. et. al.: The Sooting Tendency of Fuels Containing Polycyclic Aromatics in a Research Combustor. AIAA Paper 82-0299. January 1982.

11. Clark, J. A.: Fuel Property Effects on Radiation Intensities in a Gas Turbine Combustor. AIAA Journal, Vol. 20, No. 2, pp. 274-281. February 1982.

12. Longwell, J. P., editor: Jet Aircraft Hydrocarbon Fuels Technology. NASA Conference Publication 2033, June 1978.

13. Russell, P. L.: Fuel Character Effects on USAF Gas Turbine Engine Afterburners. AFWAL TR-82-2114. November 1982.

14. Odgers, J. and C. Carrier: Modeling of Gas Turbine Combustors; Considerations of Efficiency and Stability. ASME Journal of Engineering for Power, Vol. 95, pp. 105-113, April 1973.

15. Mellor, A. M. and R. M. Washam: Characteristic Time Correlations of Pollutant Emission from an Annular Gas Turbine Combustor. AIAA Journal of Energy, Vol. 3, No. 4, pp. 250-253. July 1979.

16. Abromovich, G. N.: The Theory of Turbulent Jets. The MIT Press, Cambridge, MA. pp. 541-544, 1963.

17. Ballal, D. R. and A. H. Lefebvre: Combustion Performance of Gas Turbine Combustors Burning Alternative Fuels. AIAA Journal of Energy, Vol. 3, No. 1, pp. 50-54. January 1979.

18. Cox, E. R.: Pressure Temperature Chart for Hydrocarbon Vapors. Industrial and Engineering Chemistry, Vol. 15, No. 6, pp. 592-593. June 1923.

19. Radcliff, A.: Section D - Fuel Injection. High Speed Aerodynamics and Jet Propulsion, Vol. XI, Design and Performance of Gas Turbine Power Plants. Princeton University Press, Princeton, NJ, 1960.

20. Simmons, H. C.: The Prediction of Sauter Mean Diameter for Gas Turbine Fuel Nozzles of Different Types. ASME Paper 79-WA/GT-5. December 1979.

21. Jasuja, A. K.: Atomization of Crude and Residual Fuel Oils. ASME Journal of Engineering for Power, Vol. 101, pp. 250-258. April 1979.

22. Simmons, H. C. and C. F. Harding: Some Effects of Using Water as a Test Fluid in Fuel Nozzle Spray Analysis. ASME Paper 80-GT-90. March 1980.

23. Dickerson, R. A. and T. A. Coultas: Breakup of Droplets in an Accelerating Gas Flow. AIAA Paper 66-611, June 1976.

24. Moffat, R. A., et al.: Development of a Transpiration Radiometer. ISA Advances in Instrumentation, Vol. 26, Pt. 2, 1971.

25. Van de Hulst, H. C.: Light Scattering by Small Particles. Wiley, New York, NY 1957.

26. Kerker, M.: The Scattering of Light and Other Electromagnetic Radiation. Academic Press, New York, NY. 1969.

27. Diermendjian, D.: Electromagnetic Scattering of Sperical Polydispersions. Elsevier, New York, NY, 1969.

28. Bonczyk, P. A.: Measurement of Particulate Size by In Situ Laser Optical Methods: A Critical Evaluation Applied to Fuel Pyrolyzed Carbon. Combustion and Flame, Vol. 35, pp. 191-206. 1979.

29. Lefebvre, A. and M. V. Herbert: Heat Transfer Processes in Gas Turbine Combustion Chambers. Proc. Institute of Mechanical Engineering, Vol. 174, No. 12, pp. 463-473, 1960.

30. Sarli, V. J. et al.: Effects of Operating Variables on Gaseous Emissions. Air Pollution Control Association Specialty Conference on Air Pollution Measurement Accuracy as it Relates to Regulation Compliance, October 1975.

31. Palmer, H. B. and H. F. Cullis: The Formation of Carbon from Gases. The Chemistry and Physics of Carbon, Vol. 1, Marcal Dekker, NY, 1965.

32. Wagner, H.: Soot Formation in Combustion. Seventeenth Symposium (International) on Combustion. The Combustion Institute, Pittsburgh, 1979.

33. Bittner, J. D. and J. B. Howard: Role of Aromatics in Soot Formation. Alternative Hydrocarbon Fuels. Vol. 62 of Progress in Astronautics and Aeronautics. AIAA, NY, 1978.

34. Street, J. C. and A. Thomas: Carbon Formation in Premixed Flames. Fuel, Vol. 34, 1955.

35. Clark, A. E. et al.: The Tendency to Smoke of Organic Compounds on Burning. Journal of Institute of Petroleum, Vol. 32, 1946.

36. Glassman, I.: Phenomenological Models of Soot Processes in Combustion Systems. AFOSR TR 79-1147, 1979.

37. Graham, S. C. et al.: The Formation and Coagulation of Soot Aerosols Generated by the Pyrolysis of Aromatic Hydrocarbons. Proceedings of the Royal Society, Series A, Vol. 344, pp. 259-285, 1975.

38. Benjamin, B. M. et al.: Pyrolysis of Tetralin. Fuel, Vol. 58, pp. 386-390, May 1979.

39. Glassman, I. and P. Yaccarino: The Temperature Effect of Sooting Diffusion Flames. Eighteenth Symposium (International) on Combustion. The Combustion Institute, Pittsburgh, 1981.

40. Naegli, D. W., et al.: Effect of Flame Temperature and Fuel Composition on Soot Formation in Gas Turbine Engines. Western States Section/The Combustion Institute Fall Meeting, Tempe, AZ, October 1981.

41. Thornberg, D. W. et al.: An Investigation of the Effects of Smoke Suppressant Fuel Additives on Engine and Test Cell Exhaust Gas Opacities. Naval Postgraduate School Report NPS-67-82-004, May 1982.

42. Bonczyk, P. A. and J. J. Sangiovanni: Optical and Probe Measurements of Soot in a Burning Fuel Droplet Stream. UTRC Report UTRC83-25 (submitted to Combustion Science and Technology), June 1983.

43. Morey, W.: Personal Communication.

TABLE 1 - Test Fuels

	Designation	Hydrogen (wt pct)	Total Aromatics (vol pct)	Naphthalenes (vol pct)	Comment
1	UTRC 2A	11.87	34.9	16.0	Parametric for hydrogen
2	ERBLS1	12.35	38.4	16.6	ERBS/BLS = 79/21 (vol)
3	UTRC 7A	12.53	26.2	14.9	Parametric for hydrogen
4	JP7	14.39	2.5	0.0	
5	JP4-Shale	14.39	15.1	0.3	Derived from oil shale
6	JP4	14.57	15.7	0.5	
7	DF2	13.46	22.9	7.9	
8	AFAPL 6	13.41	21.4	6.7	
9	AFAPL 2	13.56	31.0	3.6	
10	UTRC 3B	12.41	24.9	14.5	Parametric for aromatics
11	UTRC 8A	12.84	16.5	13.4	Parametric for aromatics
12	ERBLS2	11.89	47.3	20.5	ERBS/BLS = 60/40 (vol)
13	UTRC 9A	12.89	30.7	1.5	Parametric for naphthalenes
14	UTRC 9B	13.10	30.1	7.3	Parametric for naphthalenes
15	Tetralin	9.14	100.0	1.5	
16	Xylene Tower Bottoms (XTB)	9.64	100.0	0.1	
17	Blending Stock (3LS)	10.36	76.0	29.7	
18	ERBLS3	11.38	59.2	26.5	ERBS/BLS = 41/59 (vol)
19	ERBS	12.94	28.4	13.5	
20	Decalin	13.10	0.2	0.0	
21	JP4-A	14.16	23.1	0.6	Highly aromatic JP4
22	Jet A	13.69	15.9	1.9	
23	JP5	13.88	16.5	2.2	
24	Gulf Mineral Seal Oil (GMSO)	14.14	9.9	1.1	
25	UTRC 1	14.97	0.0	0.0	

TABLE 2 - Candidate Blending Components

Component	Specific Gravity	Hydrogen (wt pct)	Total Aromatics (vol pct)	Naphthalenes (vol pct)
Jet A	0.812	13.69	15.9	1.9
JP7	0.803	14.39	2.5	0.0
No. 2 Fuel Oil	0.851	12.82	31.3	11.2
ERBS	0.842	12.95	28.4	13.5
JP4-A	0.766	14.16	23.1	0.6
BLS	0.896	10.36	73.3	24.6
A400	0.871	8.33	100.0	62.1
Methy-naphthalene	1.109	7.29	100.0	90.0
XTB	0.860	9.64	100.0	0.1
Decalin	0.888	13.10	0.2	0.0

TABLE 3 - Parametric Variations of Chemical Properties

Fuel	Component (vol fraction)	H (wt pct)	Blend Properties Aromatic (vol pct)	Naphthalenes (vol pct)
Hydrogen Variation				
ERBLS1	ERBS (0.79) Blending Stock (0.21)	12.35	38.4	16.6
UTRC 2A	JP7 (0.533) Methyl naphthalenes (0.175) Xylene tower bottoms (0.189) Decalin (0.103)	11.87	34.9	16.0
ERBS	ERBS (1.00)	12.95	28.4	13.5
UTRC 7A	JP7 (0.660) Methyl naphthalenes (0.149) Xylene tower bottoms (0.118) Decalin (0.073)	12.53	26.2	14.9
Total Aromatic Variation				
ERBLS1	As above	12.35	38.4	16.6
UTRC 3B	Jet A (0.60) No. 2 (0.10) Methyl naphthalenes (0.15) Decalin (0.15)	12.41	24.9	14.5
ERBS	ERBS (1.00)	12.95	28.4	13.
UTRC 8A	JP7 (0.75) Methyl naphthalenes (0.15) Decalin (0.10)	12.64	16.5	13.4
Naphthalene Variation				
ERBS	ERBS (1.00)	12.95	28.4	13.5
UTRC 9A	Jet A (0.50) JP7 (0.20) Xylene tower bottoms (0.20) Decalin (0.10)	12.89	30.7	1.5
UTRC 9B	Jet A (0.40) No. 2 (0.45) ERBS (0.10) Xylene tower bottoms (0.05)	13.10	30.1	7.3

TABLE 4 - Fuel Analysis Methods

Property	Method
Hydrogen (wt pct)	ASTM D 3178
Flash point, tag closed (K)	D 56 Note 1
Distillation (vol pct at T (K))	D 86
Freeze point (K)	D 2386
Smoke point (mm)	D 1322
Specific gravity (@ 289K)	D 1298
Viscoisty @ 293K (cst)	D 445
Viscosity @ 253K (cst)	D 445
Reid vapor pressure	D 323 Note 1
Net heat of combustion (MJ/kg)	D 240
Mercaptan sulfur (wt pct)	D 3227
Total sulfur (wt pct)	D 2622
Nitrogen (wt pct)	Antek Chemiluminescence
Saturates (vol pct)	D 1319
Olefins (vol pct)	D 1319
Aromatic (vol pct)	D 1319
Naphthalenes (vol pct)	D 1840
Mass spectrometry for hydrocarbon types (wt pct)	D 2425 Note 2
Surface tension (dyne/cm)	Tensiometer

NOTES:

[1] Flash point determined only for fuels with initial boiling point (IBP) greater than 373K. Reid vapor pressure determined only for fuels with IBP less than 373K

[2] Mass spectrometric analysis by ASTM D2425 performed only for fuels with iBP greater than 373K. For fuels with IBP less than 373K, a modified ASTM D-2789 mass spectrometric analysis was performed on a de-pentanized smaple.

TABLE 5 - Fuel Analyses

Fuel	Specific Gravity	Flash Pt (K)	Reid VP	Freeze Pt (K)	Smoke Pt (mm)	Net Ht of Combustion (MJ/kg)	Viscosity (cst)			Surf. Tension (dyne/cm)	
							253K	293K	313K	297K	313K
1. UTRC 2A	0.8618	323	-	233	11.3	42.32	4.46	1.76	-	27.54	-
2. ERBLS 1	0.8524	327	-	252	10.8	42.82	6.67	2.35	-	27.46	-
3. UTRC 7A	0.8478	329	-	234	15.9	42.63	4.99	1.91	-	27.84	-
4. JP7	0.8026	337	-	227	32.3	43.21	5.80	2.21	1.59	25.90	24.50
5. JP4-S	0.7649	-	0.5	216	28.9	43.88	2.17	1.06	-	22.96	-
6. JP4	0.7620	-	2.1	217	28.7	43.24	1.85	1.03	-	23.01	-
7. DF2	0.8413	346	-	266	17.2	43.42	-	5.50	-	27.90	-
8. AFAPL b	0.8378	342	-	266	19.9	42.45	-	3.90	-	27.67	-
9. AFAPL 2	0.7852	-	2.0	215	17.8	42.74	1.88	0.99	-	23.96	-
10. UTRC 3B	0.8581	324	-	240	12.9	42.41	5.88	2.19	-	27.64	-
11. UTRC 8A	0.8468	341	-	251	16.7	42.98	5.31	2.23	-	27.75	-
12. ERBLS 2	0.8628	320	-	252	9.1	42.41	5.83	2.13	-	27.30	-
13. UTRC 9A	0.8309	315	-	217	15.8	43.14	3.71	1.59	-	26.55	-
14. UTRC 9B	0.8348	323	-	257	14.7	42.73	7.42	2.46	-	27.02	-
15. Tetralin	0.9712	345	-	242	6.2	40.41	--	2.30	1.60	35.10	32.40
16. XTB	0.8602	308	-	-	7.1	40.48	1.60	0.87	0.70	28.20	27.40
17. BLS	0.8961	307	-	255	8.3	40.43	4.30	1.70	-	29.59	-
18. ERBLS 3	0.8729	316	-	251	8.2	41.88	5.22	1.99	-	28.36	-
19. ERBS	0.8423	336	-	251	15.5	42.16	8.05	2.67	-	27.71	-
20. Decalin	0.8877	328	-	-	24.5	42.35	8.21	3.08	2.13	31.00	28.10
21. JP4-A	0.7657	-	2.9	214	20.6	43.94	1.76	0.94	-	22.21	-
22. Jet A	0.8123	317	-	225	21.2	43.16	4.76	1.91	1.38	25.90	23.90
23. JP5	0.8160	336	-	230	23.2	42.64	6.14	2.23	-	26.62	-
24. GMSO	0.8217	400	-	269	26.6	43.54	--	6.08	3.66	27.50	26.80
25. UTRC 1	0.7835	345	-	<210	40.0	44.42	12.89	3.37	-	24.38	-

NOTE: Viscosity and surface tension data were acquired at an elevated temperature only for six fuels.

TABLE 5 - Fuel Analyses
(continued)

Fuel	C (wt pct)	H (wt pct)	Sulfur (wt pct) Merc 10^{-4}	Total	Nitrogen (wt pct)	H/C-FIA (vol pct) Sat	Olefin	Arom	Naphthalene UV (vol pct)	H/C-Mass Spec (vol pct) Arom	Naphthalene
1. UTRC 2A	87.50	11.87	1	0.15	0.105	60.8	0.9	38.3	13.7	34.9	16.0
2. ERBLS 1	87.54	12.35	4	0.04	0.006	56.4	1.0	42.6	13.5	38.4	16.6
3. UTRC 7A	86.06	12.54	1	0.13	0.088	69.1	1.4	29.5	11.4	26.2	14.9
4. JP7	85.41	14.39	<1	<0.01	<0.001	95.0	0.0	5.0	0.1	2.5	0.0
5. JP4-S	85.72	14.39	<1	<0.01	0.016	84.3	0.0	15.7	0.2	15.1	0.3
6. JP4	85.65	14.57	2	0.01	<0.001	86.4	0.0	13.6	0.5	15.7	0.5
7. DF2	86.22	13.46	1	0.30	0.010	72.9	1.1	26.0	7.0	22.9	7.9
8. AFAPL 6	86.16	13.41	1	0.21	0.007	73.8	0.0	26.2	5.8	21.4	6.7
9. AFAPL 2	86.15	13.56	1	<0.01	<0.001	72.3	0.0	27.7	3.6	31.0	3.6
10. UTRC 3B	86.98	12.41	2	0.19	0.092	71.0	0.9	28.1	13.6	24.9	14.5
11. UTRC 8A	86.71	12.84	2	0.13	0.100	80.0	0.5	19.5	12.7	16.5	13.4
12. ERBLS 2	87.06	11.89	<1	0.05	0.007	48.6	1.0	50.4	15.4	47.3	20.5
13. UTRC 9A	87.76	12.89	3	0.03	<0.001	66.3	1.3	32.4	0.7	30.7	1.5
14. UTRC 9B	86.80	13.10	2	0.12	0.006	67.8	0.9	31.3	6.3	30.1	7.3
15. Tetralin	90.46	9.14	<1	<0.01	0.002	0.0	0.0	100.0	0.1	100.0	1.5
16. XTB	89.08	9.64	<1	<0.01	<0.001	0.0	0.0	100.0	0.1	100.0	0.1
17. BLS	89.79	10.36	2	0.08	0.008	14.8	0.8	84.4	20.5	73.3 (76.0)*	24.6 (29.7)*
18. ERBLS3	88.23	11.38	2	0.06	0.007	38.0	0.3	61.7	17.0	59.2	26.5
19. ERBS	86.99	12.95	3	0.04	0.005	68.9	0.0	31.1	11.6	28.4	13.5
20. Decalin	86.63	13.10	<1	<0.01	<0.001	97.6	0.3	2.1	0.0	0.2	0.0
21. JP4-A	85.84	14.16	2	<0.01	<0.001	77.3	0.7	22.0	0.7	23.1	0.6
22. Jet A	85.68	13.69	6	0.08	<0.001	80.1	0.3	19.6	1.4	15.9	1.9
23. JP5	86.33	13.88	3	0.04	<0.001	80.4	1.0	18.6	1.5	16.5	2.2
24. GMSO	85.80	14.1?	3	<0.01	<0.001	83.2	0.5	16.3	0.6	9.9	-.0
25. UTRC 1	84.96	14.97	3	<0.01	<0.001	96.0	0.8	3.2	0.0	0.4	0.0

*Values indicated in parentheses are corrected values based on ERBS/BLS blend analysis.

TABLE 5 - Fuel Analyses
(continued)
Hydrocarbon Type by Mass Spectrometry (wt pct)

Fuel	Saturates Total	Paraffins	Monocyclo Paraffins	Dicyclo Paraffins	Tricyclo Paraffins	Total Aromatics	Alkyl Benzene	Indanes	Indenes	C10 Naphthalene	C11+ Naphthalene	Acenaphthenes	Acenaphthalenes	Tricyclic Aromatics
1. UTRC 2A	61.0	22.9	25.7	11.3	1.1	39.0	17.5	1.1	0.0	1.2	14.1	4.2	0.6	0.3
2. ERBLS 1	56.5	34.6	14.0	6.4	1.4	43.5	13.9	7.5	0.0	0.0	14.4	3.4	2.0	2.3
3. UTRC 7A	69.8	29.4	27.1	11.8	1.5	30.2	10.3	1.5	0.0	1.0	12.8	3.7	0.5	0.3
4. JP7	97.0	49.3	37.0	9.7	1.0	3.0	1.6	1.2	0.0	0.0	0.1	0.0	0.0	0.0
5. JP4-S	81.7	61.8	17.9	1.6	0.1	17.6	14.5	2.5	-	0.2	0.3	-	-	*
6. JP4	77.2	57.2	15.8	3.6	0.4	18.4	15.3	2.2	-	0.3	0.5	-	-	-
7. DF2	73.2	38.6	21.1	10.5	2.9	26.8	7.9	5.3	2.4	0.0	6.0	2.4	1.2	1.6
8. AFAPL 6	75.2	41.5	23.4	8.3	2.0	24.8	9.0	5.2	1.3	0.6	5.8	1.3	0.6	1.0
9. AFAPL 2	59.8	44.5	12.5	2.4	0.3	35.5	26.5	4.1	-	1.8	3.0	-	-	*
10. UTRC 3B	71.2	25.9	30.0	13.8	1.5	28.8	6.7	3.7	0.5	1.1	12.1	3.7	0.6	0.4
11. UTRC 8A	80.0	31.3	32.7	14.4	1.6	20.0	1.7	1.4	0.2	0.9	11.4	3.5	0.5	0.3
12. ERBLS 2	47.6	29.4	11.5	5.4	1.3	52.4	18.4	7.5	0.0	0.0	17.3	4.1	2.6	2.6
13. UTRC 9A	66.7	25.4	27.6	12.3	1.4	33.3	28.7	2.6	0.0	0.0	1.6	0.2	0.0	0.1
14. UTRC 9B	67.8	37.8	20.5	7.8	1.7	32.2	15.3	7.0	0.7	1.5	6.3	1.9	0.0	1.1
15. Tetralin	0.0	0.0	0.0	0.0	0.0	100.0	0.0	98.5	0.0	0.0	0.0	0.0	0.0	0.0
16. XTB	0.0	0.0	0.0	0.0	0.0	100.0	99.9	0.0	0.0	0.0	0.1	0.0	0.0	0.0
17. BLS	23.1	16.7	2.8	2.8	0.7	76.9	40.5	5.5	0.0	0.0	20.6	4.5	2.6	3.4
18. ERBLS 3	35.4	22.8	7.7	4.0	0.9	64.6	25.3	6.0	0.0	0.0	21.8	5.0	3.0	3.5
19. ERBS	66.6	40.4	17.7	7.0	1.5	33.4	8.0	7.2	0.1	0.0	11.8	2.8	1.6	1.9
20. Decalin	99.8	0.0	0.0	99.7	0.1	0.2	0.2	0.0	-	0.0	0.0	0.0	0.0	*
21. JP4-A	71.3	56.1	11.7	3.1	0.3	26.9	22.7	3.2	0.6	0.4	0.5	-	-	-
22. Jet A	81.7	43.2	28.2	8.7	1.6	18.3	10.7	4.5	0.8	0.2	2.0	0.2	0.0	0.1
23. JP5	80.8	44.4	24.3	10.0	2.7	19.2	9.5	6.1	2.0	0.0	2.3	0.2	0.0	0.1
24. GMSO	88.2	52.7	25.1	7.6	2.8	11.8	4.5	4.0	0.0	0.0	0.5	0.6	0.3	0.0
25. UTRC 1	99.6	80.0	16.9	2.6	0.1	0.4	0.4	0.0	0.0	0.0	0.0	0.0	0.0	0.0

*These fuels analyzed by a modified ASTM D 2789

TABLE 5 - Fuel Analyses
(continued)

Distillation (K)

Fuel	IBP	5	10	15	20	30	40	50	60	70	80	90	95
1. UTRC 2A	435	447	452	456	460	466	472	479	485	491	498	510	520
2. ERBLS 1	435	452	459	464	469	481	491	500	510	522	537	562	586
3. UTRC 7A	442	456	460	464	467	472	477	482	487	491	498	507	518
4. JP7	466	474	477	478	479	481	482	484	486	489	494	502	511
5. JP4-S	394	405	407	411	414	419	425	432	439	446	454	465	481
6. JP4	340	364	371	376	381	392	405	420	445	468	486	502	514
7. DF2	465	492	507	515	522	535	545	556	566	578	592	611	626
8. AFAPL 6	462	479	486	492	496	507	517	529	542	560	580	603	624
9. AFAPL 2	342	364	375	382	388	400	414	432	449	465	483	503	515
10. UTRC 3B	440	453	460	462	466	473	480	486	493	502	512	528	546
11. UTRC 8A	468	475	476	477	478	480	482	485	489	494	500	510	520
12. ERBLS 2	425	439	445	451	459	473	487	500	513	526	541	565	586
13. UTRC 9A	424	436	440	443	446	451	458	466	474	481	491	505	519
14. UTRC 9B	431	449	456	461	467	477	489	500	510	525	594	573	597
15. Tetralin	474	475	475	475	475	476	476	476	476	476	476	476	476
16. XTB	416	419	420	420	420	421	422	423	424	426	429	433	437
17. BLS	410	420	423	426	431	443	458	496	526	539	551	571	592
18. ERBLS ?	417	431	437	442	450	464	481	499	514	528	544	565	585
19. ERBS	460	473	475	479	482	489	494	501	510	520	535	560	582
20. Decalin	459	460	461	461	461	461	461	461	462	462	462	462	463
21. JP4-A	340	354	363	371	377	390	404	424	447	467	483	500	513
22. Jet A	435	449	454	458	461	467	474	480	487	495	504	516	526
23. JP5	459	471	474	476	479	482	486	491	496	502	509	520	530
24. GMSO	536	543	545	547	550	552	556	559	563	567	573	581	589
25. UTRC 1	474	482	483	484	485	487	490	492	496	501	507	516	522

TABLE 6 - Combustor Open Area Distribution

Section		Number	Area Distribution Diameter (mm)	Area (cm^2)
Dome	Cooling	60	1.78	
(4 rings)		60	1.47	
		60	1.47	
		60	1.09	4.09
Louver 1	Cooling	96	1.98	2.96
	Combustion	6	12.7	7.13
Louver 2	Cooling	96	1.98	2.96
	Combustion	6	12.7	7.13
Louver 3	Cooling	96	1.98	2.96
	Combustion	6	12.7	7.13
Louver 4	Cooling	96	1.98	2.96
Louver 5	Cooling	48	1.98	1.48
	Combustion	6	12.7	7.13
Louver 6	Cooling	48	1.98	1.48

TABLE 7 - Liner Effective Area Distribution

Section		Effective Area (cm^2) Individual	Adjusted	Percent of Total (with Swirler)
Dome	Cooling	3.2	3.0	8.1
Louver 1	Cooling	2.65	2.5	6.8
	Combustion	4.90	4.6	12.5
Louver 2	Cooling	2.65	2.5	6.8
	Combustion	4.91	4.6	12.5
Louver 3	Cooling	2.57	2.4	6.5
	Combustion	4.76	4.5	12.2
Louver 4	Cooling	2.81	2.6	7.1
Louver 5	Cooling	1.25	1.2	3.3
	Combustion	4.90	4.6	12.5
Louver 6	Cooling	1.40	1.3	3.5
Sum of Components		36.0	33.8	91.8
Measured Total Liner		33.8		
Swirler		3.0	3.0	8.2
Total Liner with Swirler		36.8	36.8	100.0

TABLE 8 – Primary Zone Equivalence Ratio Variation for Jet A

Overall Fuel-Air Ratio	0.C15	0.018	0.022
Overall Equivalence Ratio	0.22	0.26	0.32

Combustor Configuration (Airflow Split)	Primary Equivalence Ratio		
Lean (0.23)	0.98	1.18	1.44
Baseline (0.195)	1.18	1.42	1.74
Rich (0.17)	1.31	1.57	1.92

TABLE 9 - Fuel Atomization Levels

Fuel Nozzle No. 35
Fuel Temperature = 295 ± 5K

Fuel	SMD (µm)/Included Cone Angle (deg)		
	Fuel Weight Flow (kg/hr)		
	118	133	162
JP4-S	41/70	26/65	8/60
JP4-A	44/70	25/65	7/60
UTRC1	44/70	30/65	13/60
JP4	45/65	27/65	8/60
AFAPL	53/75	35/70	21/65
GMSO	55/75	45/70	23/65
JP7	56/70	40/65	18/60
UTRC 9A	56/75	41/75	14/65
JP5	58/75	46/70	24/65
Jet A	60/75	39/70	20/65
UTRC 7A	60/70	47/70	19/65
UTRC 8A	64/75	47/75	21/70
UTRC 2A	64/80	47/75	22/70
DF2	64/70	48/70	26/65
XTB	65/75	52/70	26/65
UTRC 9B	66/70	51/70	16/65
ERBS	68/70	47/70	20/65
UTRC 3B	69/75	48/75	28/70
BLS	73/75	55/75	37/70
ERBLS1	74/75	55/75	22/70
ERBLS2	74/75	48/75	22/70
ERBLS3	74/75	54/70	26/70
AFAPL 6	83/75	55/70	22/65
Decalin	83/75	63/70	42/65
Tetralin	83/75	67/75	45/70

TABLE 10 - Fuel Temperature Influence on Atomization

Fuel Nozzle No. 35

Fuel	Fuel Temperature (K)	SMD (μm)/Included Cone Angle (deg) Fuel Weight Flow (kg/hr)		
		118	133	162
Jet A	299	60/75	39/70	20/65
	311	53/75	38/70	23/65
	328		31/70	
Tetralin	299	83/75	67/75	45/70
	311	90/80	78/75	49/70
	328	83/80	68/75	45/70

TABLE 11 - Fuel Nozzle Number Influence on Atomization

Fuel Temperature = 298K

Fuel	Nozzle Number	SMD (μm)/Included Cone Angle (deg)				
		Fuel Weight Flow (kg/hr)				
		83	96	118	133	162
Jet A	35	-	-	60/75	39/70	20/65
	30	-	-	30/70	21/65	-
	20	29/65	15/60	-	-	-
Tetralin	35	-	-	-	67/75	45/70
	30	-	-	-	46/70	26/85
	20	-	-	-	12/70	-

TABLE 12 - Fuel Nozzle Specification

Fuel	SMD for NN=35 (μm)	Test Nozzle (NN)	SMD for Test Nozzle (μm)
JP4-S	26	40	39
JP4-A	25	40	38
UTRC 1	30	40	45
JP4	27	40	41
AFAPL 2	35	35	35
GM 0	45	35	45
JP7	40	35	40
UTRC 9A	41	35	41
JP5	46	35	46
Jet A	39	35	39
UTRC 7A	47	32	36
UTRC 8A	47	32	36
UTRC 2A	47	32	36
DF2	48	32	36
X7B	52	32	39
UTRC 9B	51	32	39
ERBS	47	32	36
UTRC 3B	48	32	36
BLS	55	32	42
ERBLS 1	55	32	42
ERBLS 2	48	32	36
ERBLS 3	54	32	41
AFAPL 6	55	32	42
Decalin	63	30	39
Tetralin	67	30	42

TABLE 13 - Airflow Influence on Atomization

Fuel Nozzle No. 35

Fuel Temperature = 298K

Fuel	Swirler Airflow Differential Pressure (kPa)	SMD (μm)/Included Cone Angle (deg) Fuel Weight Flow = 130 kg/hr
Jet A	0	42/70
	4.92	33/55
	26.2	4/45
Tetralin	0	67/75
	4.92	59/60
	26.2	13/45

TABLE 14 - Test Facility Instrumentation

Symbol	Measurement		Description
	Device	Range	
PVAUP	P/T	2.7 MPa	Air pressure upstream of venturi
TVAUP	T/C	Type K	Air temperature upstream of venturi
PVATH	P/T	2.0 MPa	Air pressure at throat of venturi
TVENT	T/C	Type T	Venturi body temperature
PHTREX	P/T	1.7 MPa	Air pressure at electrical heater exit
PFPUMP	P/T	6.9 MPa	Fuel pressure at pump discharge
TFPUMP	T/C	Type K	Fuel temperature at pump discharge
PFINJ	P/T	6.9 MPa	Fuel pressure in line entering rig
TFINJ	T/C	Type K	Fuel temperature at nozzle
WF	Micromotion	--	Fuel mass flow
FUEL FLAG	MV	--	Indicator of fuel valve actuation
P31	P/T	1.7 MPa	Air pressure at combustor inlet, R = 5.7 cm
P32	P/T	1.7 MPa	Air pressure at combustor inlet, R = 3.8 cm
P33	P/T	1.7 MPa	Air pressure at combustor inlet, R = 1.9 cm
P34	P/T	1.7 MPa	Air pressure at combustor inlet, R = 1.0 cm
T31	T/C	Type K	Air temperature at combustor inlet, R = 2.5 cm
T32	T/C	Type K	Air temperature at combustor inlet, R = 5.0 cm
T33	T/C	Type K	Air temperature at combustor inlet, R = 2.5 cm
T34	T/C	Type K	Air temperature at combustor inlet, R = 5.0 cm
PCASE 1	P/T	1.7 MPa	Liner airflow pressure, Z = 9.2 cm
PCASE 2	P/T	1.7 MPa	Liner airflow pressure, Z = 20.3 cm
PCASE 3	P/T	1.7 MPa	Liner airflow pressure, Z = 31.4 cm
TL01060 - TL62060	T/C	Type K	Liner temperature along row (13 total), θ = 60 deg
TL01180 - TL62180	T/C	Type K	, θ = 180 deg
TL01300 - TL62300	T/C	Type K	, θ = 300 deg
PRADN2	P/T	3.4 MPa	Nitrogen pressure upstream of venturi for transpiration radiometers
TRADN2	T/C	Type T	Nitrogen temperature upstream of venturi
PRAD1	P/T	1.7 MPa	Nitrogen pressure in radiometer, θ = 90 deg
PRAD2	P/T	1.7 MPa	Nitrogen pressure in radiometer, θ = 300 deg
TCRAD1	T/C	Type T	Radiometer coolant temperature, θ = 90 deg
TCRAD2	T/C	Type T	Radiometer coolant temperature, θ = 300 deg
QDOME1	mv	--	Signal from transpiration radiometer, θ = 90 deg
QDOME2	mv	--	Signal from transpiration radiometer, θ = 300 deg

TABLE 14

(Continued)

RAD1	mv	--	Signal from thermopile radiometer, Z = 9.2 cm
RAD2	mv	--	Signal from thermopile radiometer, Z = 14.8 cm
RAD3	mv	--	Signal from thermopile radiometer, Z = 20.3 cm
T401-T422	T/C	Type B	Gas temperature at combustor exit
P4	P/T	1.7 MPa	Gas pressure at combustor exit
PMT1	mv		Photomultiplier tube output for scattered light at 45 deg from forward
PMT2	mv		Photomultiplier tube output for scattered light at 135 deg from forward
LPOWER	mv		Laser powermeter output
TCR1	T/C	Type T	Coolant exit temperature, ring 1
TCR2	T/C	Type T	Coolant exit temperature, ring 2
TCR3	T/C	Type T	Coolant exit temperautre, ring 3
TCR4	T/C	Type T	Coolant exit temperature, adapter spool
TCTC	T/C	Type T	Coolant exit temperature, T/C rake
TCXI	T/C	Type T	Coolant exit temperature, emissions rake
TCSNIN	T/C	Type T	Coolant inlet temperature, smoke probe
TCSNEX	T/C	Type T	Coolant exit temperature, smoke probe
PXI	P/T	1.7 MPa	Gaseous sample pressure
TXI	T/C	Type K	Gaseous sample temperature
PSN	P/T	1.7 MPa	Smoke sample pressure
UHC	FID		Signal from UHC analyzer
RUHC	mv		Signal UHC analyzer range
O2	Paramagnetic		Signal from O2 analyzer
RO2	mv		Signal denoting O2 analyzer range
NOX	Chemiluminescent		Signal from NOX analyzer
RNOX	mv		Signal denoting NOX analyzer range
CO	NDIR		Signal from CO analyzer
RCO	mv		Signal from CO analyzer range
CO2	NDIR		Signal from CO2 analyzer range
RCO2	mv		Signal denoting CO2 analyzer

NOTES:

1. P/T = pressure transducer, strain gauge
2. T/C = thermocouple
3. All P/T readings with range = 1.7 MPa performed with a single pressure scanner
4. Coordinate reference position -
    R is the radial coordinate with R = 0 on combustor axial center line
    Z is the axial coordinate with Z = 0 at the combustor dome flange
    θ is the azimuthal angle about the axial center line (clockwise positive viewing downstream) with θ = 0 through the igniter location
5. SAE smoke filter samples manually obtained; no interface with data system
6. Liner temperature nomenclature: TLXXYYZZZ
    where XX = louver number, TT = T/C position, ZZZ = θ

TABLE 15 - Emissions Analysis Instrumentation

Component	Range	Instrument Detection Method	Instrument Error % Full Scale
THC	0-1 ppmv Intermediate ranges 0-10%	Flame Ionization Detector	± 5.0% ± 1.0% ± 1.0%
NO_x	0-2.5 ppmv Intermediate ranges (6) 0-10,000 ppmv	Chemiluminescence Detector TECO Model 10A	± 1.0% ± 1.0% ± 1.0%
CO	0-200 ppmv 0-1000 ppmv 0-5000 ppmv	Nondispersive Infrared Beckman Model 865	± 1.0%
CO_2	0-2% 0-5% 0-15%	Nondispersive Infrared Beckman Model 315	± 1.0% ± 1.0% ± 1.0%
O_2	0-1% 0-5% 0-10% 0-25%	Paramagnetic Analyzer Scott Model 150	± 1.0% ± 1.0% ± 1.0% ± 1.0%

TABLE 16 Test Conditions

	Condition 1	Condition 2	Condition 3
Combustor upstream air pressure (MPa)	1.32	1.32	1.32
Combustor upstream air temperature (K)	700	700	700
Combustor total air flow (kg/s)	1.84	1.84	1.84
Combustor ideal exit temperature (K)	1246	1346	1473

TABLE 17 - Measured or Derived Performance Parameters

	Parameter Type	Correction Technique	Precision Assessment
Airflow rate	M*	--	--
Fuel flow rate	M*	--	--
Burner entrance average total pressure	M*	--	--
Burner entrance average total temperature	M*	--	--
Fuel manifold pressure	M	IC	X
Fuel injector pressure drop	C	Eqn	X
Fuel temperature at injector	M	--	X
Fuel-air ratio metered	C	Eqn	X
Average combustor exit total temperature	M	IC	X
Average combustor exit static pressure	M	IC	X
Average combustor exit total pressure	C	Eqn	X
Combustor total pressure loss	C	Eqn	X
Primary zone flow split	*	--	--
Primary zone fuel-air ratio	C	Eqn	--
Primary zone flame temperature	C	Eqn	--
Combustor liner temperature	M	IC	X
Combustor thermal radiation flux	M	Eqn	X
Emission indices, CO, UHC, NOx	M	Cor	X
Percent CO_2, O_2	M	IC	X
Average SAE Smoke Number	M	--	X
Combustion efficiency - ΔT	C	Eqn	X
Combustion efficiency - emissions	C	Eqn	X
Combustor reference velocity	C	Eqn	X
Sample-line temperature, pressure	M	--	--
Burner exit pattern factor	C	Eqn	X
Fuel-air ratio - emissions	C	Eqn	X

Symbols: M   - Measured
            C   - Calculated
            Eqn - Corrected values obtained as equation results using corrected
                  parameter values
            IC - Corrected by use of influence coefficients
            Cor - Corrected by use of correlation relating derived and measured
                  parameters
            *   - Test parameter

TABLE 18 Local Equivalence Ratio

	Test Condition		
	1	2	3
	Overall Equivalence Ratio		
	0.22	0.26	0.32
	Local Equivalence Ratio		
Combustor Section			
Primary zone	1.2	1.4	1.7
Louver 1	1.2	1.4	1.7
Louver 2	0.8	1.0	1.2
Louver 3	0.5	0.6	0.7

NOTE: (1) Baseline combustor configuration

       (2) Lquivalence ratios are for Jet A

TABLE 19 Regression Analysis Results

Variable	Condition	Regression Form	R^{2*}	C1	C2	C1/C2
Dome Radiation	1	H^{C1}	0.83	-1.5		
	2		0.87	-1.7		
	3		0.84	-1.4		
	1	SP^{C1}	0.92	-0.41		
	2		0.91	-0.43		
	3		0.92	-0.36		
	1	$H^{C1}(100-N)^{C2}$	0.87	-1.4	-0.47	3.0
	2		0.92	-1.5	-0.30	3.0
	3		0.91	-1.2	-0.54	2.2
Liner Temperature Rise	1	H^{C1}	0.84	-0.57		
	2		0.78	-0.56		
	3		0.68	-0.42		
	1	SP^{C1}	0.92	-0.15		
	2		0.90	-0.15		
	3		0.89	-0.12		
	1	$H^{C1}(100-N)^{C2}$	0.90	-0.50	-0.20	2.5
	2		0.90	-0.47	-0.25	1.9
	3		0.81	-0.33	-0.24	1.4
Smoke Number	1	H^{C1}	0.81	-1.7		
	2		0.78	-2.0		
	3		0.76	-2.3		
	1	SP^{C1}	0.93	-0.50		
	2		0.84	-0.57		
	3		0.91	-0.67		
	1	$H^{C1}(100-N)^{C2}$	0.88	-1.6	-0.62	2.6
	2		0.36	-1.7	-0.75	2.3
	3		0.81	-2.0	-0.64	3.1

*These anlyses performed in log plane (i.e., log (radiation)).
 Similar quality expected in real plane.
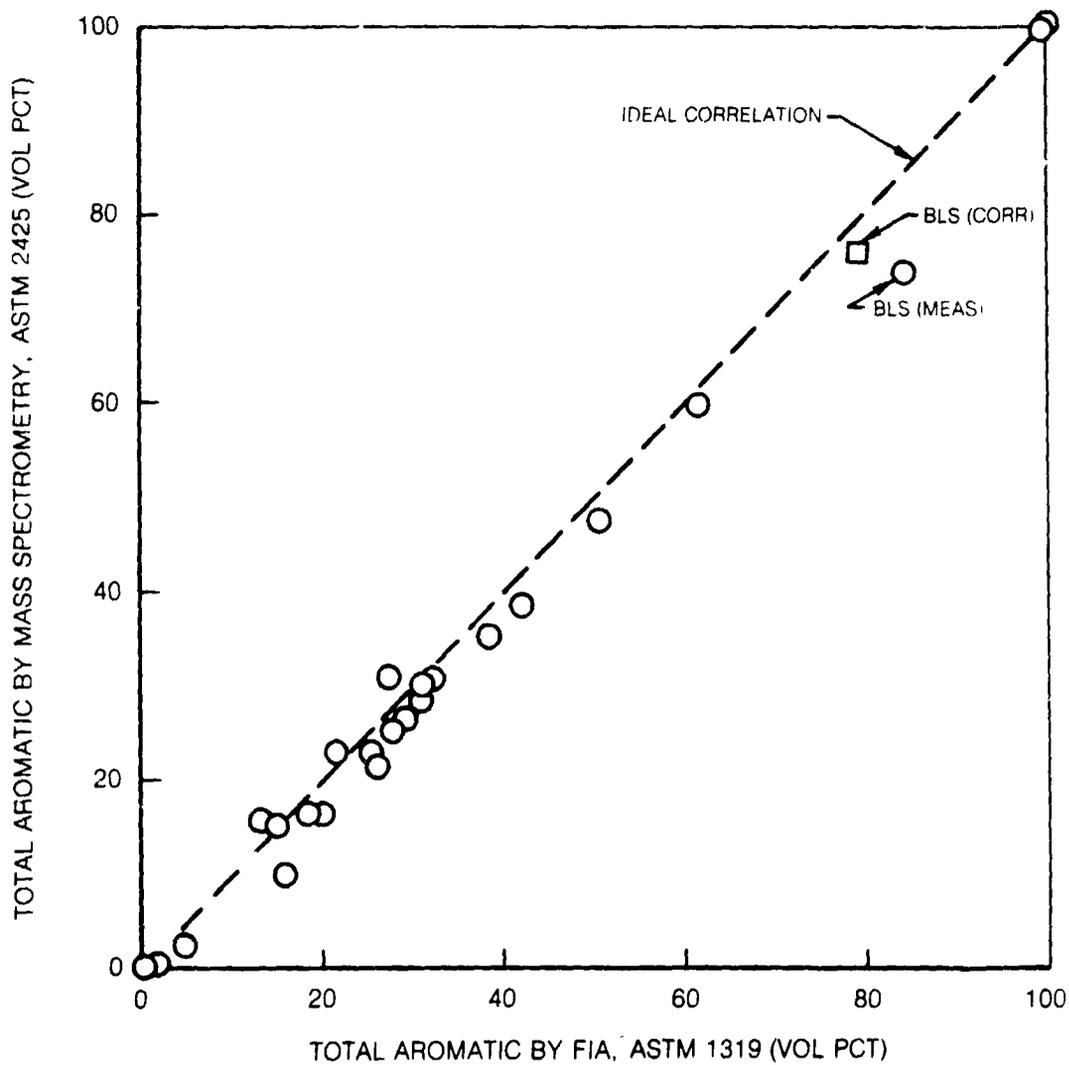
Fig. 1 Comparison of Total Aromatic Content for Two Analysis Techniques
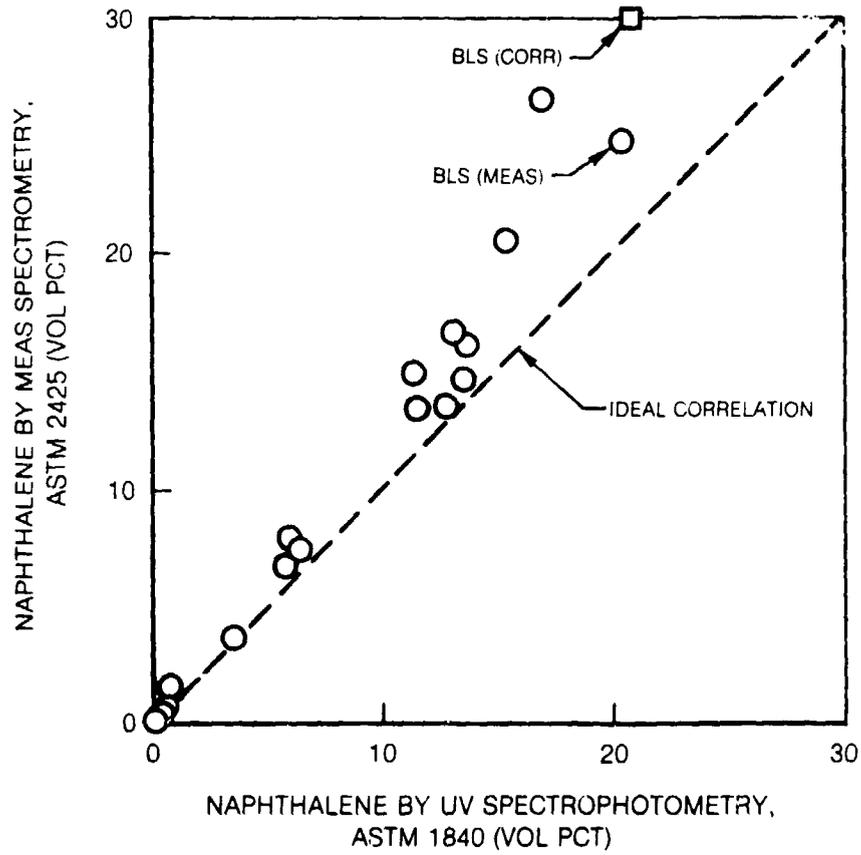
Fig. 2 Comparison of Naphthalene Content for Two Analysis Techniques
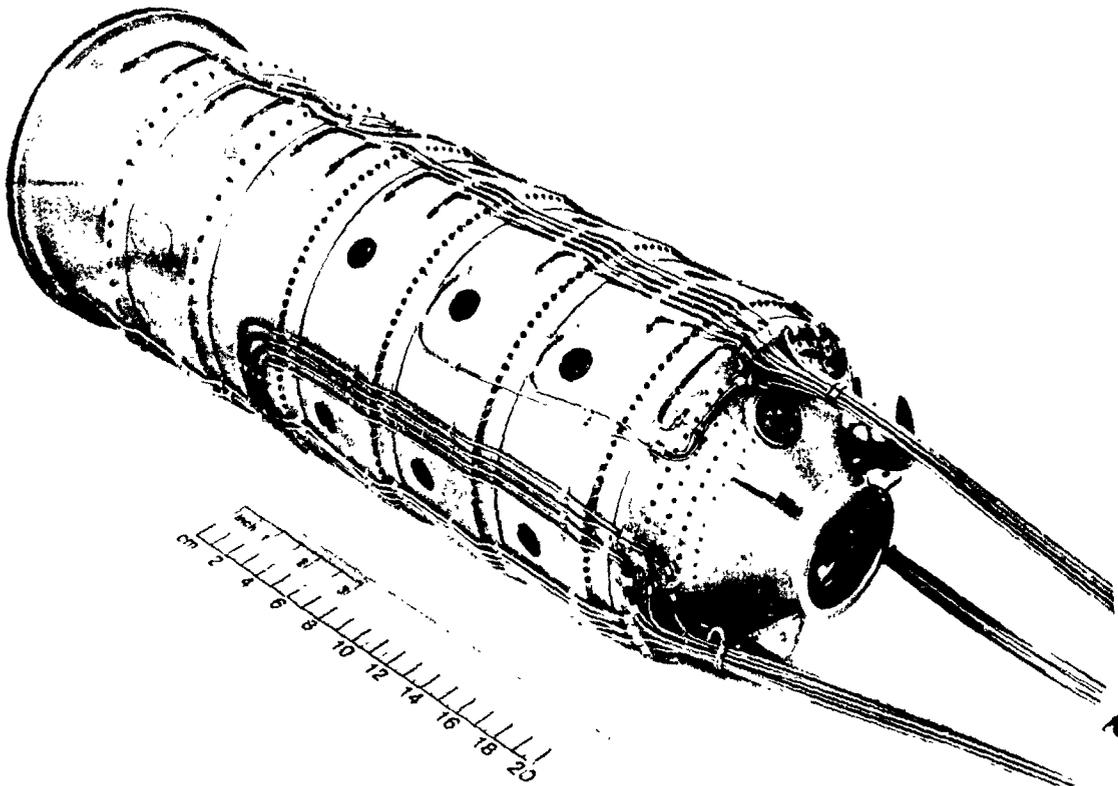
Fig. 3 Generic Gas Turbine Combustor

83-7-29-3
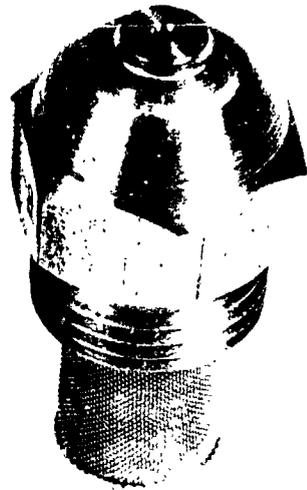
a) SIMPLEX PRESSURE ATOMIZING INJECTOR
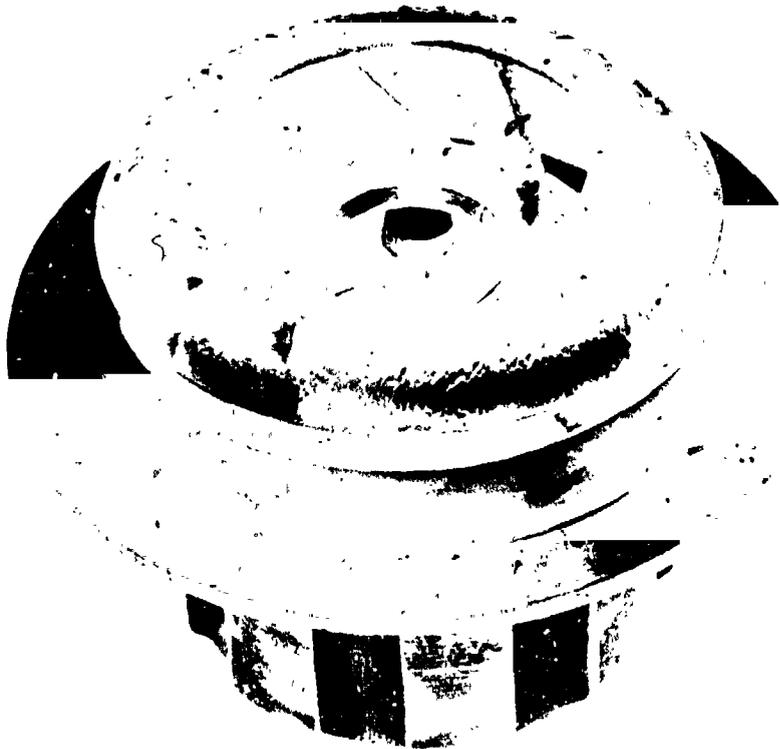
b) AIRFLOW SWIRLER

Fig. 4 Fuel Nozzle and Air Swirler
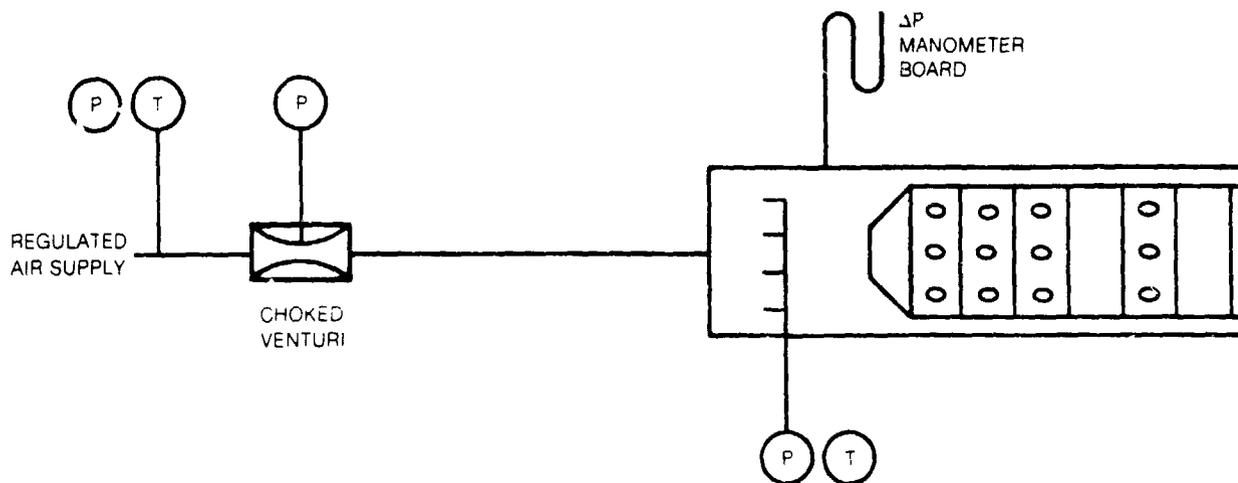
Fig. 5 Test Setup for Effective Area Determination

(a) SAMPLING PROBE

5 cm DIA   10 cm DIA

OPEN CIRCLES SET 1
CLOSED CIRCLES SET 2
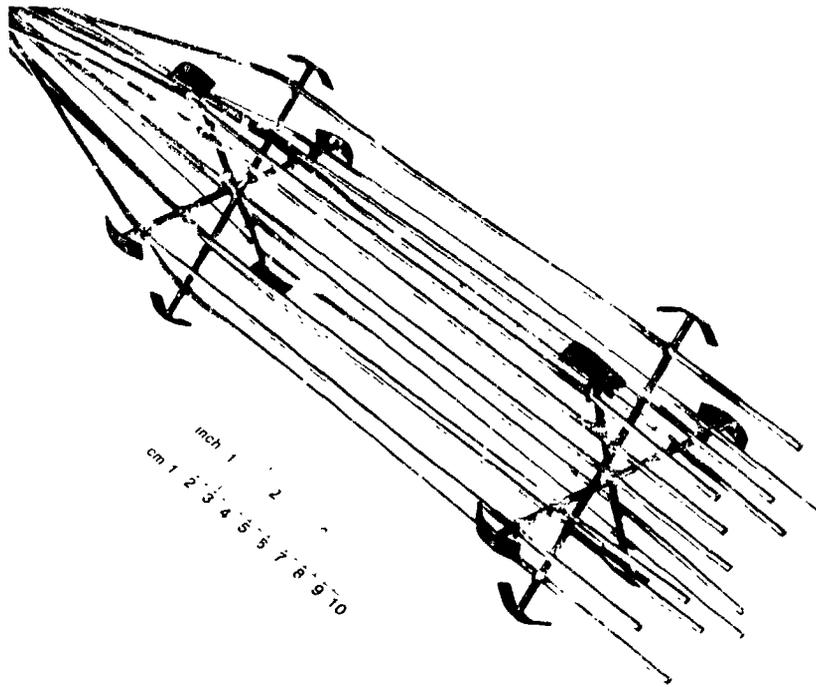
COMBUSTOR WALL
12.7 cm DIA
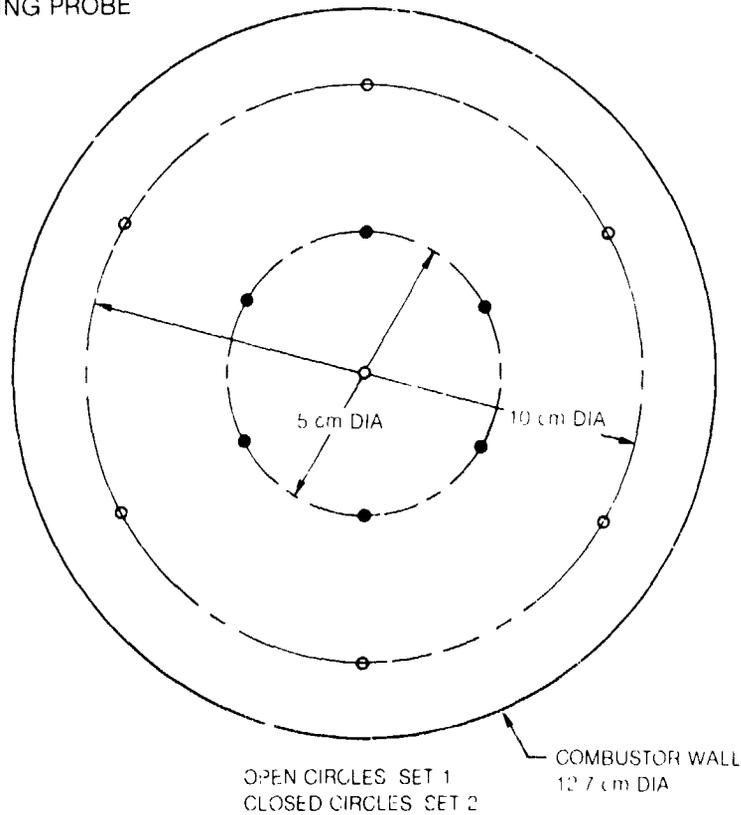
(b) SAMPLING TUBE LAYOUT

Fig. 6 Primary Airflow Sampling Probe

83 7 29-6
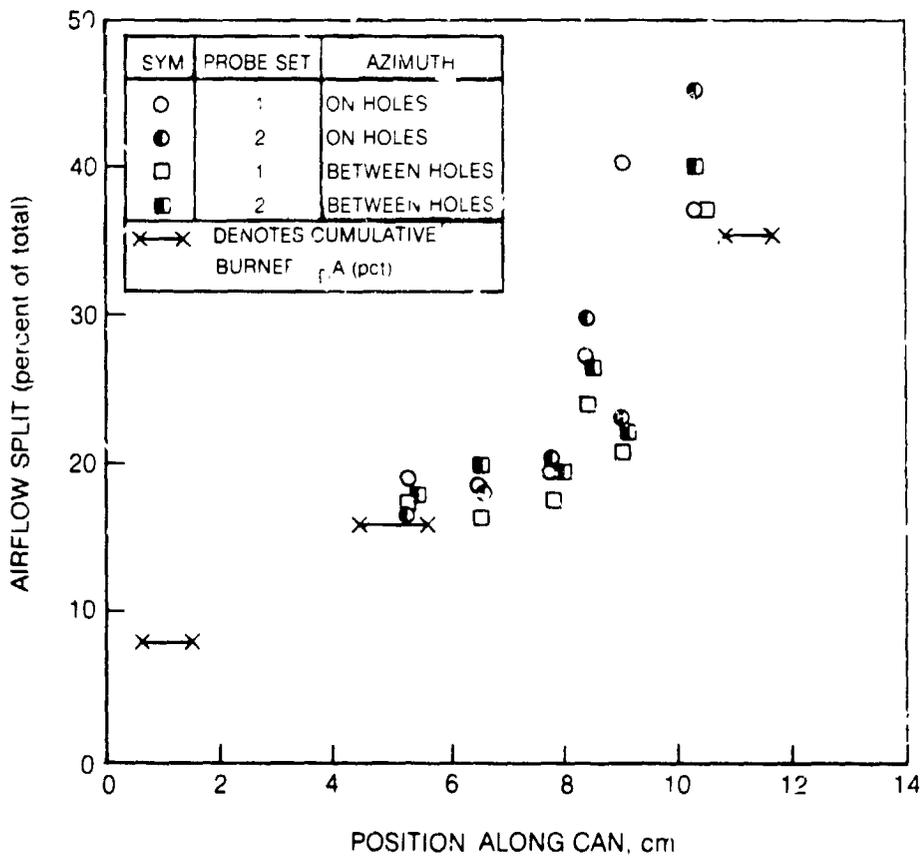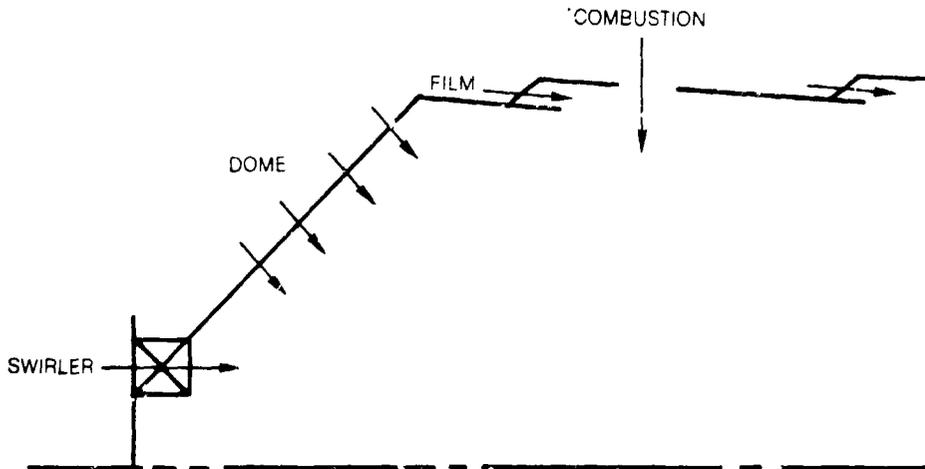
Fig. 7 Calculated Combustor Airflow Split

82—8—1:0—1
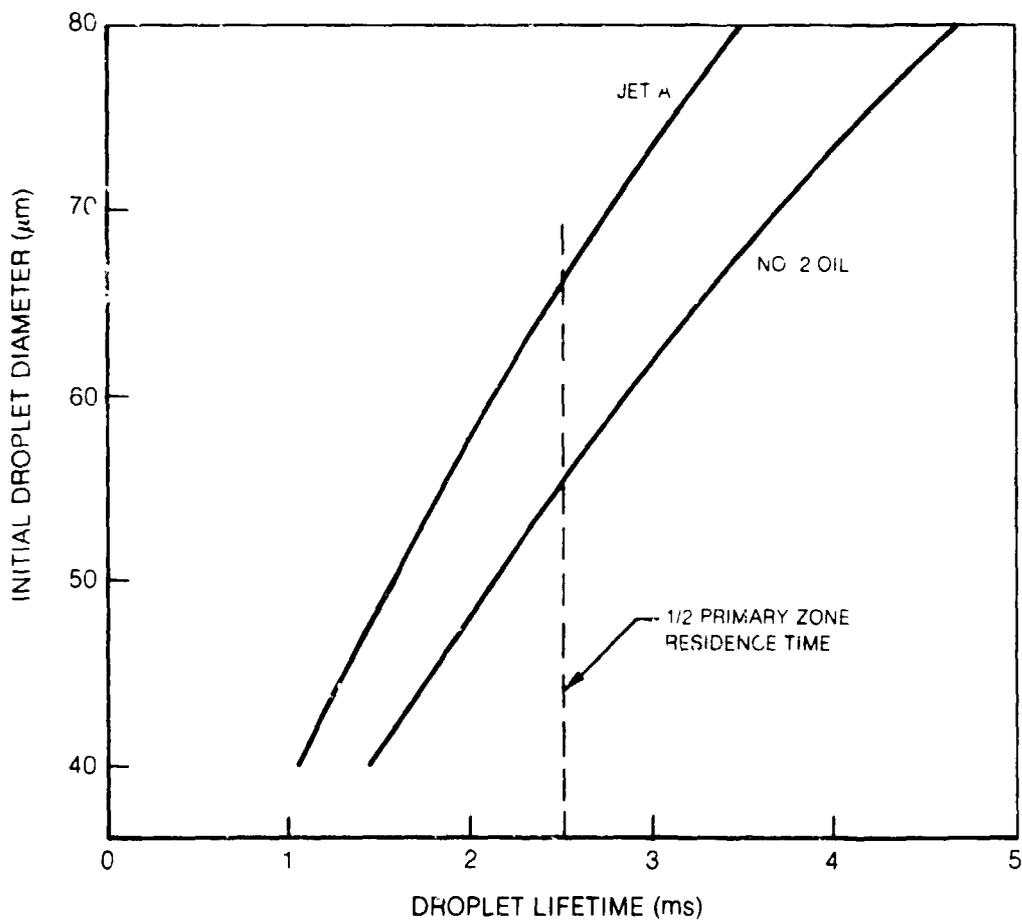
Fig. 8 Predicted Droplet Lifetime in Primary Zone with 20 pct Turbulence

83-7-29-7
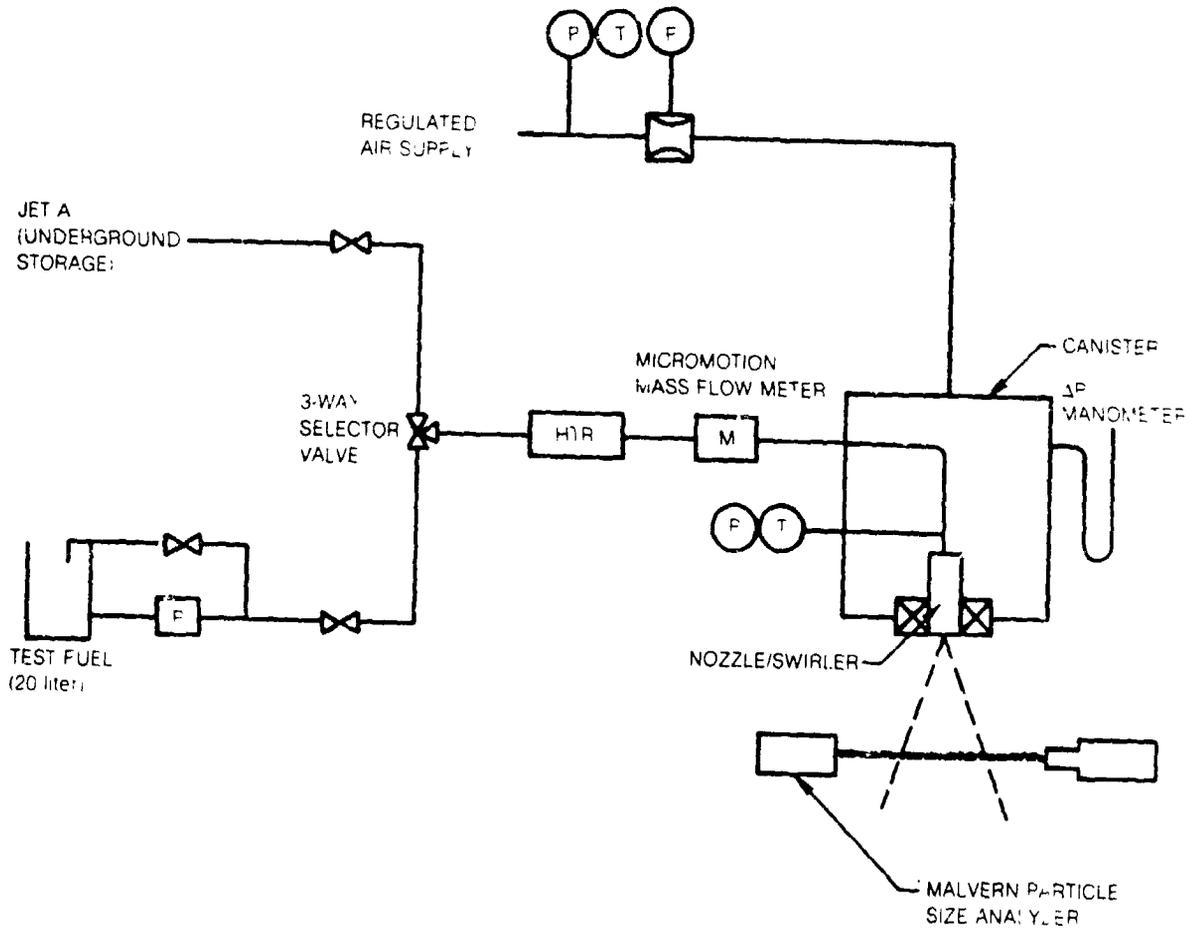
Fig. 9 Fuel Spray Characterization Facility
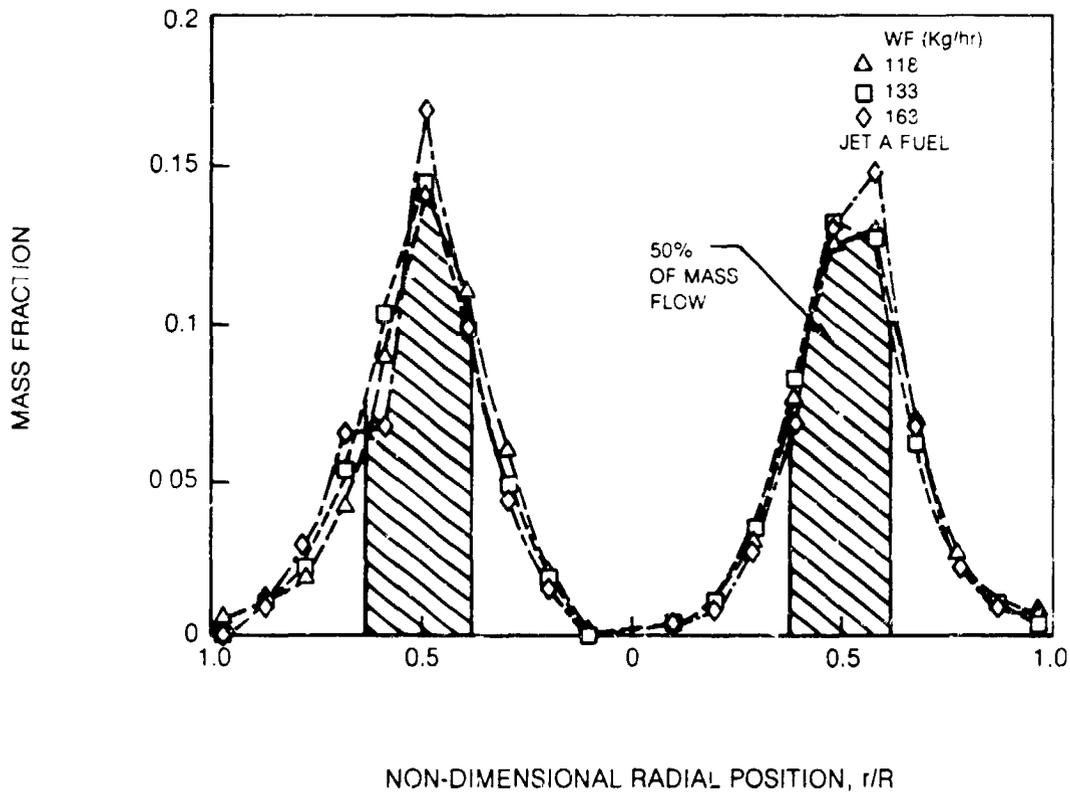
Fig. 10 Fuel Spray Mass Distribution for No. 35 Nozzle
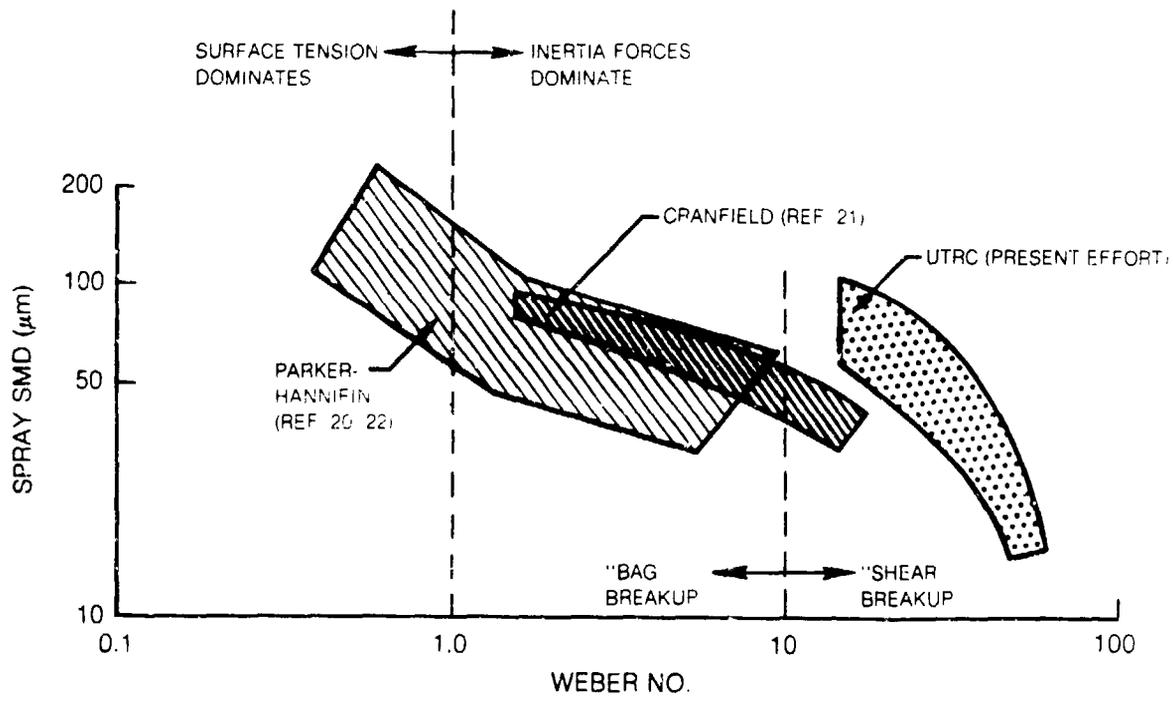
Fig. 11 Weber Number Regimes

R84-915908-29
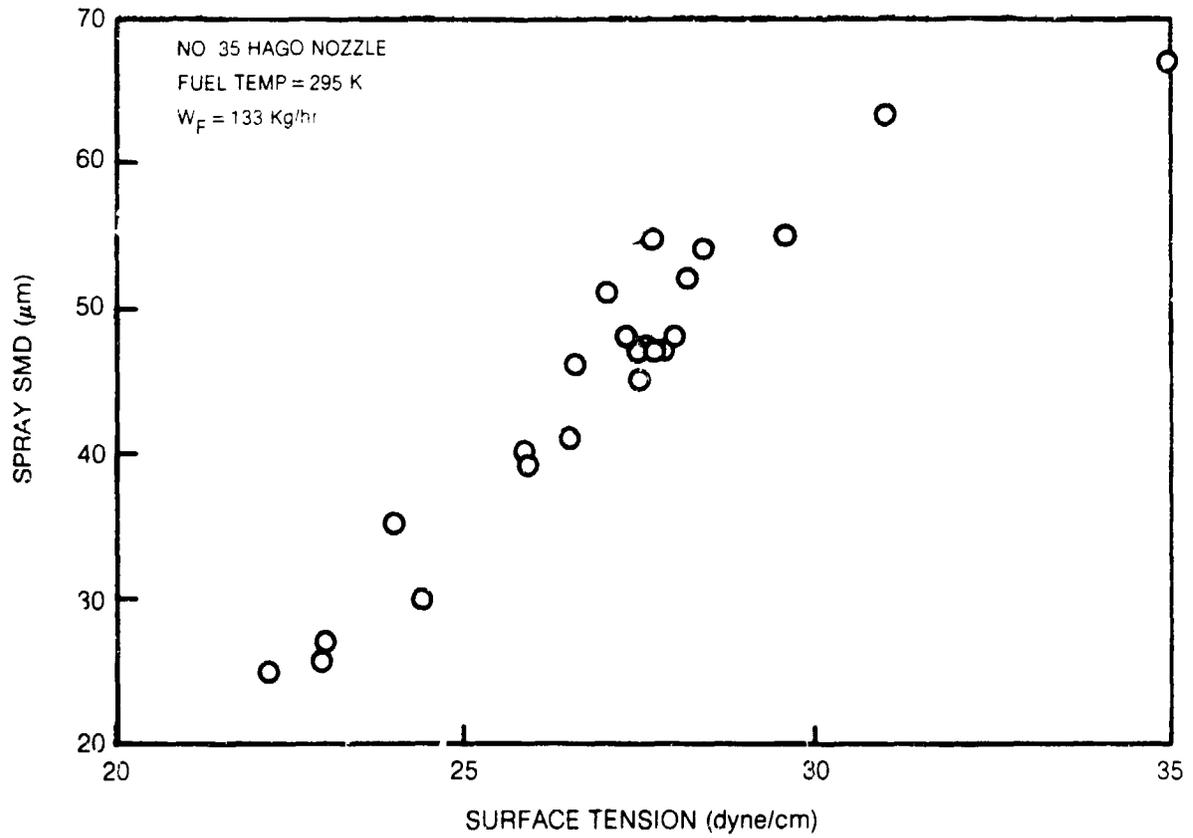
Fig. 12 Influence of Fuel Surface Tension on Measured Atomization

83—7—29—10
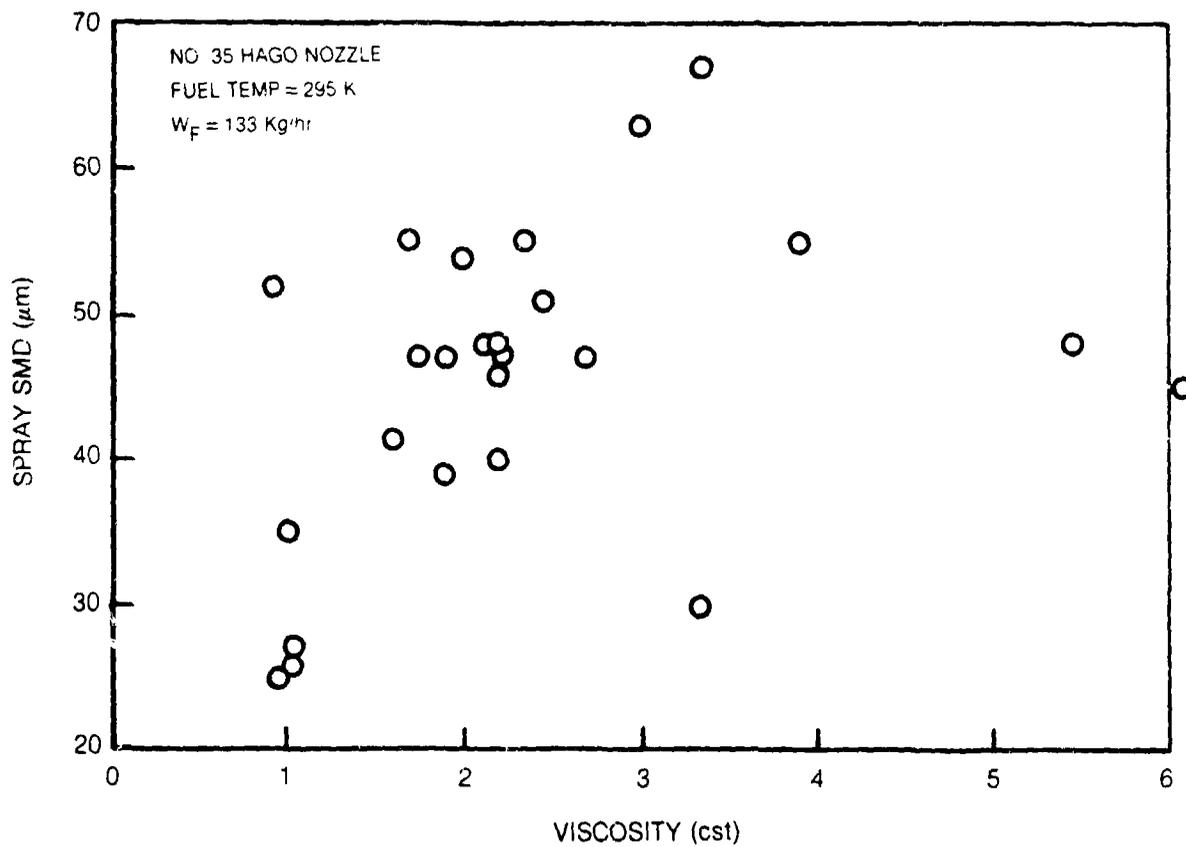
Fig. 13 Influence of Fuel Viscosity on Measured Atomization
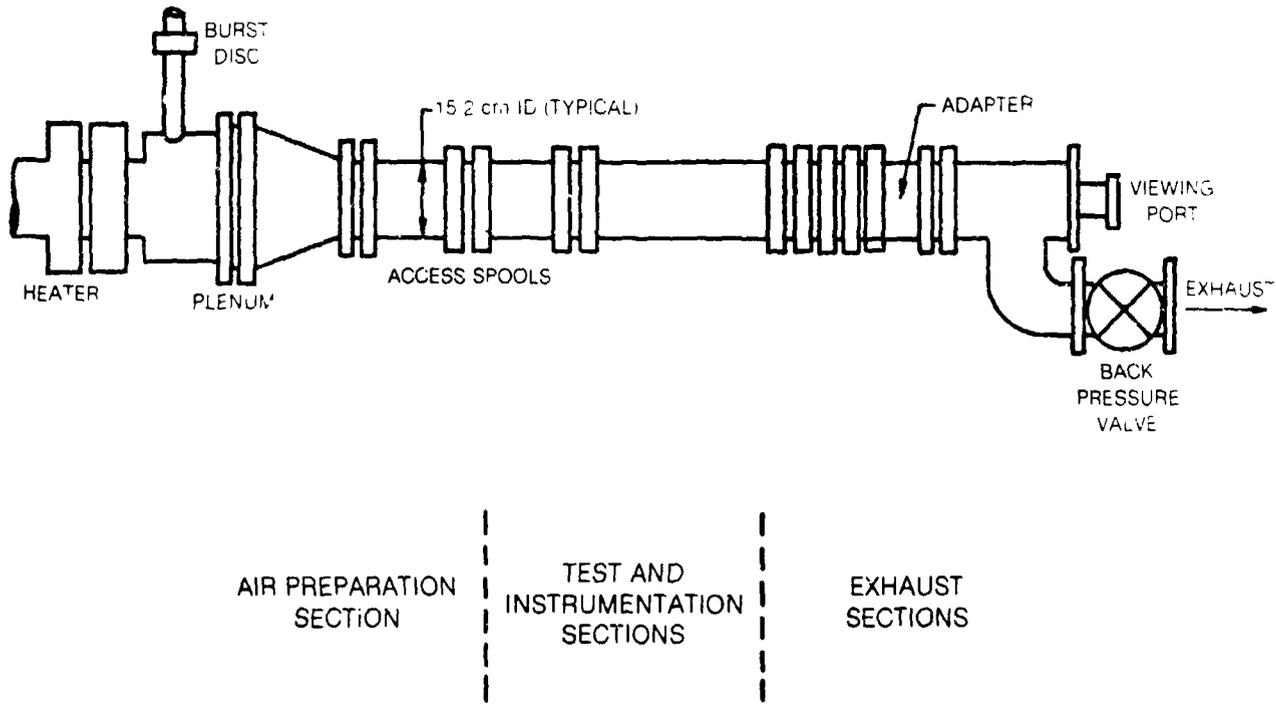
Fig. 14 Aviation-Fuel Property Effects Test Facility

81—6—64—4
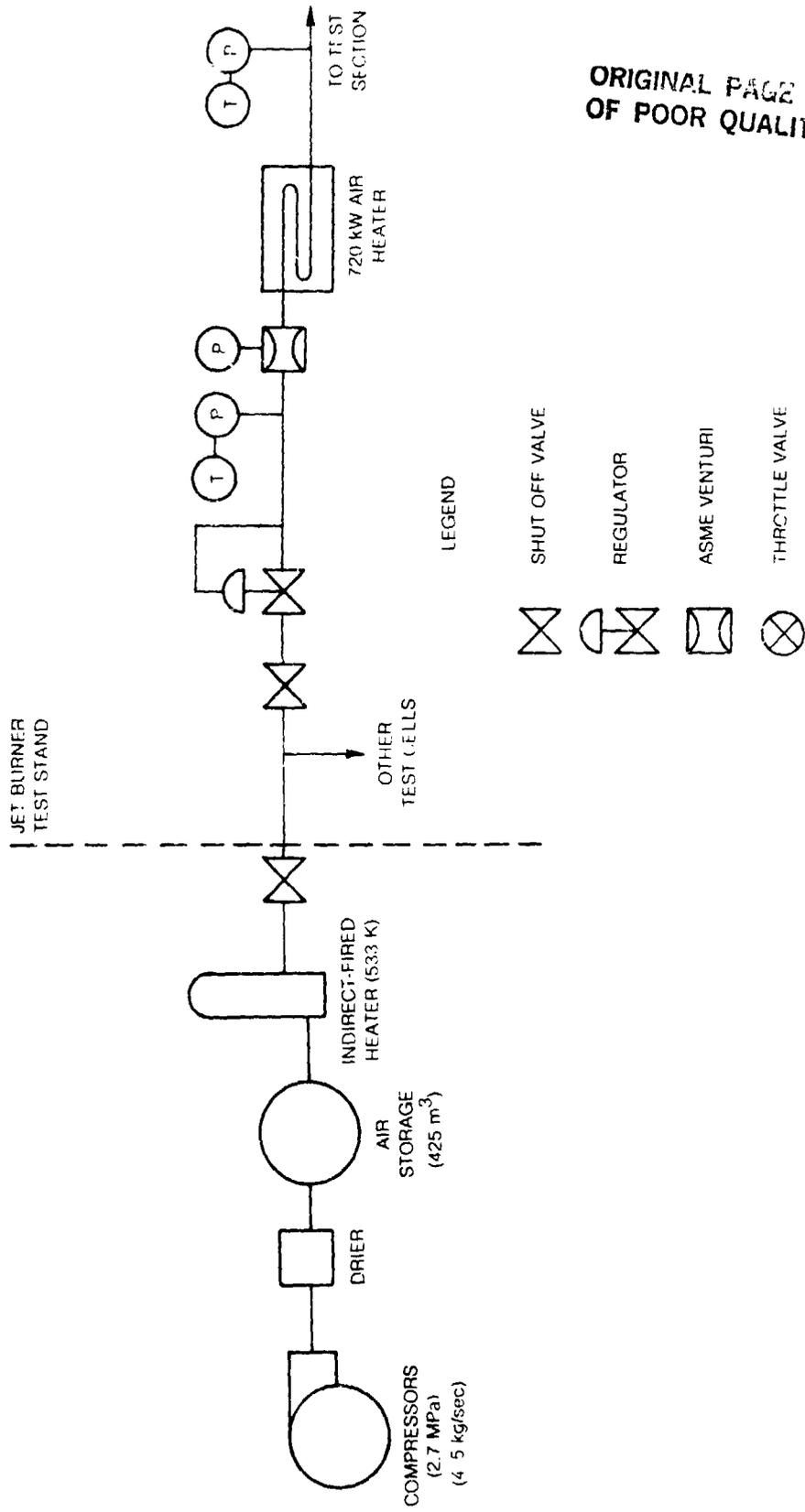
Fig. 15 Air Supply System for Test Rig

LEGEND

SHUT OFF VALVE

REGULATOR

ASME VENTURI

THROTTLE VALVE

81—6—64—7

Fig. 16 Test Rig Support Systems and Instrumentation
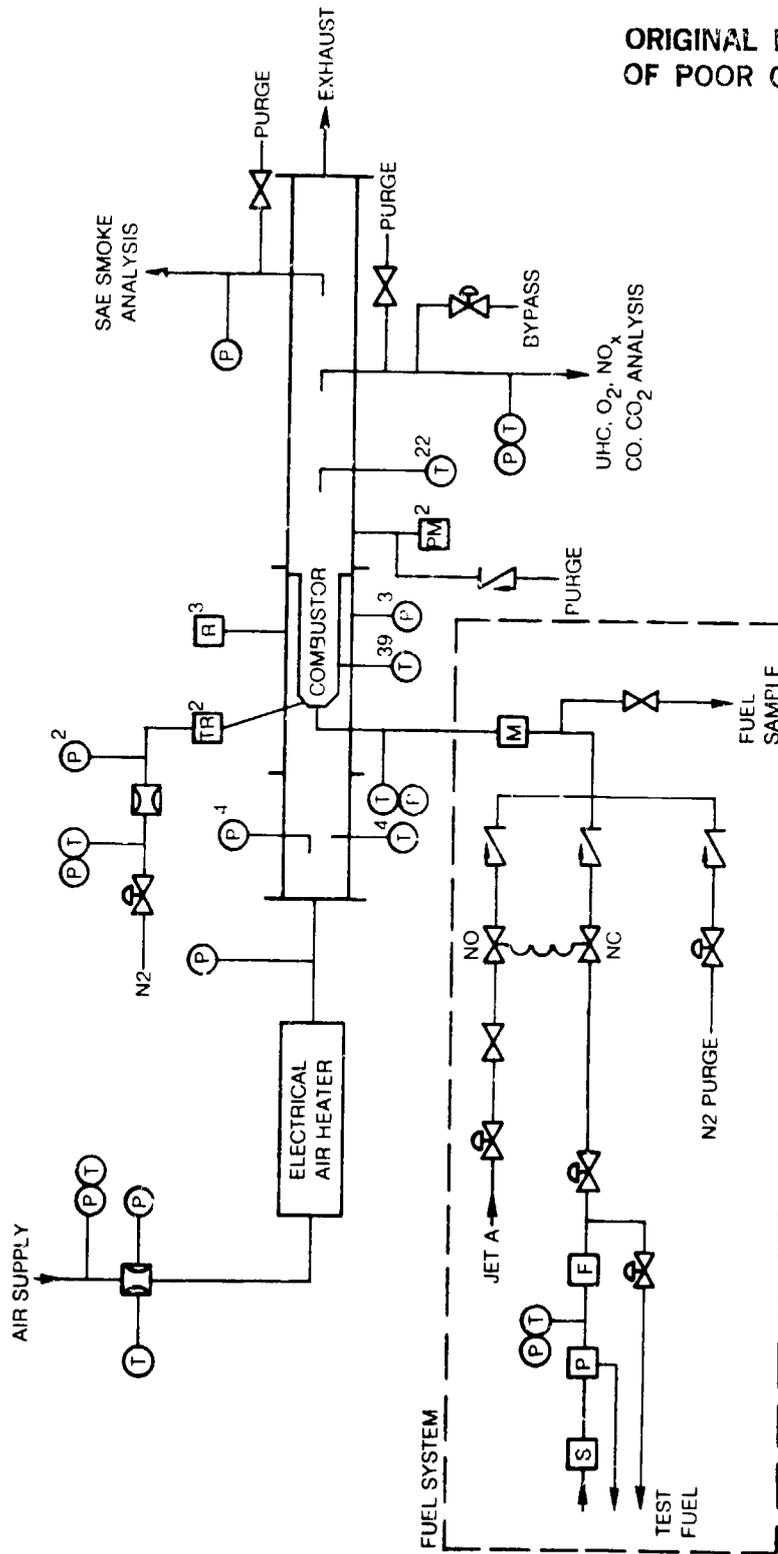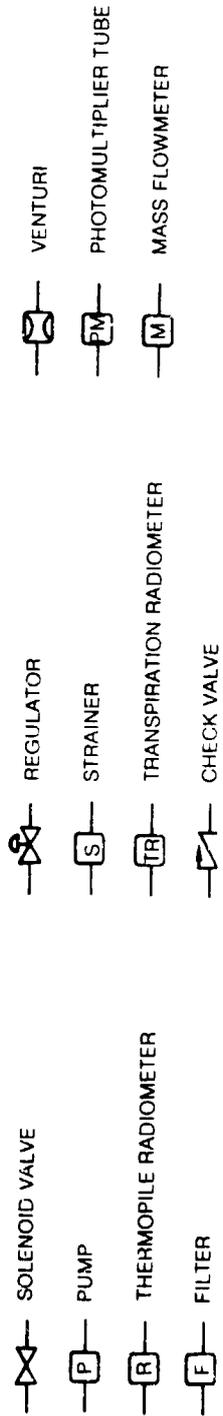
NOTES: SUPERSCRIPT INDICATES MULTIPLE MEASUREMENTS, COOLANT TEMPERATURE MEASUREMENTS NOT INDICATED

a) PROBE BODY
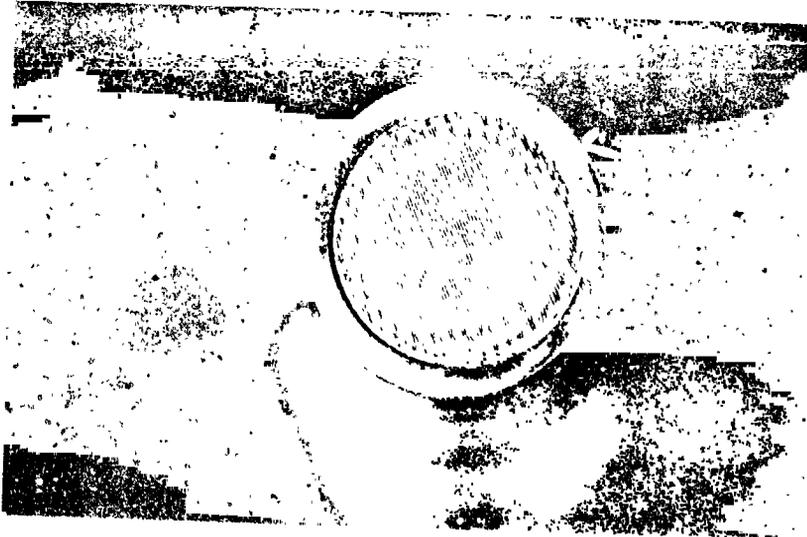
b) TIP SCREEN

Fig. 17 Transpiration Radiometer

82-292-B
82-292-A

83-7 29- 12

R84-915908-29
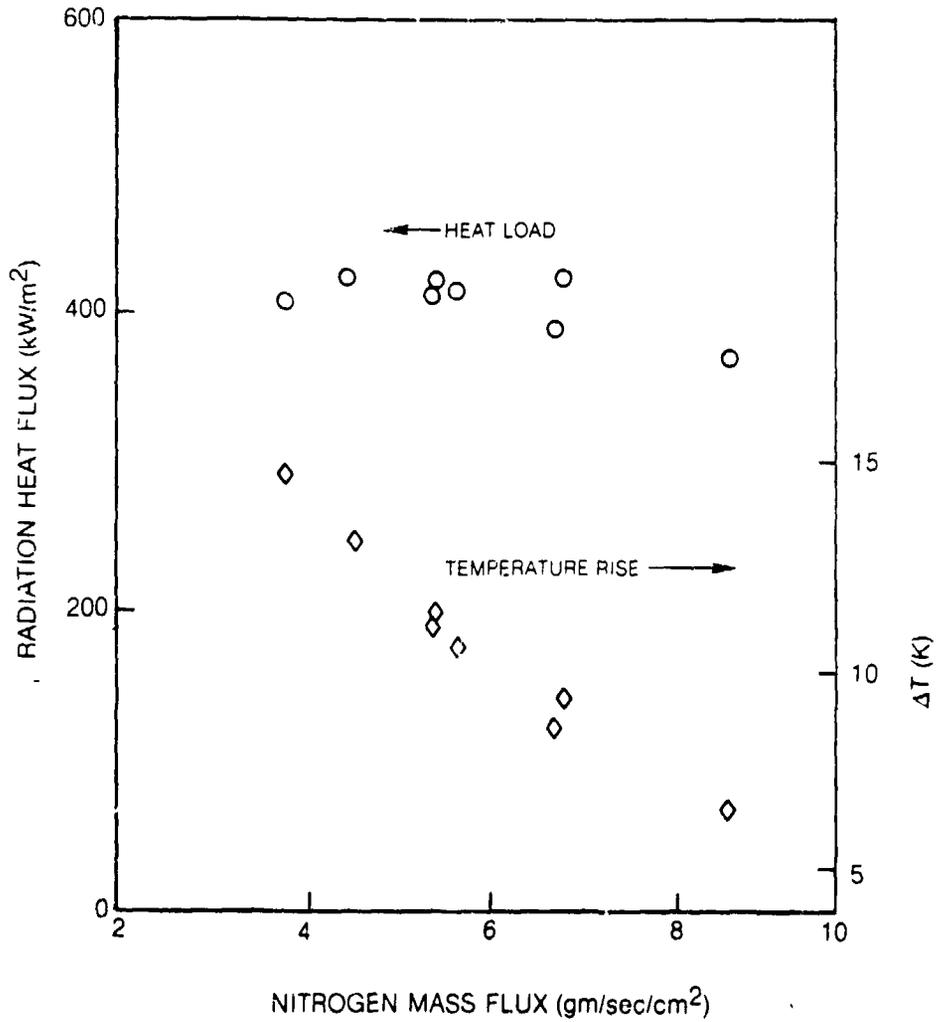
Fig. 18 Operational Characteristics of Transpiration Radiometer

82-11-38-1
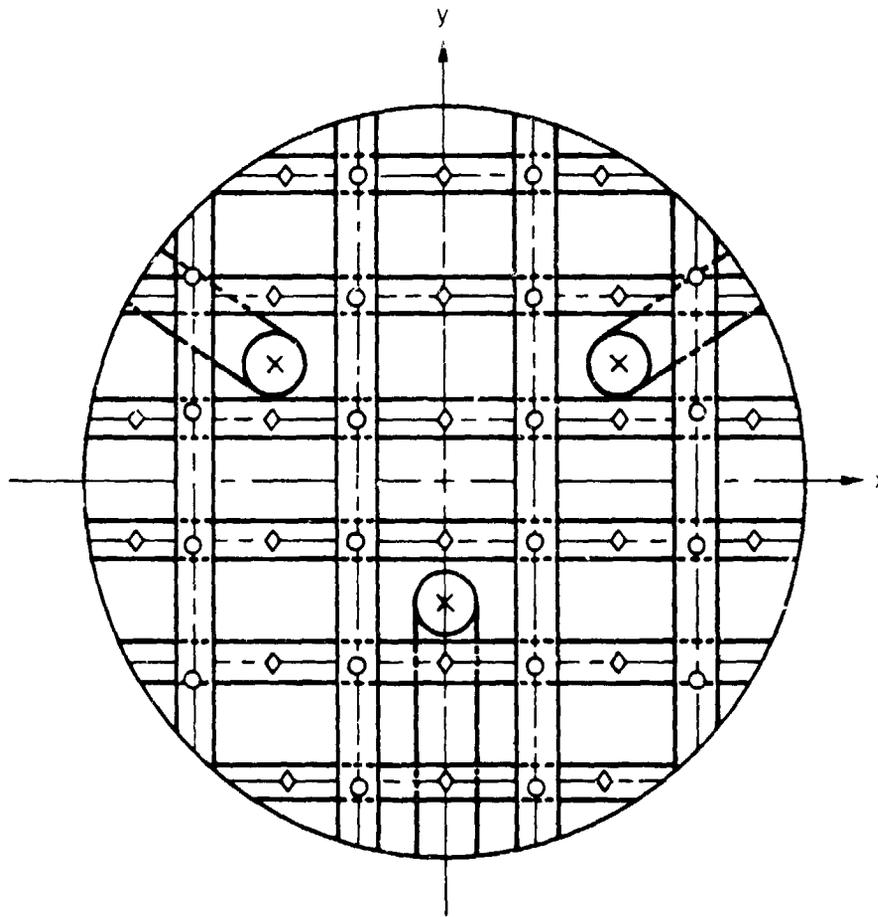
○ EMISSION SAMPLE INLET (20 TOTAL) RAKES AT X = ± 1 58, ± 4 44 cm

◇ TYPE B THERMOCOUPLE (22 TOTAL) RAKES AT y = ± 1 02, ± 3 05, ± 5 08 cm

✗ SMOKE SAMPLE INLET (3 TOTAL) INLETS AT X = ± 3 05, y = 2 03 cm
$$X = 0 00 \quad y = -2 03 \text{ cm}$$

Fig. 19 Probe Distribution at Combustor Exit

81-11-23-1

$$\frac{I(45)}{I(135)}$$

n = 1 94 − 0 66ı

n = 1 56 − 0 46ı

PARTICLE DIAMETER (μm)
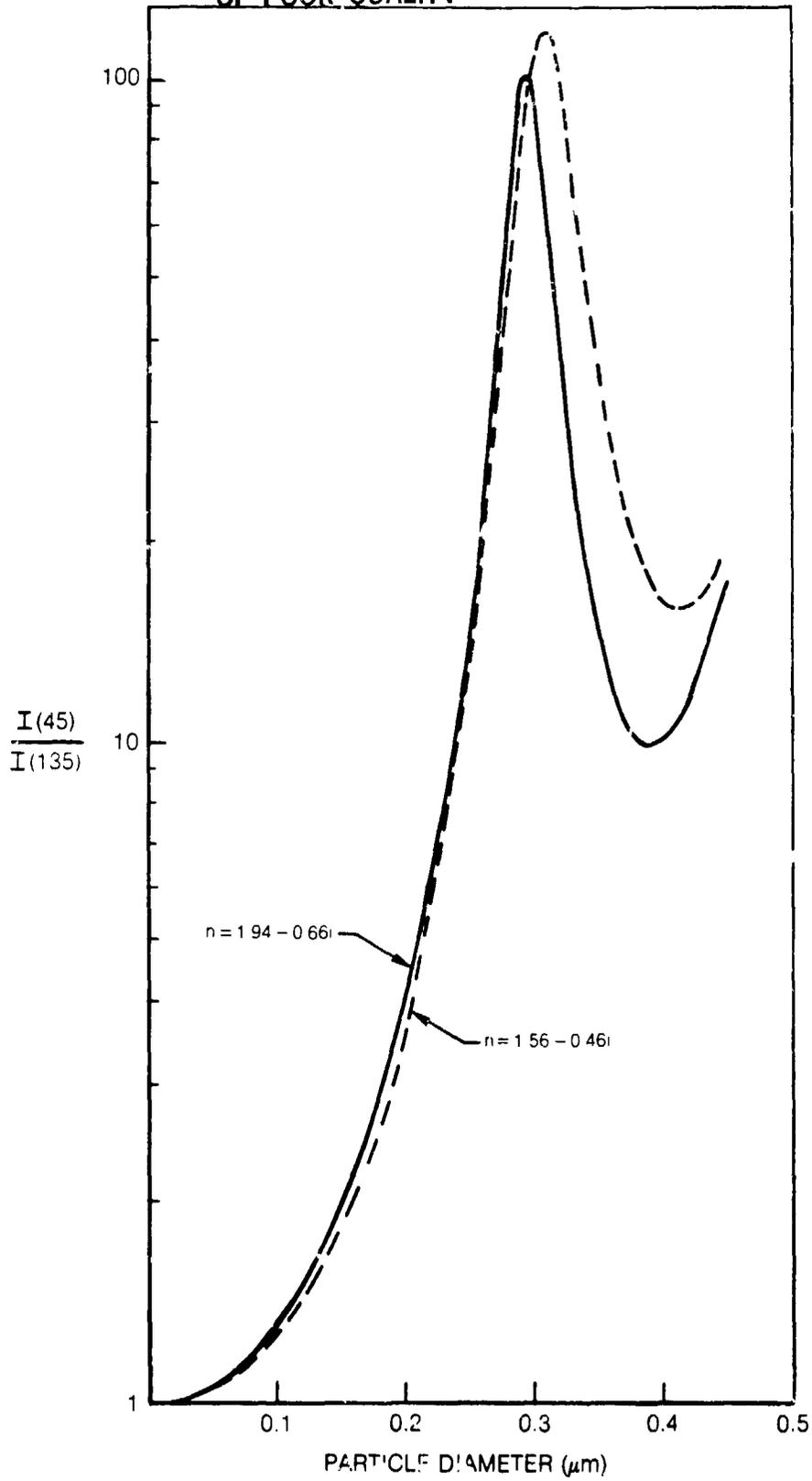
Fig. 20 Scattered-Light Ratio Dependence on Particle Diameter

83−7−29−13

OUTPUT TO LOCK-IN AMPLIFIER

PMT

PMT

F
W
A
P
A
A
A
P
DETECTOR
ASSEMBLY

ALIGNMENT
WINDOW

AL
PR
C
L
W
F
W
L
PM
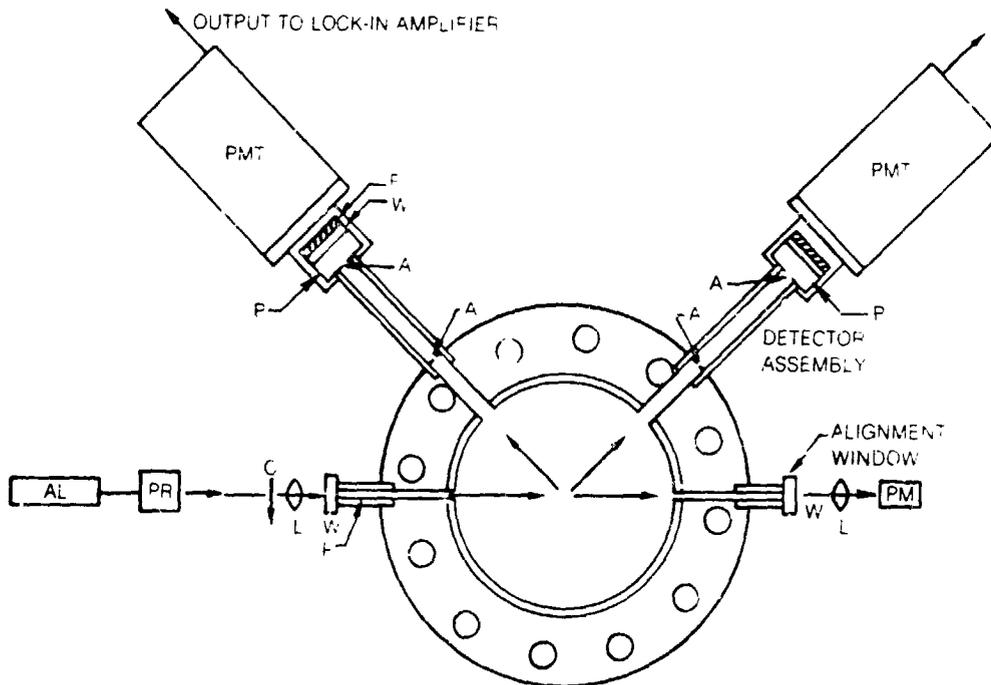
A	APERTURE
AL	ARGON-ION LASER
C	MECHANICAL CHOPPER
F	NARROW BAND OPTICAL FILTER AND POLARIZER
L	LENSE
P	NITROGEN PURGE
PM	POWER METER
PMT	PHOTOMULTIPLIER
PR	POLARIZATION ROTATOR
W	WINDOW

Fig. 21 Layout of Particle Sizing Apparatus

NOTE EACH SYMBOL REPRESENTS A DIFFERENT TEST DAY

DOME RADIATION (kW/m^2)

NOZZLE NUMBER (NN)

RELATIVE ATOMIZATION   SMD(NN)/SMD(NN = 30)
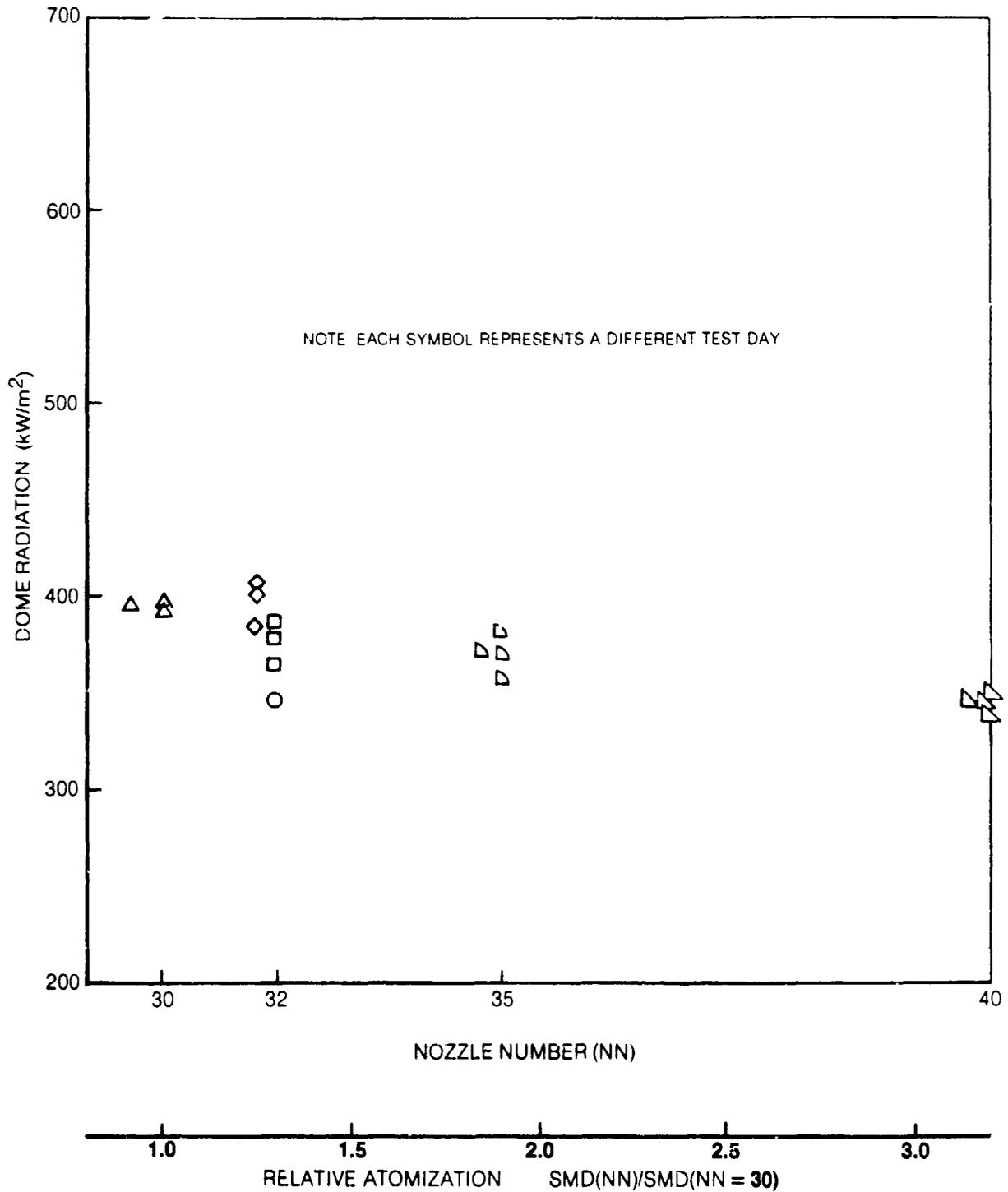
Fig. 22 Variation of Dome Radiation for Jet A-U Fuel

	FUEL	TEST CONDITION
◇	JET A-U	1
▢	ERBS	1
○	ERBS	2
△	ERBS	3
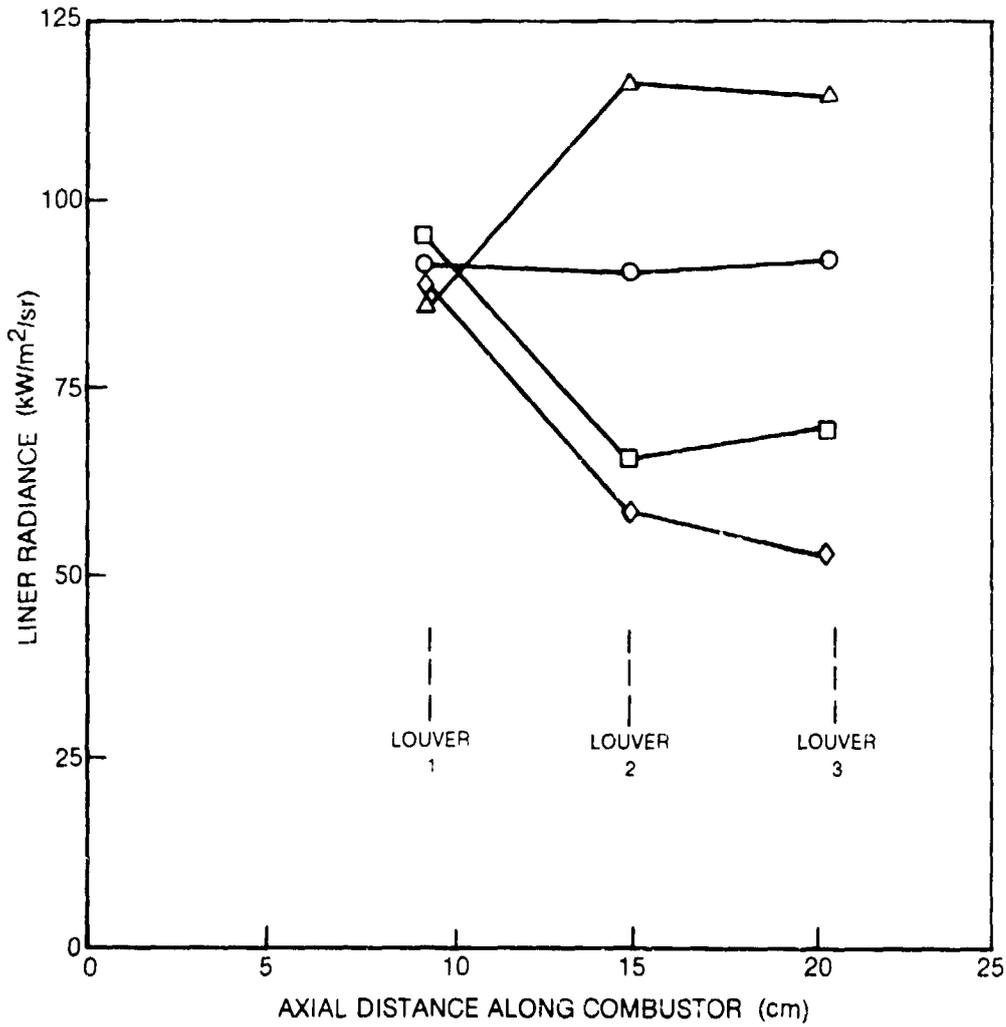
Fig. 23 Axial Distribution of Liner Radiance for ERBS Fuel
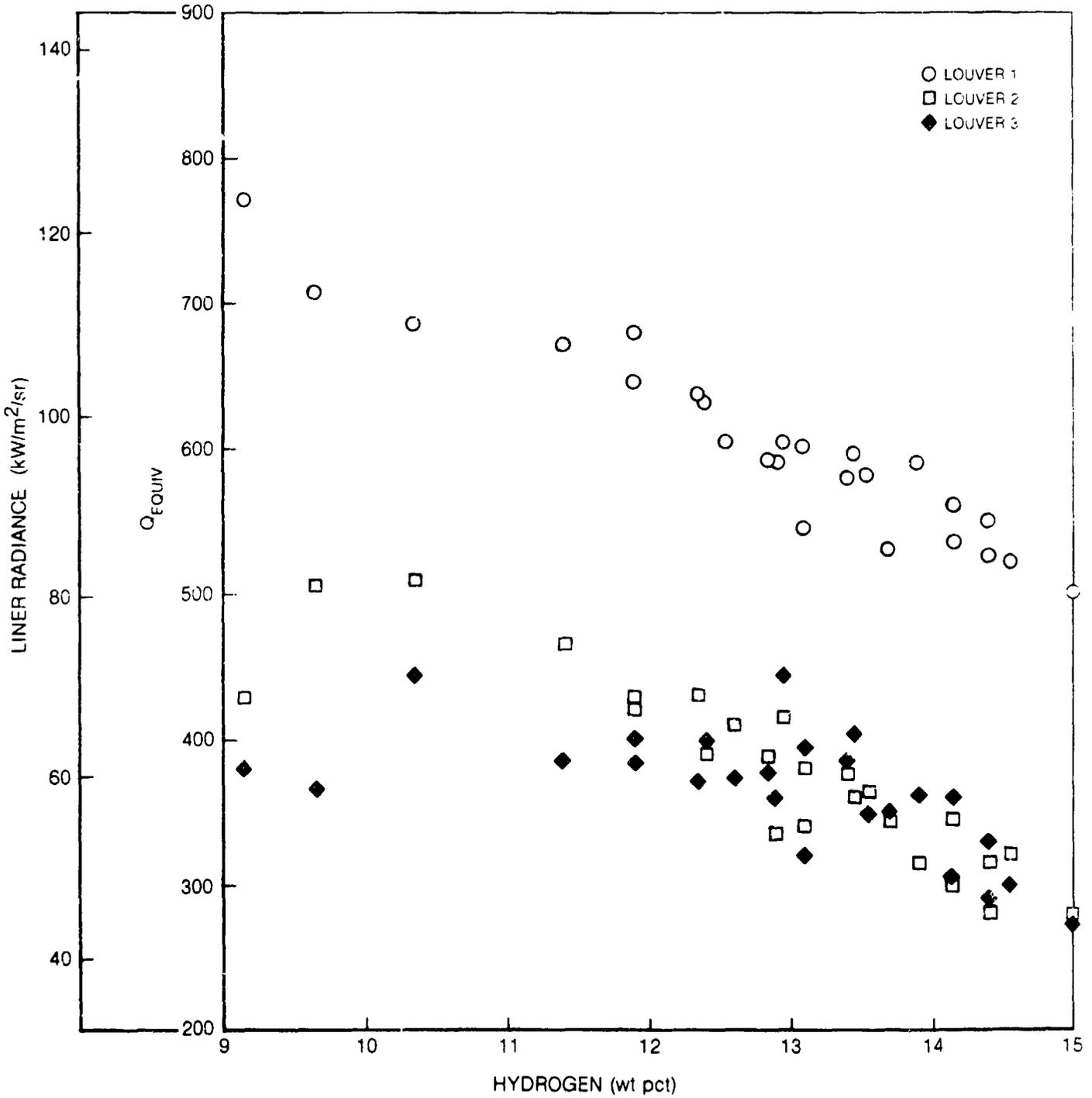
Fig. 24 Variation of Liner Radiance for Test Condition 1

ORIGINAL PAGE IS
OF POOR QUALITY
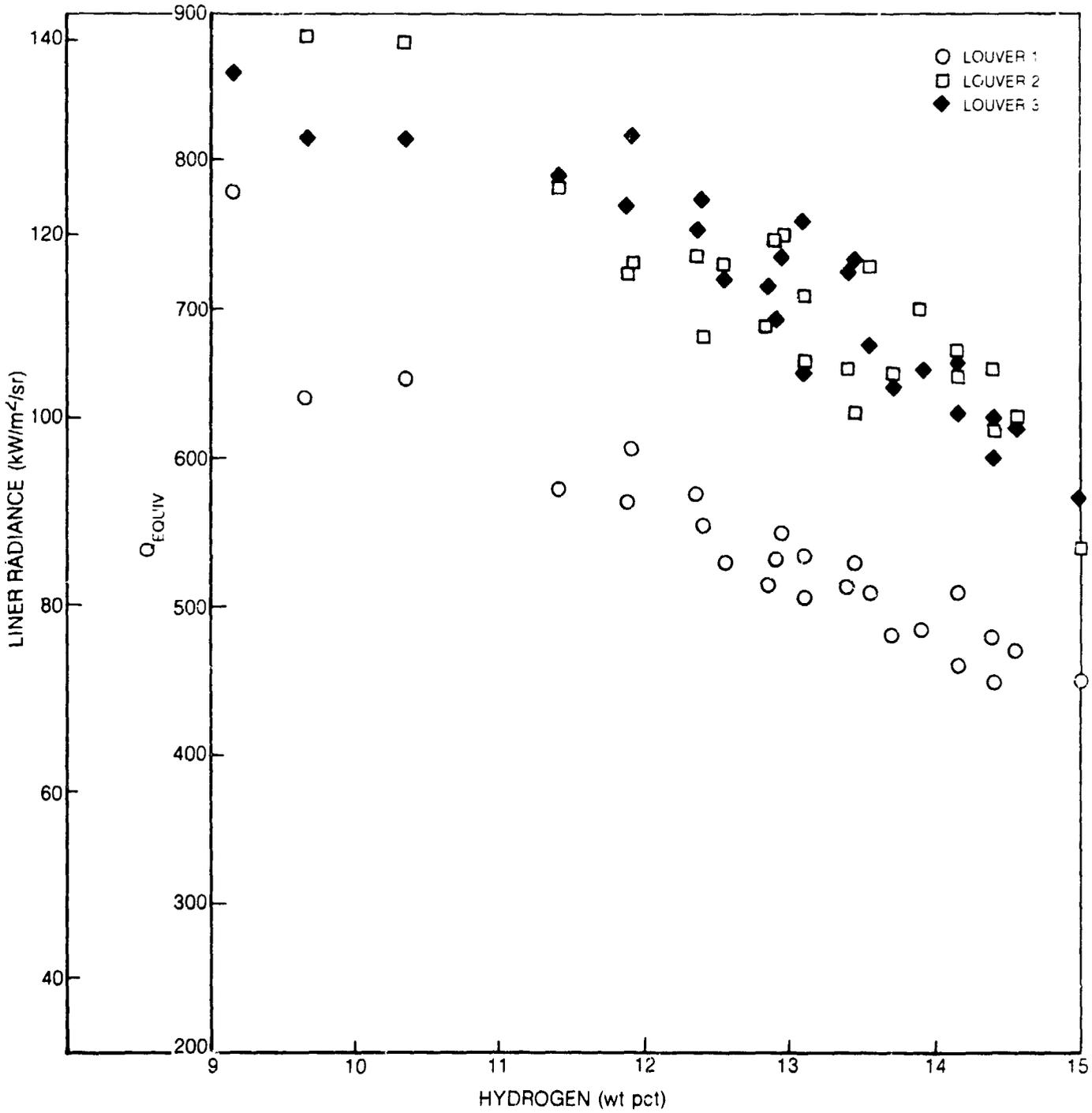
Fig. 25 Variation of Liner Radiance for Test Condition 3

83-7-29-25
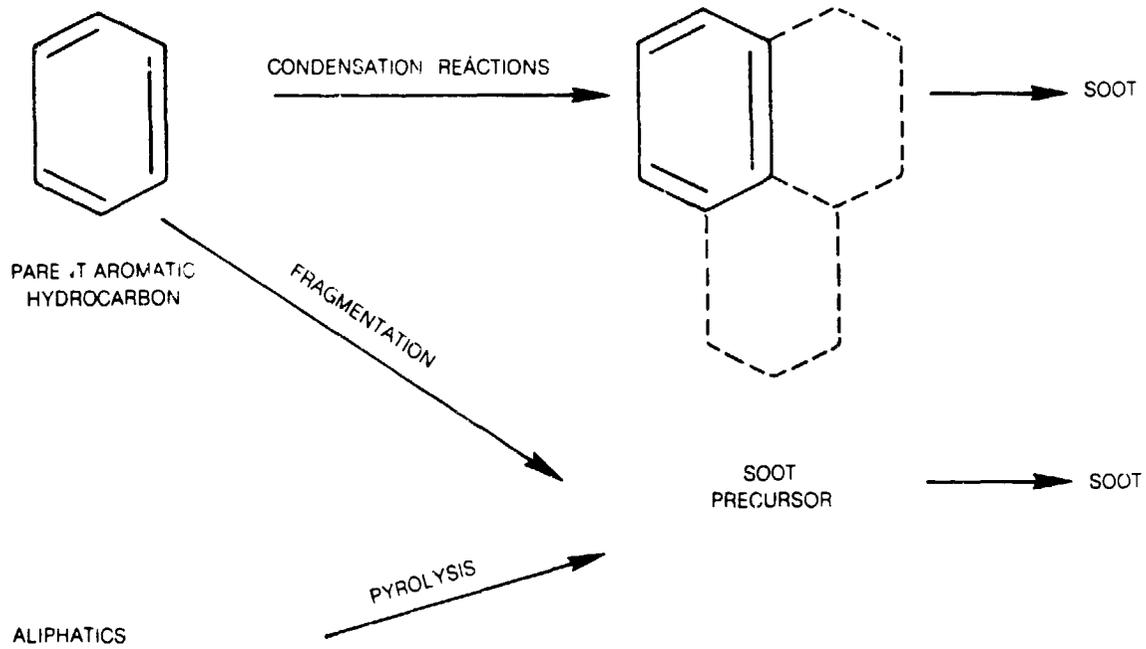
Fig. 26 Active Sooting Mechanisms for Aviation Fuels
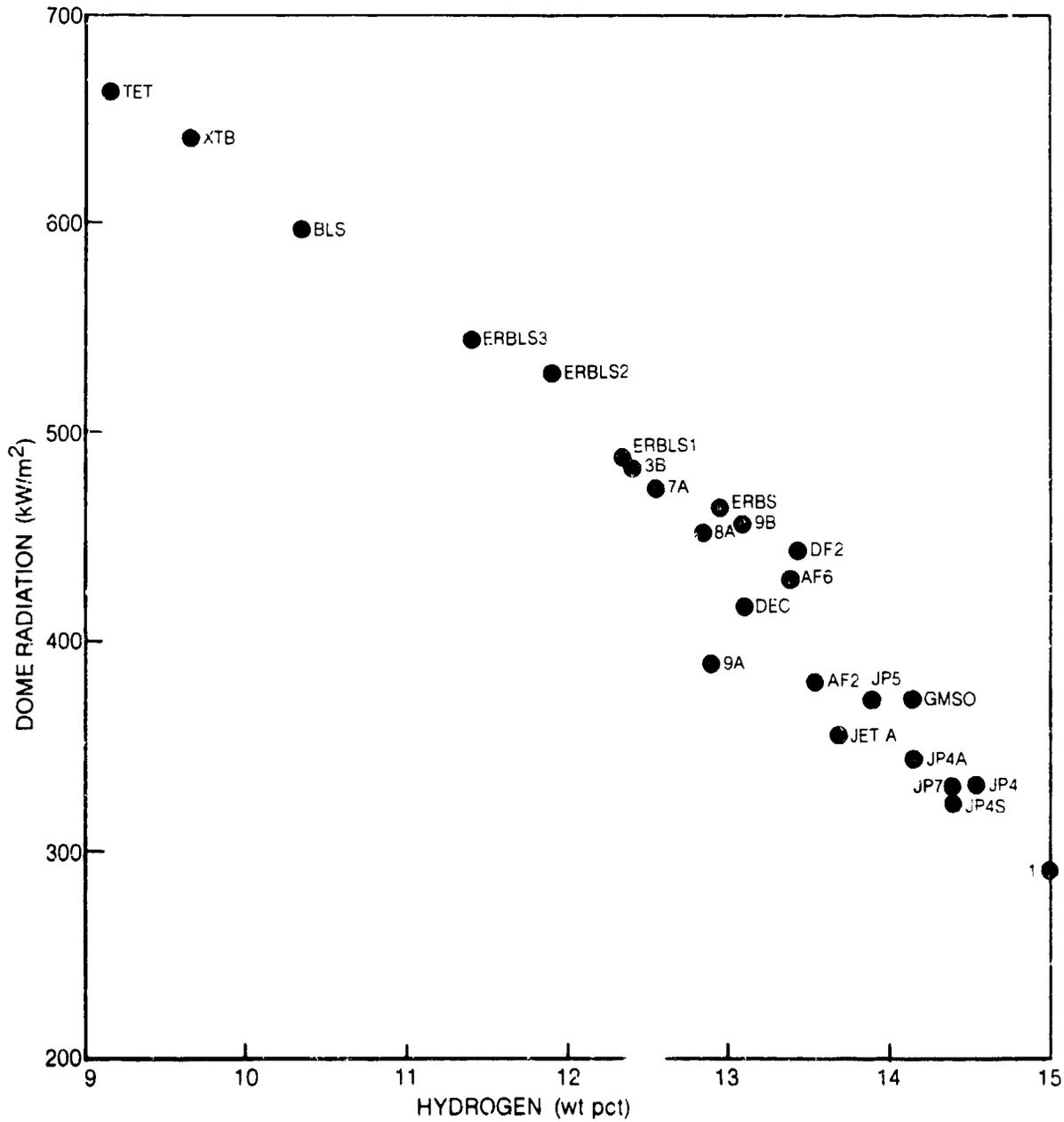
Fig. 27 Dependence of Dome Radiation on Fuel Hydrogen Content for Test Condition 2
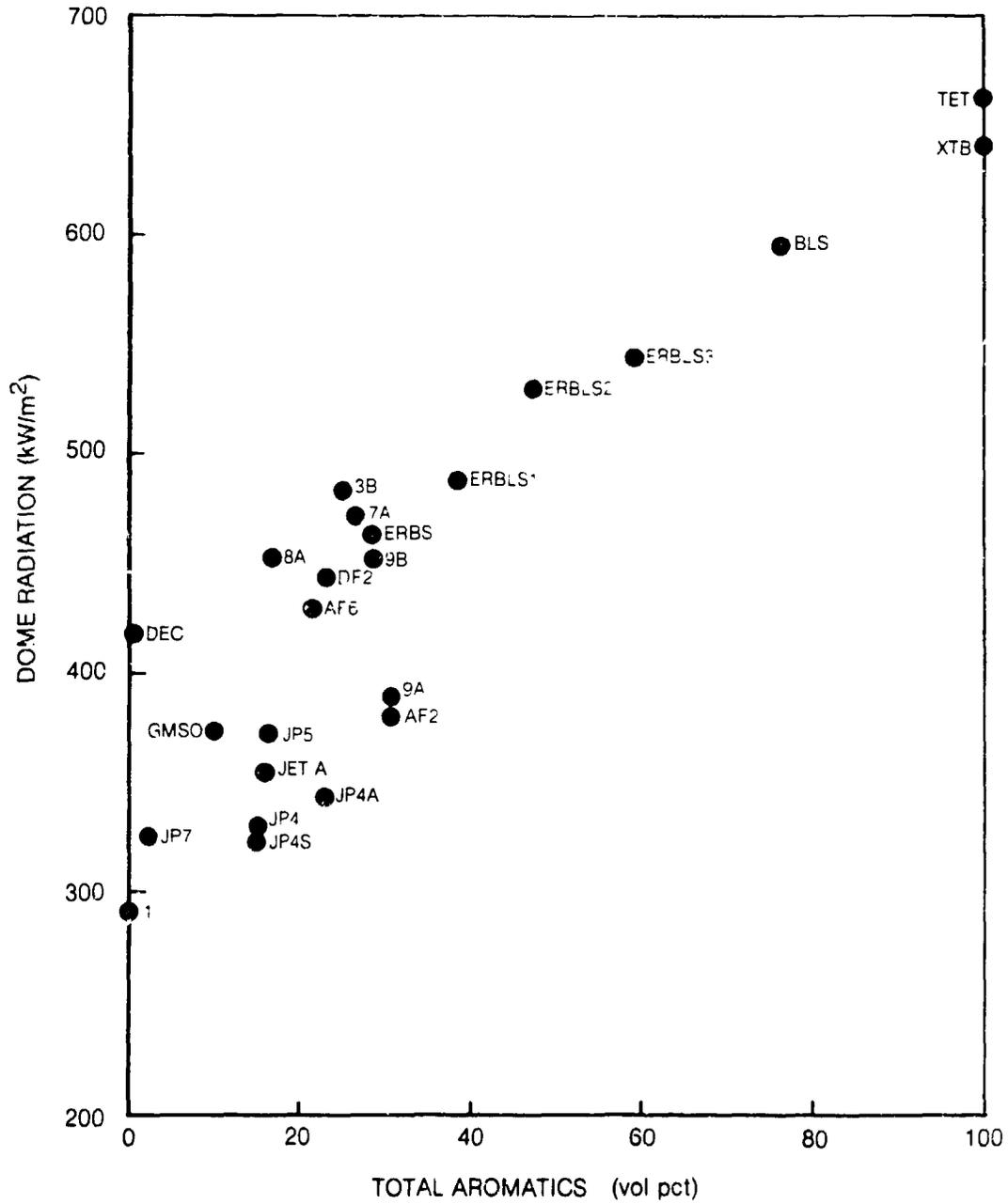
Fig. 28 Dependence of Dome Radiation on Fuel Total Aromatic Content for Test Condition 2
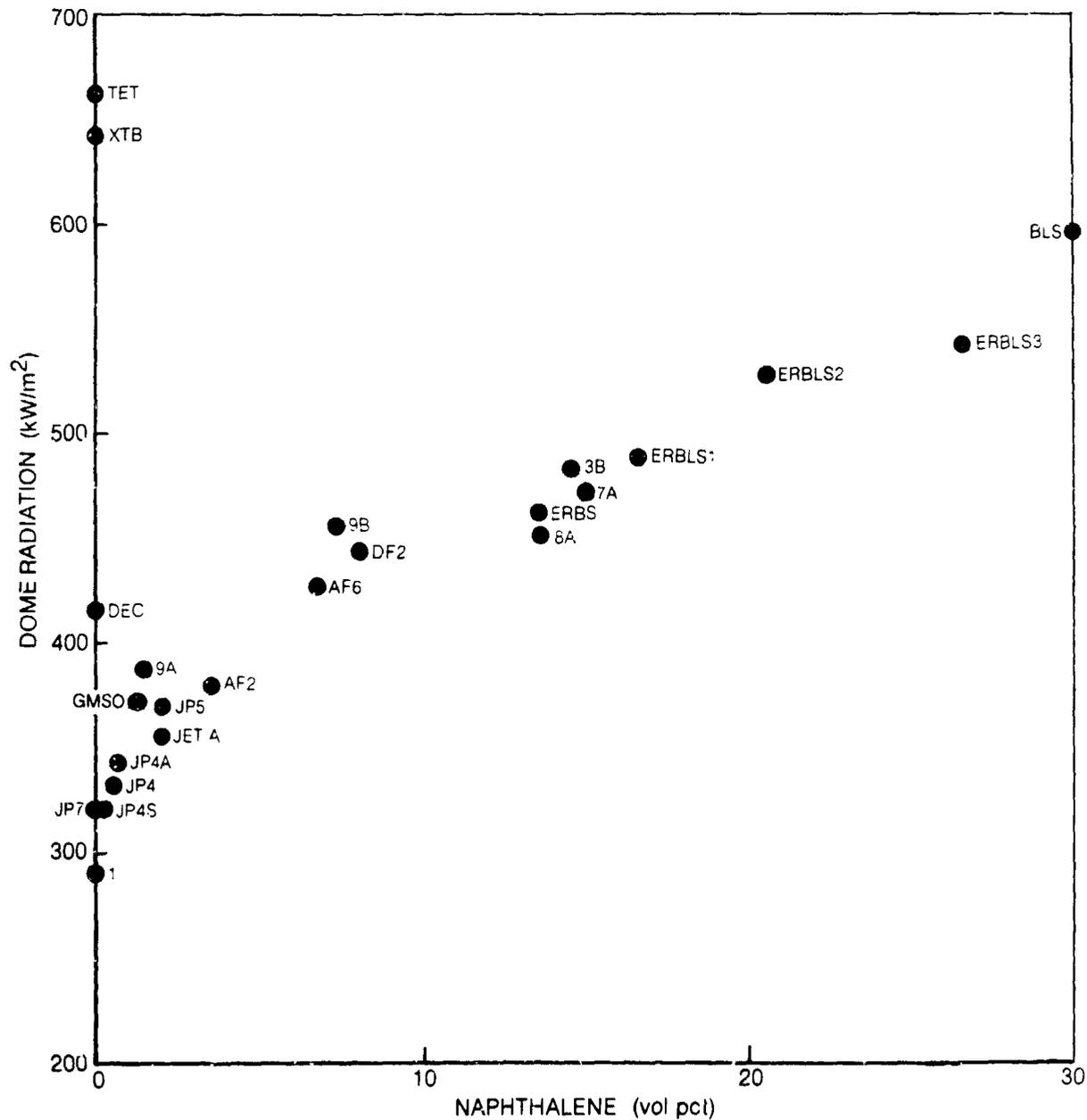
Fig. 29 Dependence of Dome Radiation on Fuel Naphthalene Content for Test Condition 2
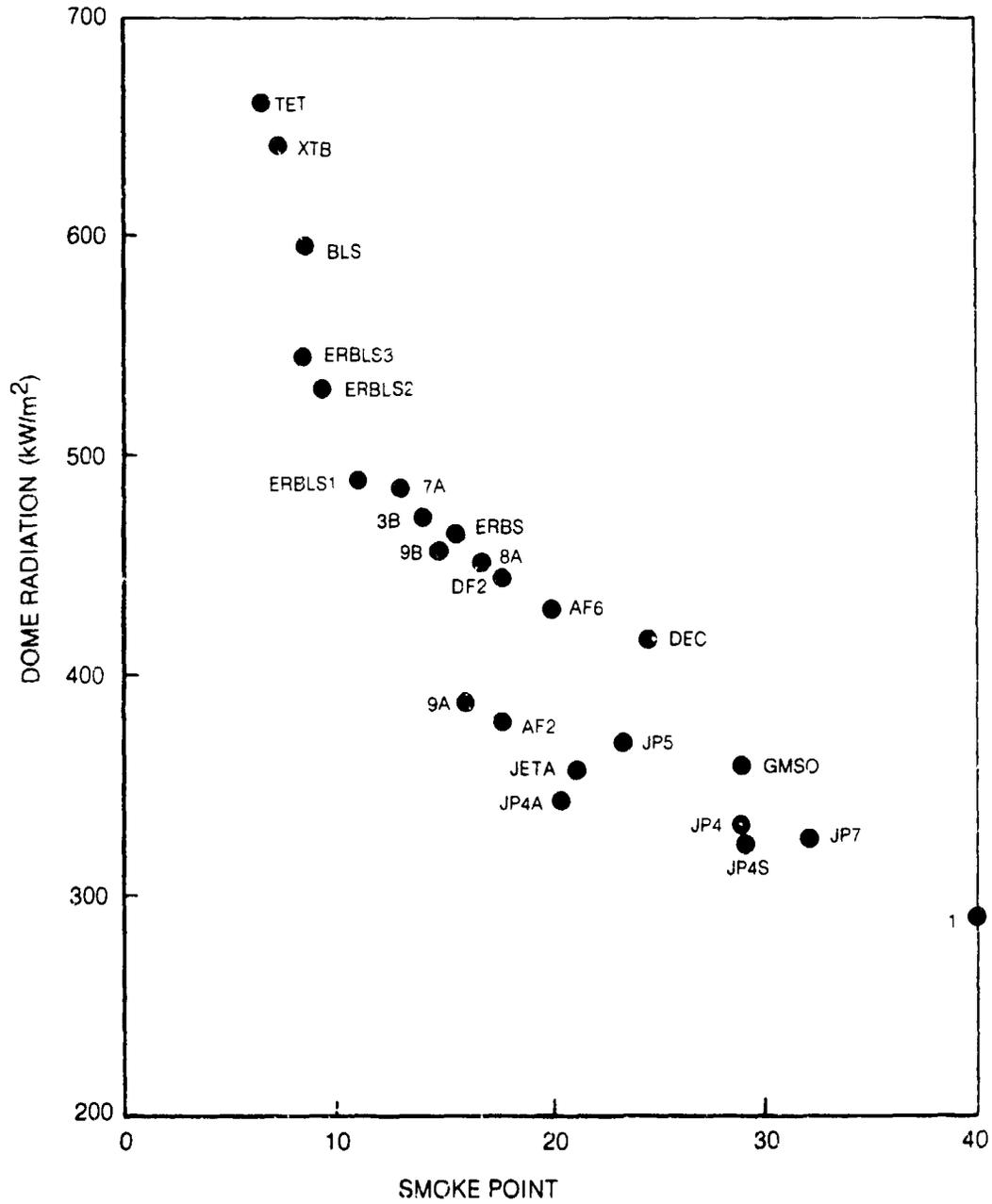
Fig. 30 Dependence of Dome Radiation on Fuel Smoke Point for Test Condition 2
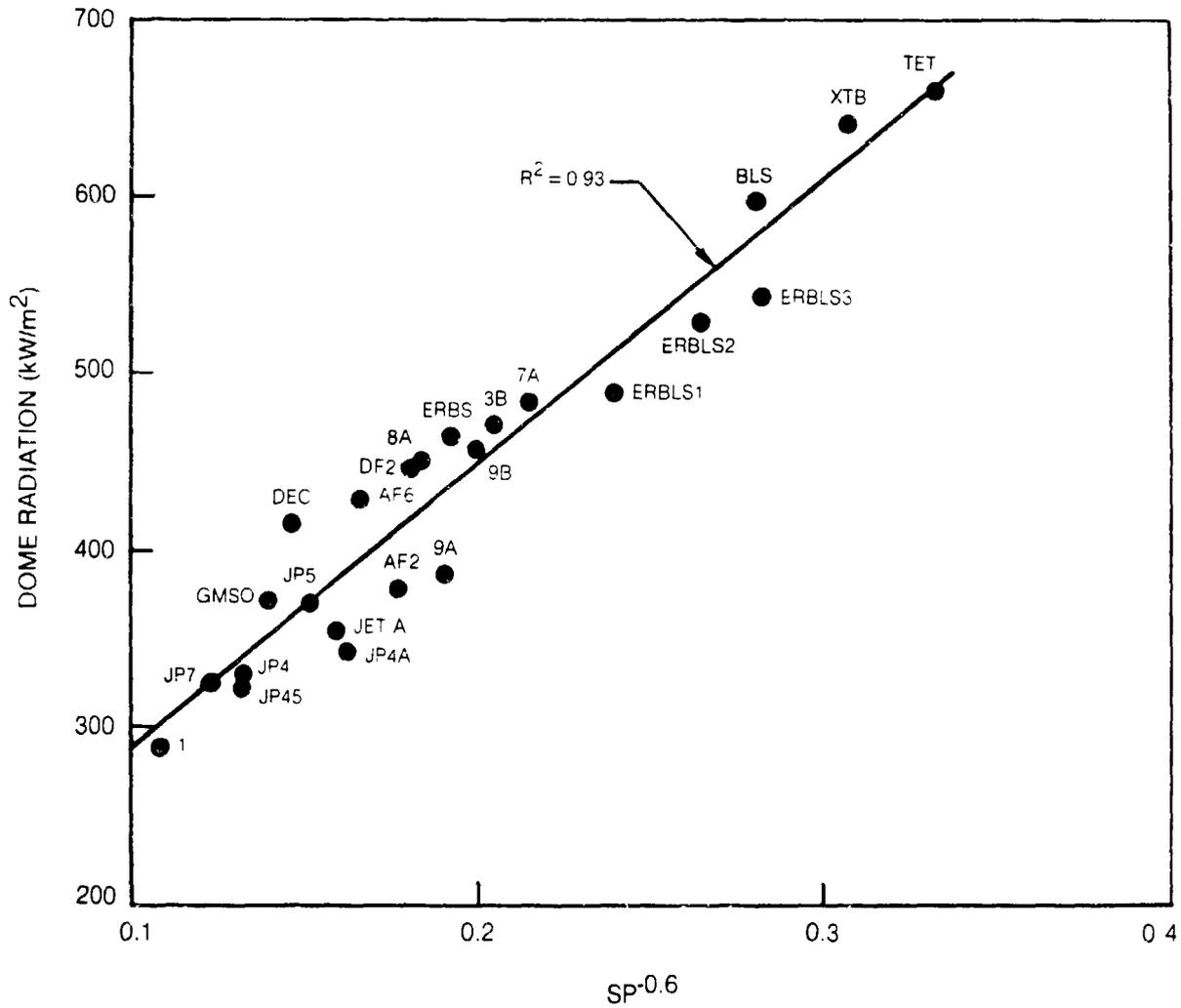
Fig. 31 Correlation of Dome Radiation with Smoke Point for Test Condition 2
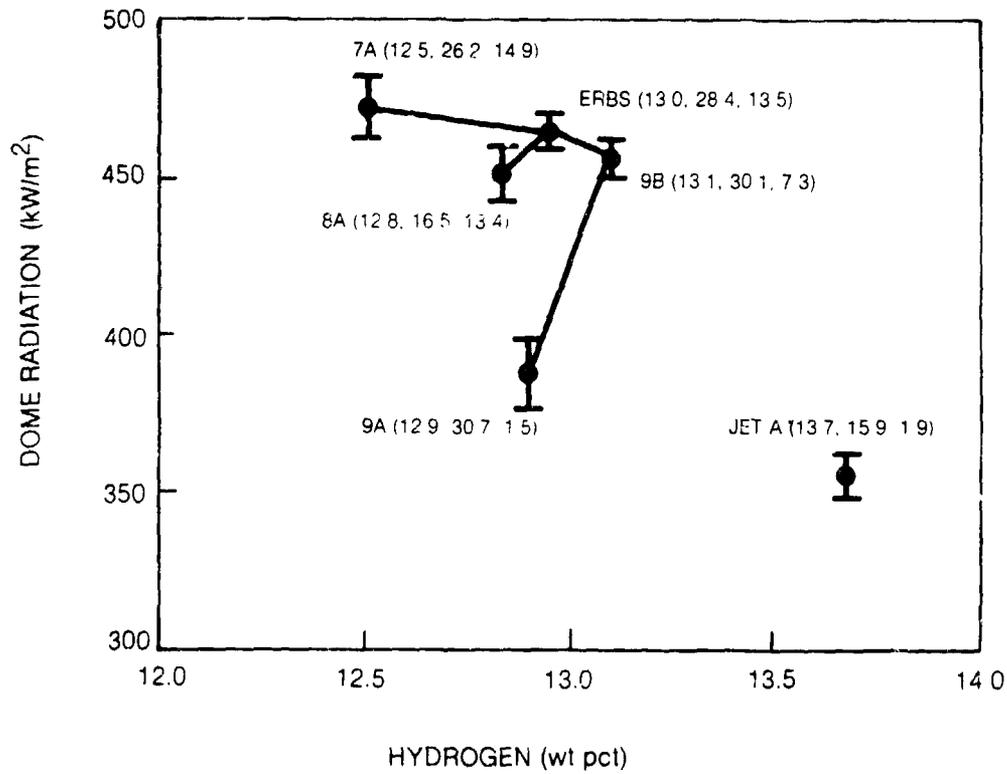
Fig. 32 Influence of Parametric Fuel Property Variations on Dome Radiation for Test Condition 2

ORIGINAL PAGE IS
OF POOR QUALITY
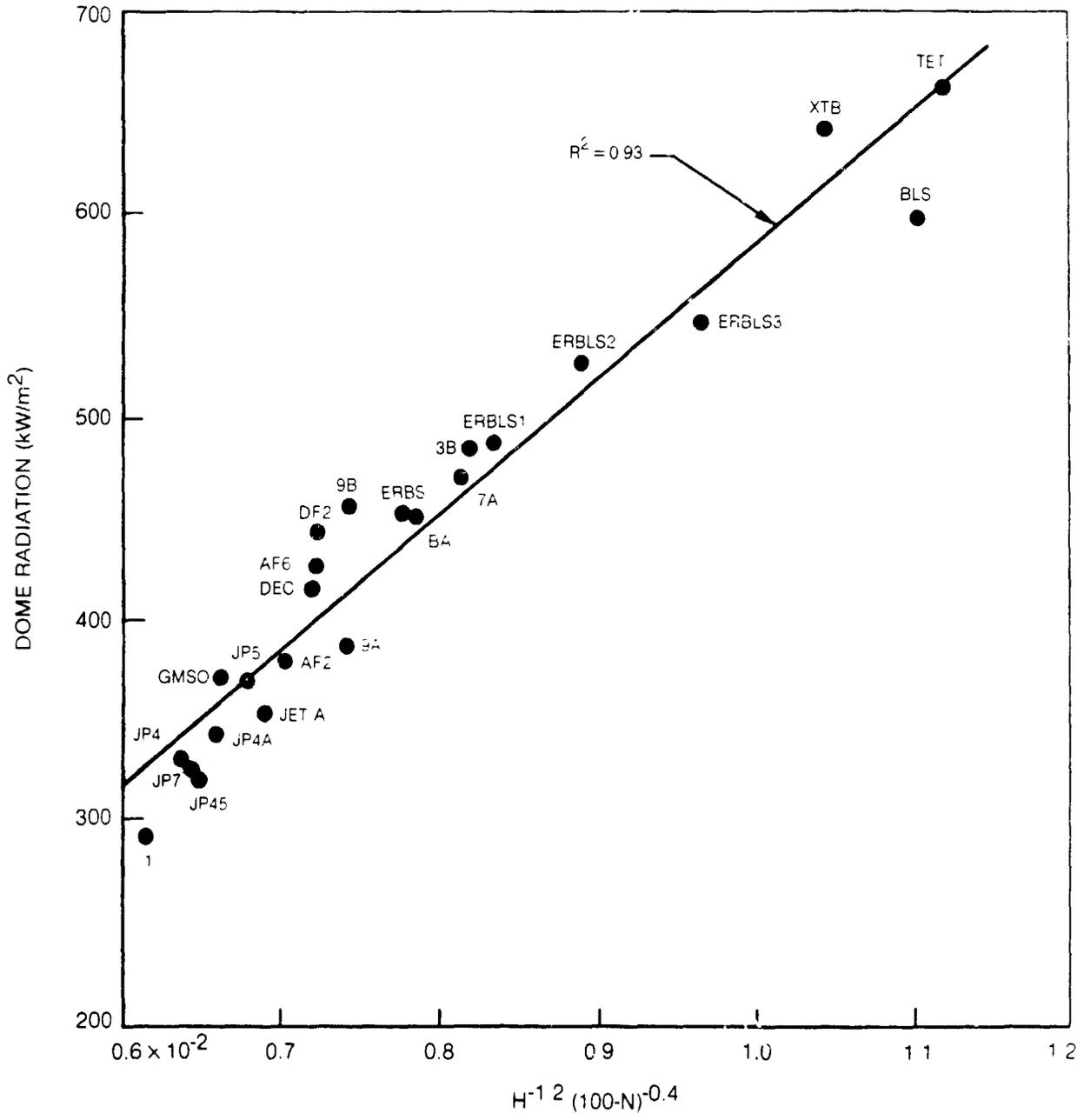
Fig. 33 Correlation of Dome Radiation with Fuel Chemical Properties
for Test Condition 2
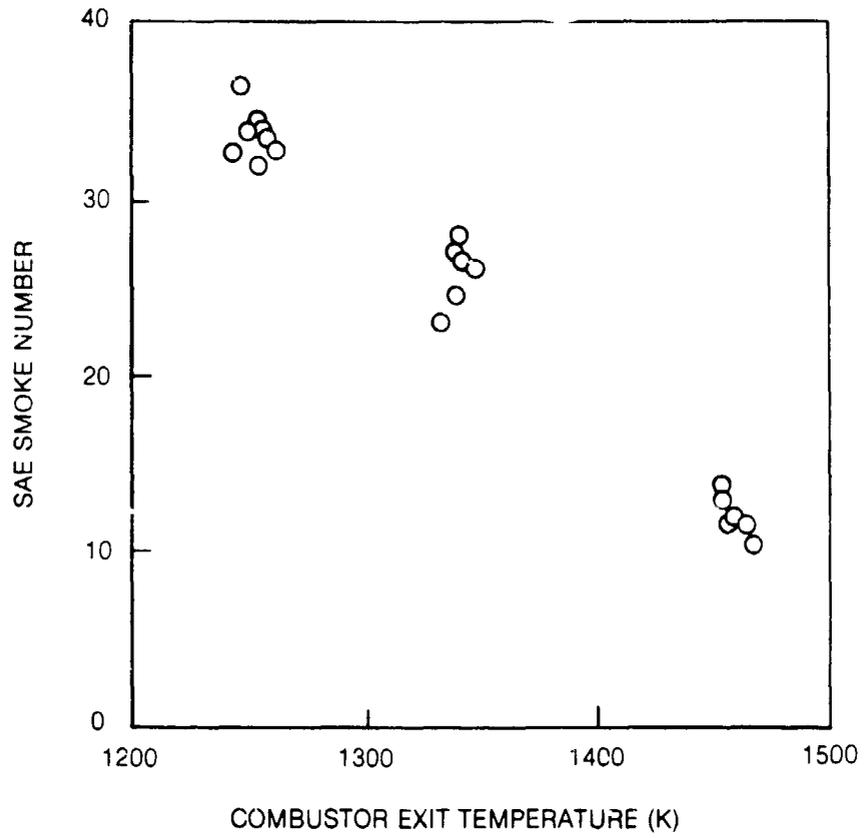
Fig. 34 Influence of Operating Condition on Smoke Number for ERBS Fuel
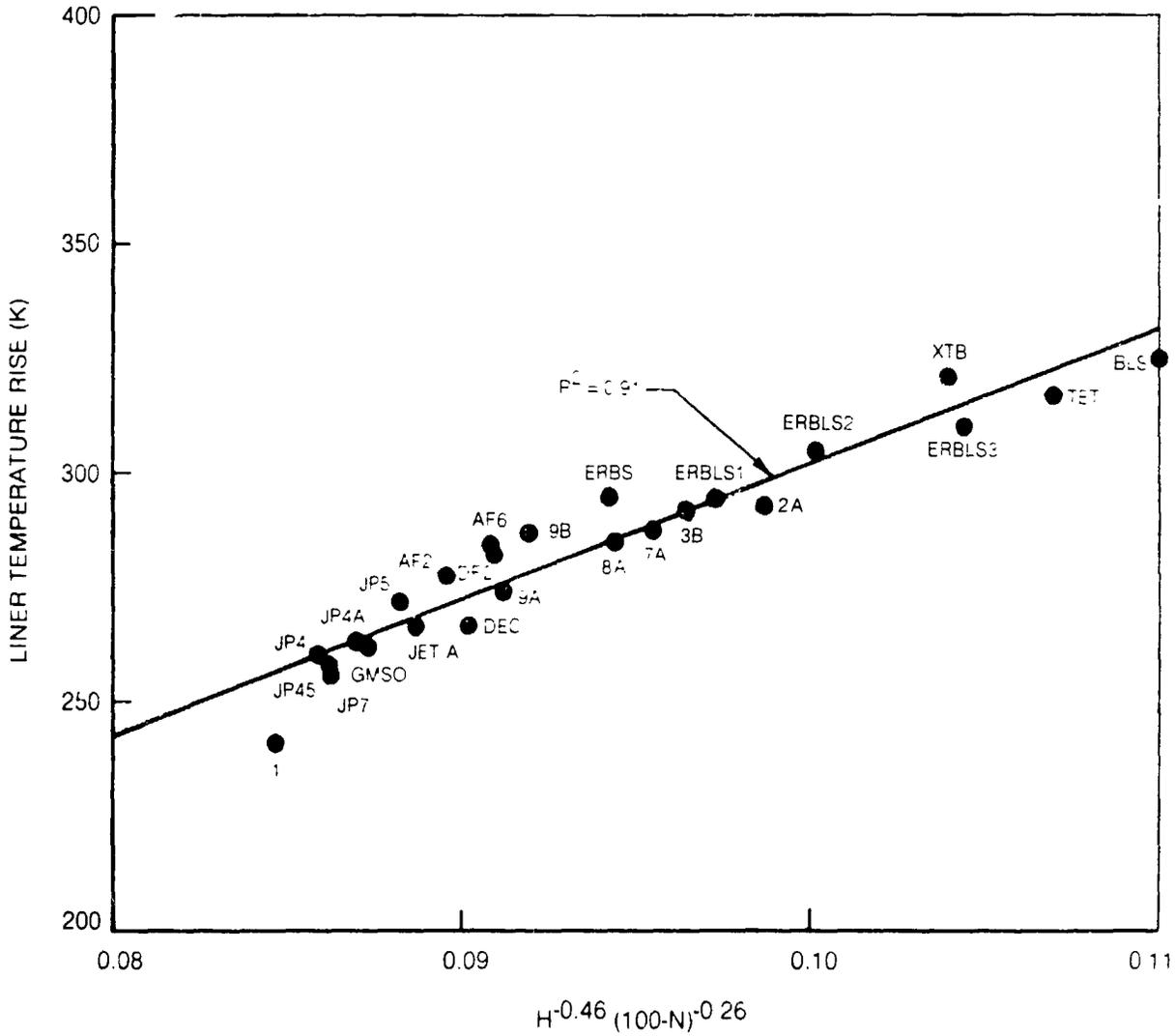
Fig. 35 Correlation of Liner Temperature Rise with Fuel Chemical Properties for Test Condition 2

84-1-104-3
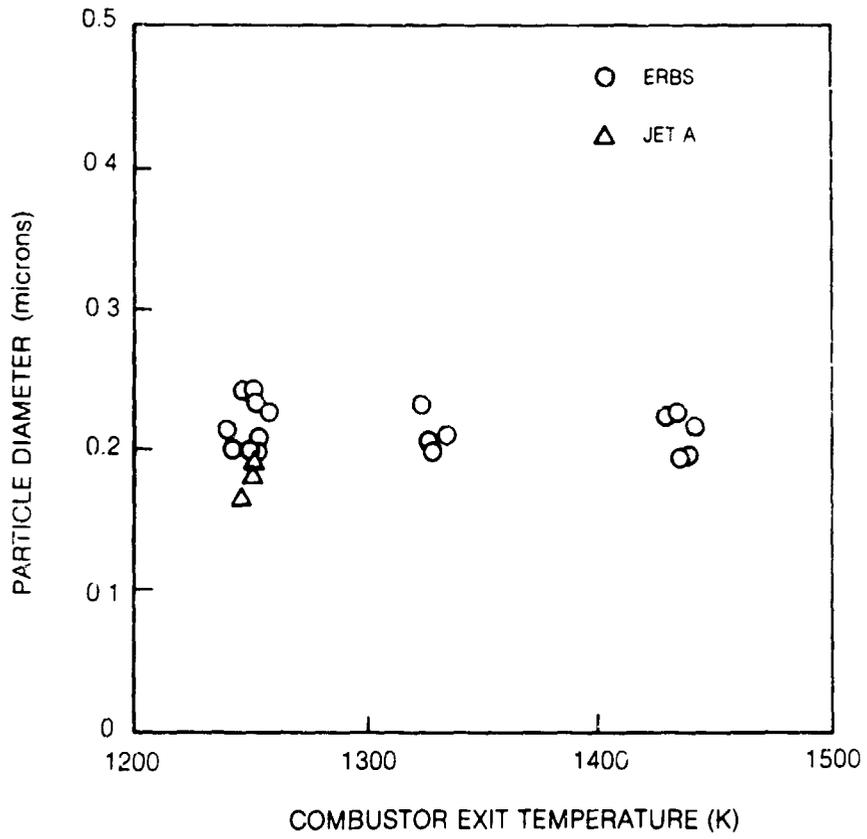
Fig. 36 Influence of Operating Condition on Particulate Diameter for ERBS Fuel
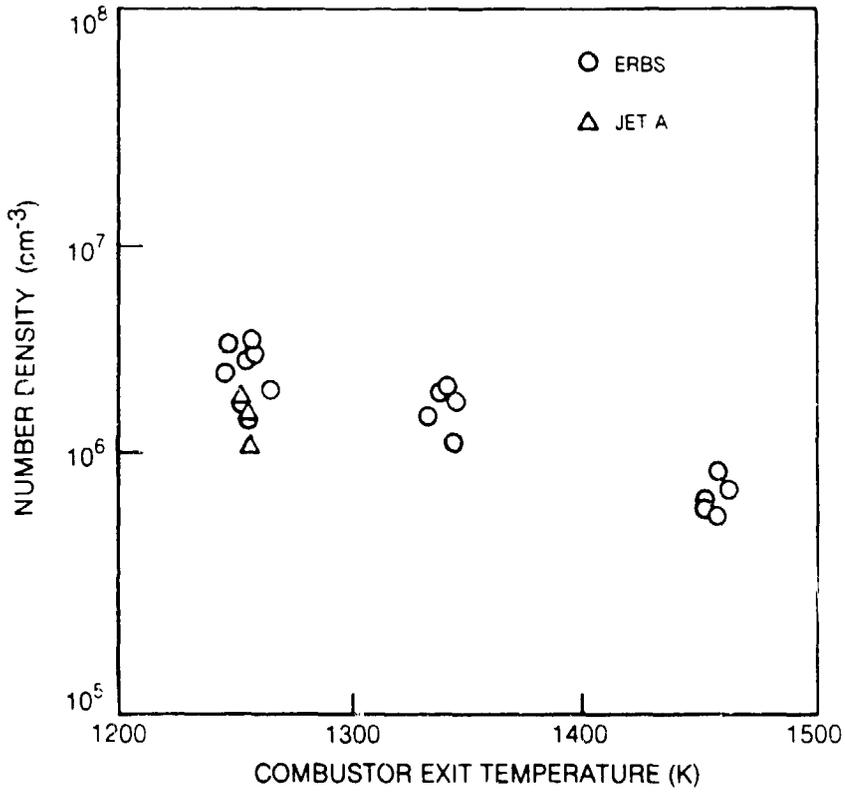
Fig. 37 Influence of Operating Condition on Particulate Number Density for ERBS Fuel

83-7-29-34

ORIGINAL PAGE IS
OF POOR QUALITY

$LOG_{10}N = 4.9 \, SN^{0.082}$

$R^2 = 0.83$

NUMBER DENSITY (cm^{-3})

SMOKE NUMBER

TEST CONDITION

○ 1
□ 2
△ 3
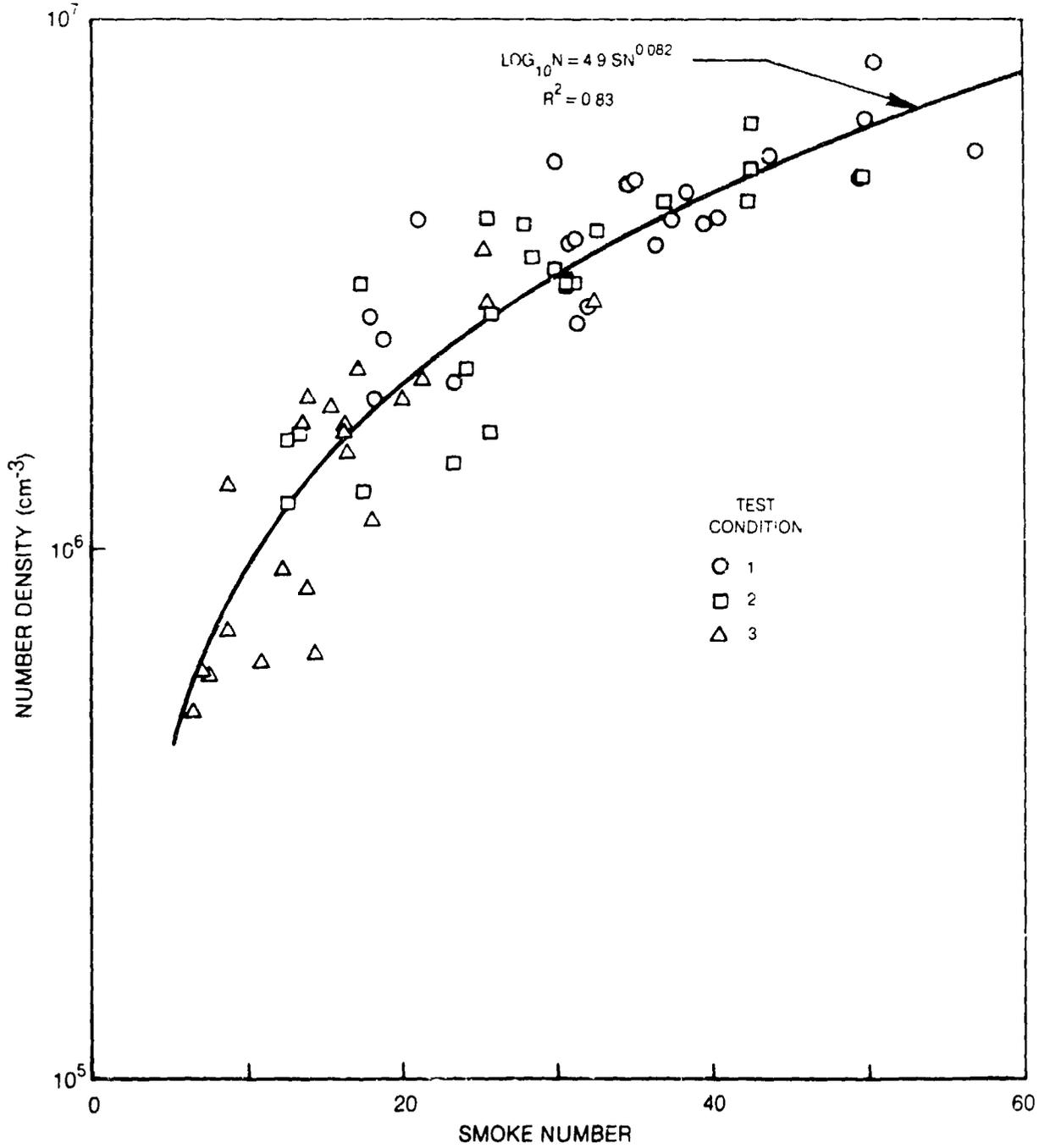
Fig. 38 Soot Number Density Correlated with Smoke Number
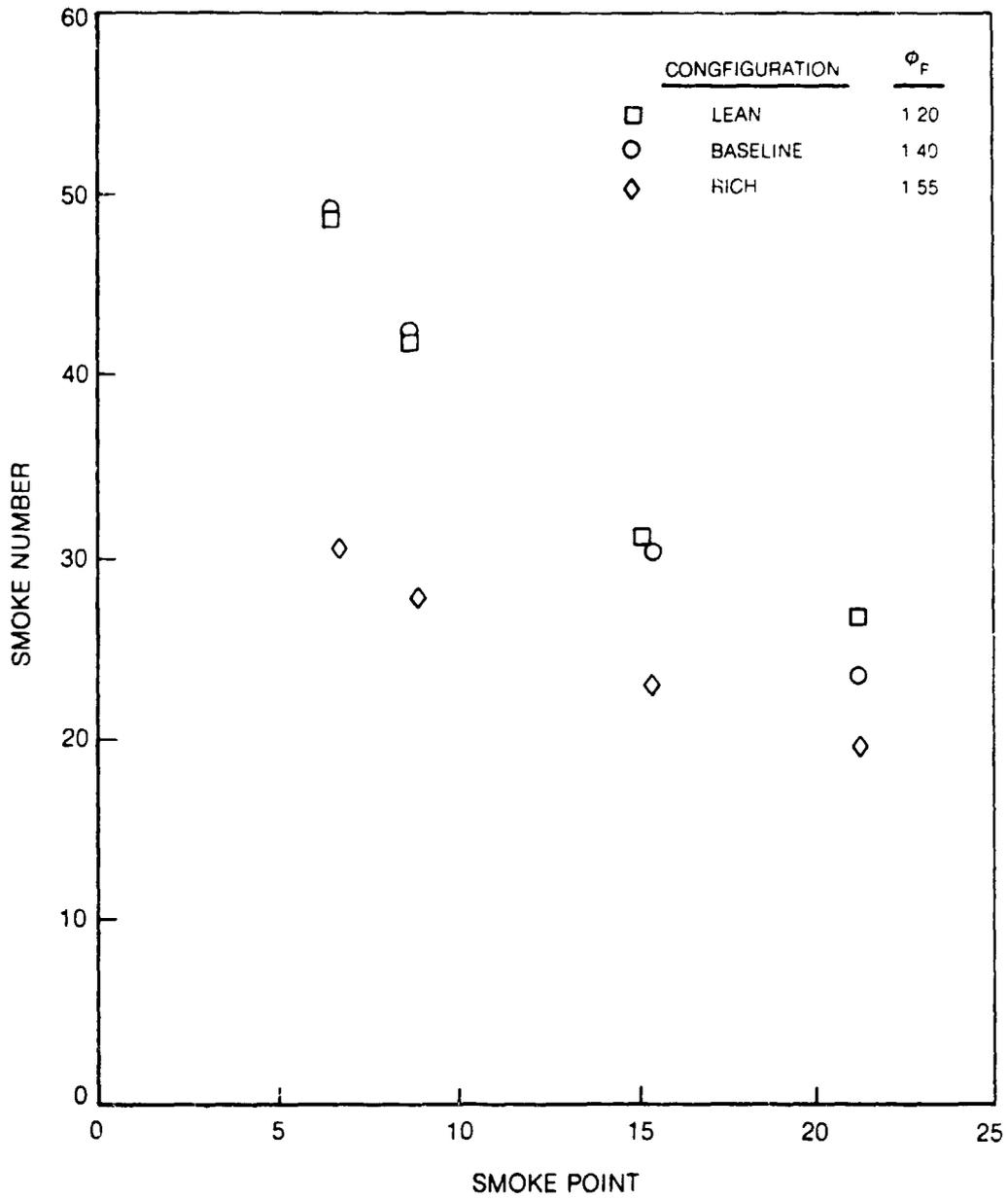
Fig. 39 Influence of Combustor Configuration on Exhaust Smoke Number
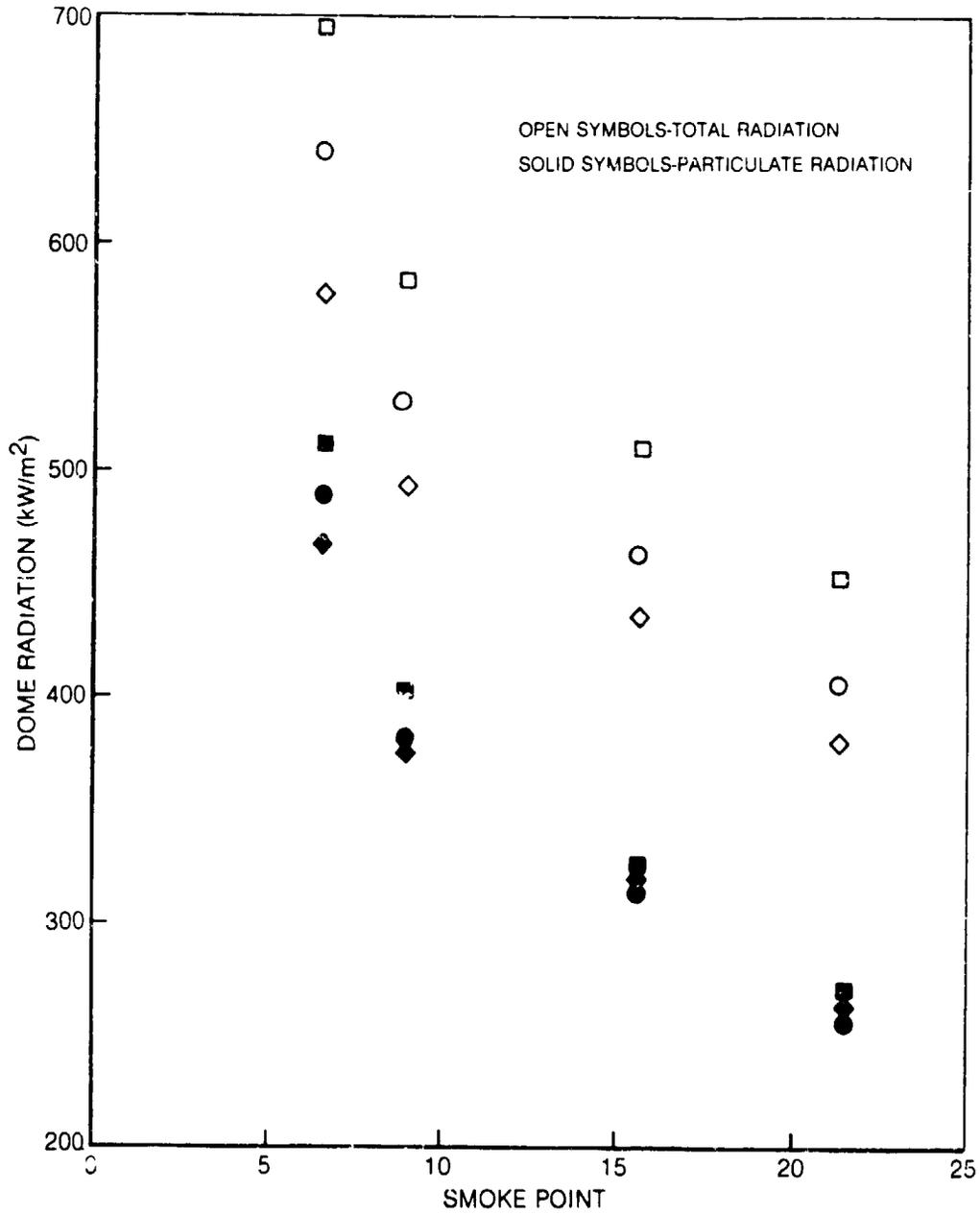
Fig. 40 Influence of Primary Zone Equivalence Ratio on Dome Radiation at Test Condition 2
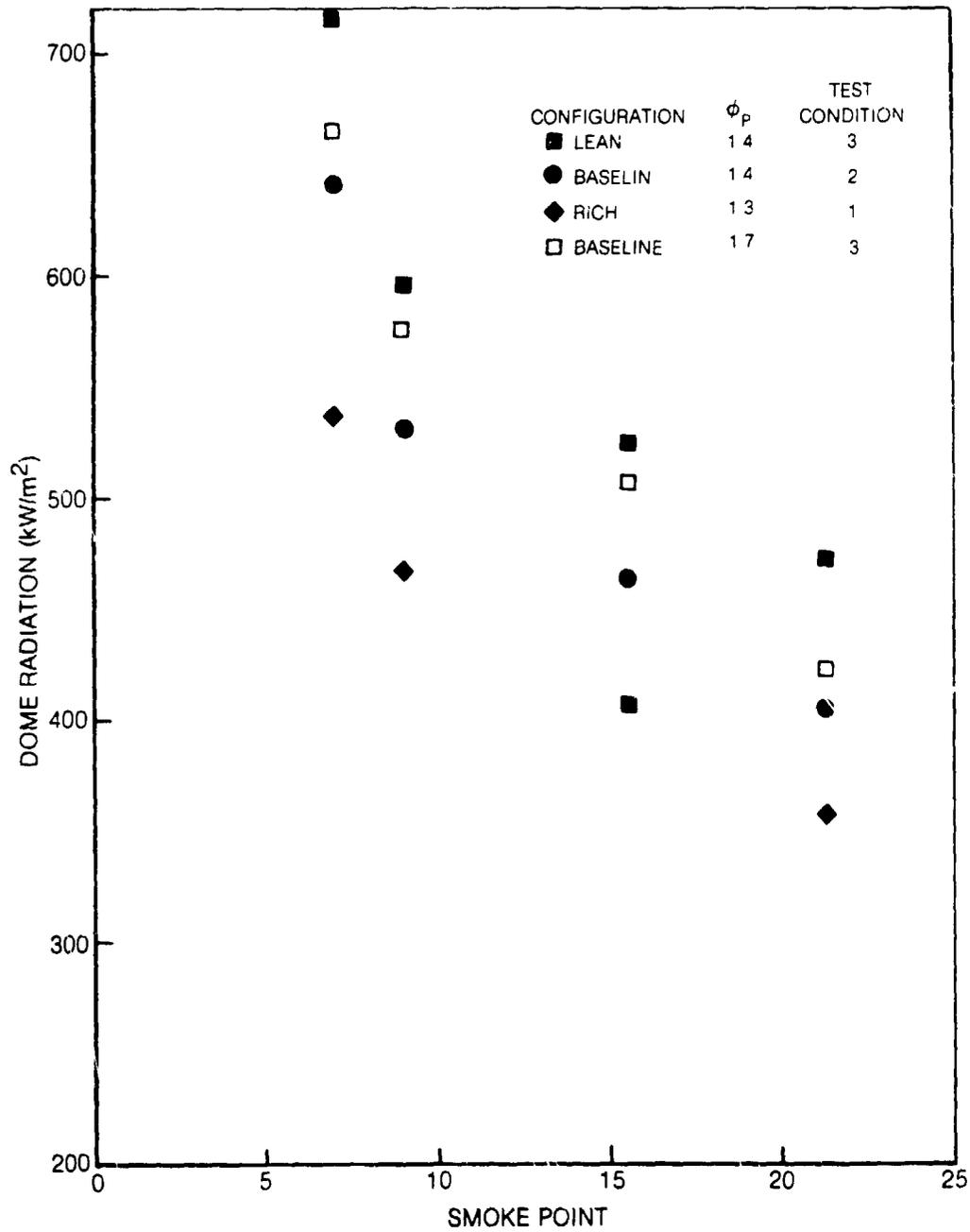
Fig. 41 Influence of Combustor Configuration on Dome Radiation

83-7-29-37

APPENDIX - DATA TABLES

This appendix presents data which supplement the discussion of fuel chemical property influences. A complete tabulation of all data is contained in the contract Comprehensive Data Report. The following data are presented in two forms. First, three tables, one for each test condition, display the normalized combustor parameters obtained for each test fuel. Second, as referenced in Section VII, plots of liner temperature rise and exhaust smoke number at Condition 2 are presented with fuel hydrogen, total aromatic, or naphthalene contents or smoke point as independent variables.

Appendix Tables

1. Normalized Data for Test Condition 1

2. Normalized Data for Test Condition 2

3. Normalized Data for Test Condition 3

Appendix Figures

A-1 Dependence of Liner Temperature Rise on Hydrogen Content at Condition 2

A-2 Dependence of Liner Temperature Rise on Total Aromatic Content at Condition 2

A-3 Dependence of Liner Temperature Rise on Naphthalene Content at Condition 2

A-4 Dependence of Liner Temperature Rise on Smoke Point at Condition 2

A-5 Dependence of Exhaust Smoke Number on Hydrogen Content at Condition 2

A-6 Dependence of Exhaust Smoke Number on Total Aromatic Content at Condition 2

A-7 Dependence of Exhaust Smoke Number on Naphthalene Content at Condition 2

A-8 Dependence of Exhaust Smoke Number on Smoke Point at Condition 2

Appendix Symbols

D   Characteristic soot particulate diameter (μm)

F/A   Overall combustor fuel-air ratio (--)

N   Soot particulate number density at combustor exit (cm^{-3})

PHIP	Primary zone equivalence ratio
QDOME1	Radiation to dome radiometer (kW/m^2)
QCASE1	Equivalent full-hemispherical radiation at Louver 1 (kW/m^2)
QCASE2	Equivalent full-hemispherical radiation at Louver 2 (kW/m^2)
QCASE3	Equivalent full-hemispherical radiation at Louver 3 (kW/m^2)
SN	Exhaust smoke number (--)
TP	Liner temperature rise parameter (K)

AVIATION FUEL PROGRAM NORMALIZED DATA — TEST CONDITION 1

FUEL NO.	FUEL NAME	F/A	PHIP	QDOME1	QCASE1	QCASE2	QCASE7	TP	SN	N	D
1	UTRC-2A										
2	ERBLS-1										
3	UTRC-7A										
4	JP7										
5	JP4-SHALE										
6	JP4										
7	DF2										
8	AFAPL-6										
9	AFAPL-2										
10	UTRC-3B										
11	UTRC-8A										
12	ERBLS-12										
13	UTRC-9A										
14	UTRC-9B										
15	TETRALIN										
16	XTB										
17	BLS										
18	ERBLS-3										
19	ERBS										
20	DECALIN										
21	JP4-A										
22	JET-A										
23	JP5										
24	GMSO										
25	UTRC-1										

AVIATION FUEL PROGRAM NORMALIZED DATA - TEST CONDITION 2

FUEL NO.	FUEL NAME	F/A	PHIP	QDOME1	QCASE1	QCASE2	QCASE3	TP	SN	N	D
1	UTRC-2A										
2	ERBLS-1										
3	UTRC-7A										
4	JP7										
5	JP4-SHALE										
6	DF2										
7	AFAPL-6										
8	AFAPL-2										
9	UTRC-3B										
10	UTRC-8A										
11	ERBLS-2										
12	UTRC-9A										
13	UTRC-9B										
14	TETRALIN										
15	XTB										
16	BLS										
17	ERBLS-3										
18	DECALIN										
19	JP4-A										
20	JET-A										
21	JP5										
24	GMSO										
25	UTRC-1										

AVIATION FUEL PROGRAM NORMALIZED DATA - TEST CONDITION 3

| FUEL NO.	FUEL NAME	F/A	PHIP	QDOME1	QCASE1	CCASE2	QCASE	TP	SN	N	D
1	UTRC-2A										
2	ERBLS-1										
3	UTRC-7A										
4	JP7										
5	JP4-SHALE										
6	JP4										
7	DF2										
8	AFAPL-6										
9	AFAPL-2										
10	UTRC-3B										
11	UTRC-8A										
12	ERBLS-12										
13	UTRC-9A										
14	UTRC-9B										
15	TETRALIN										
16	XTB										
17	BLS										
18	ERBLS-3										
19	ERBS										
20	DECALIN										
21	JP4-A										
22	JET-A										
23	JP5										
24	GMSO										
25	UTRC-1										

Fig. A-1 Dependence of Liner Temperature Rise on Fuel Hydrogen Content for Test Condition 2
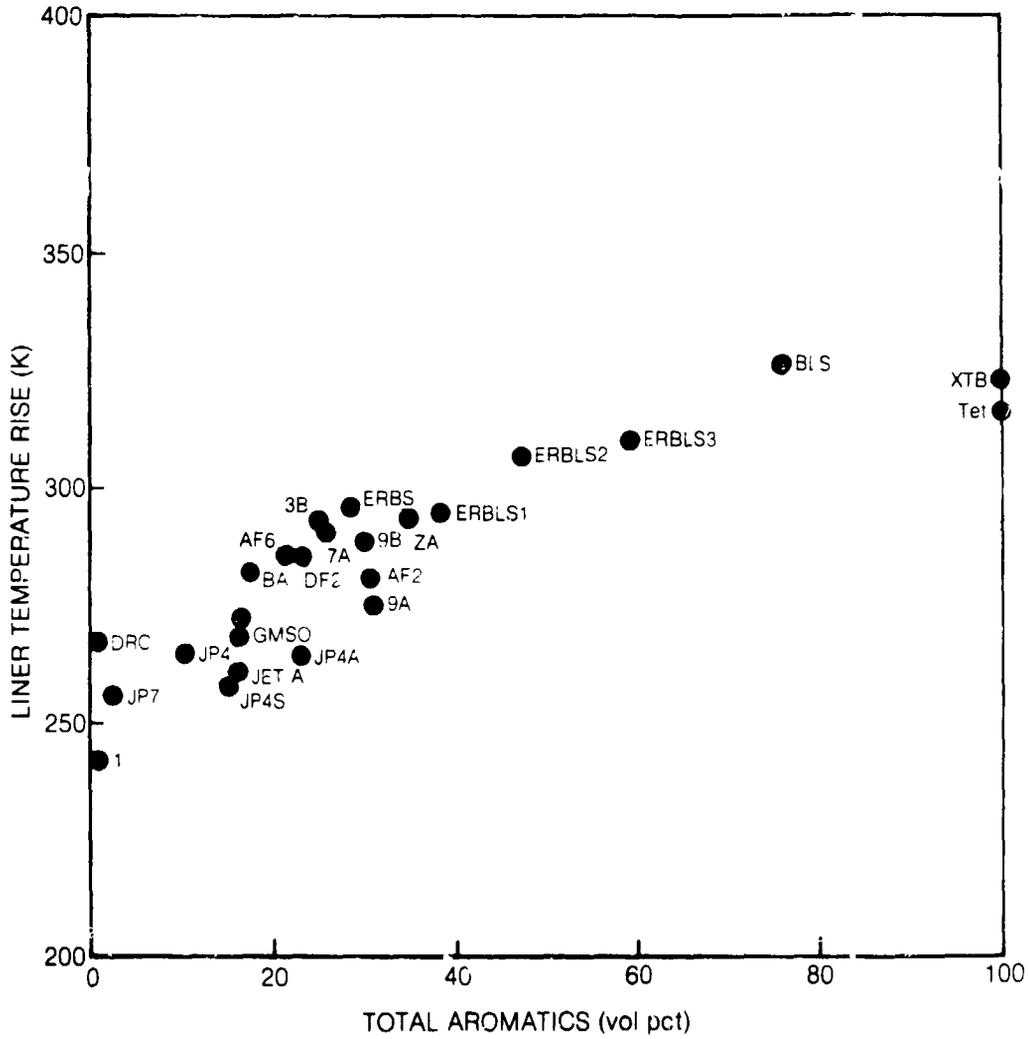
**Fig. A-2 Dependence of Liner Temperature Rise on Fuel Total Aromatic Content for Test Condition 2**

ORIGINAL PAGE IS
OF POOR QUALITY
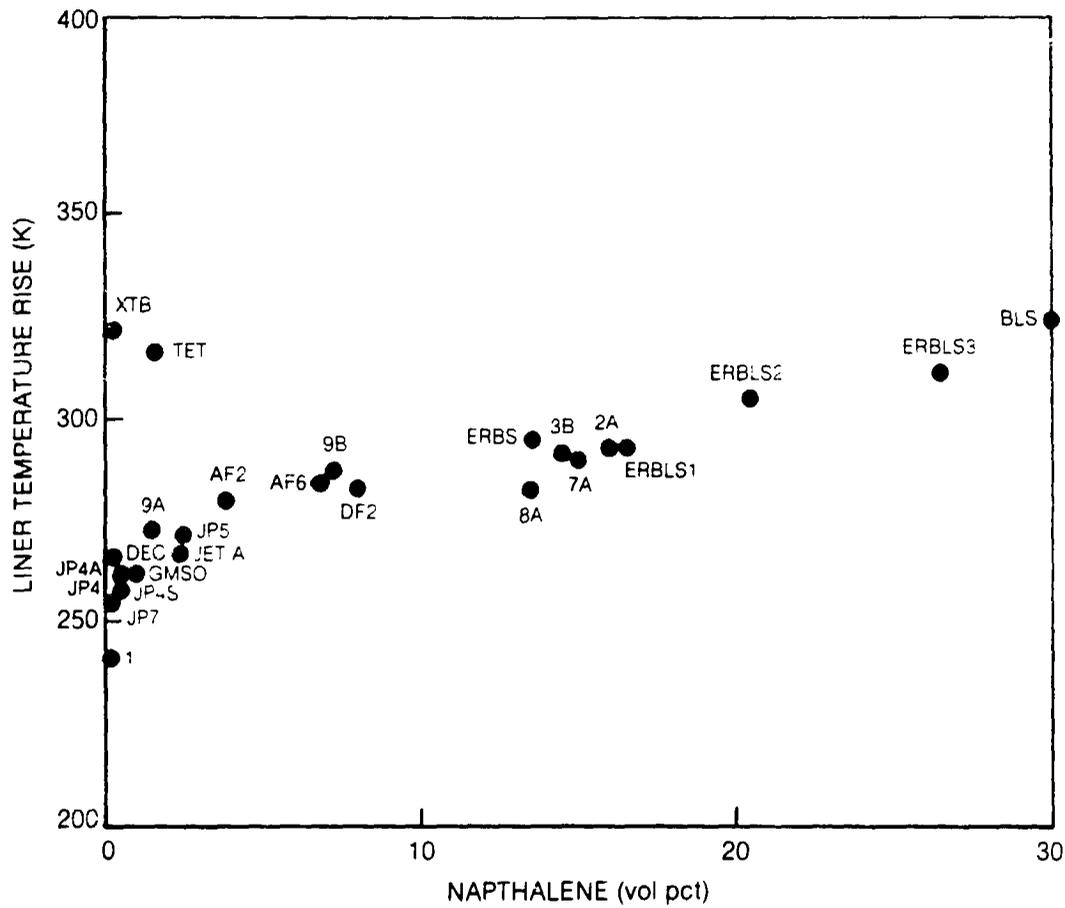
Fig. A-3 Dependence of Liner Temperature Rise on Fuel Napthalene Content
for Test Condition 2

83-7-29-20
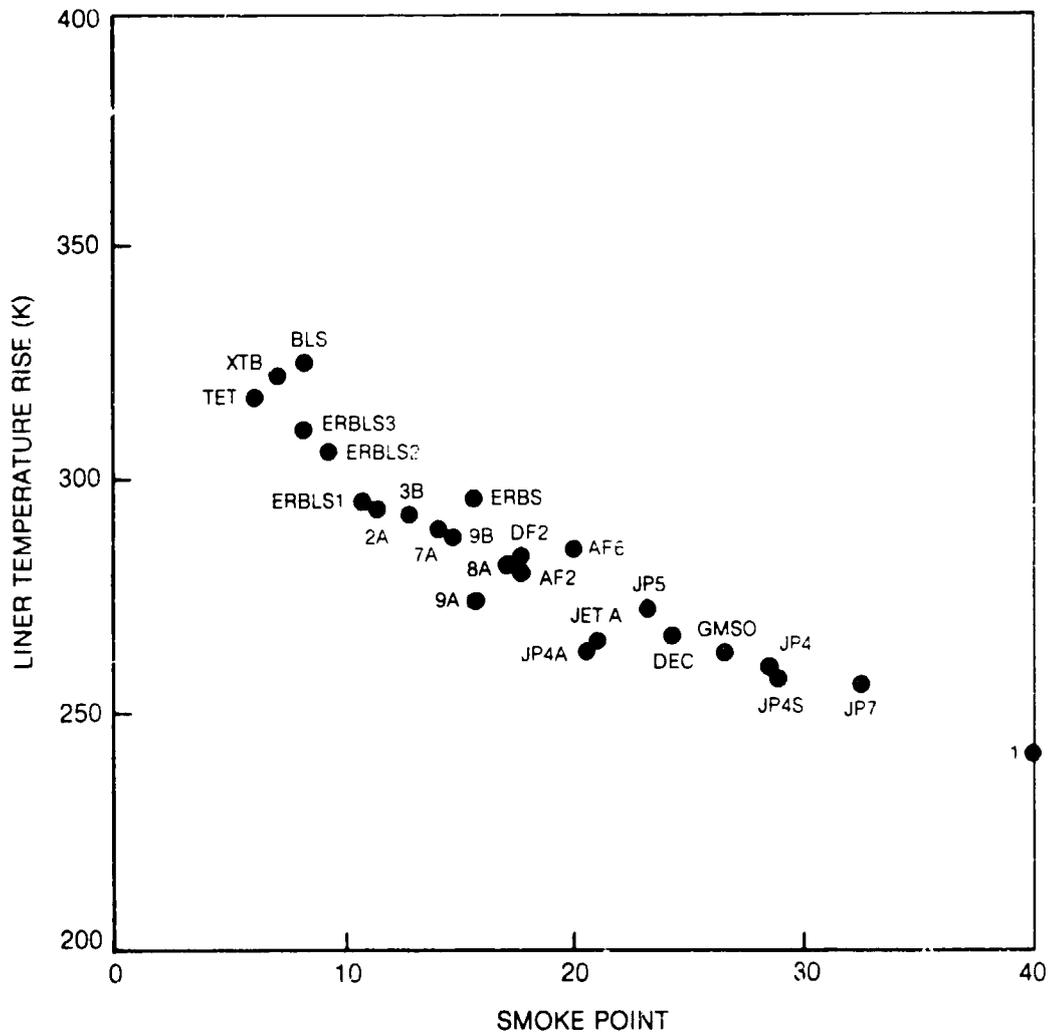
**Fig. A-4 Dependence of Liner Temperature Rise on Smoke Point
for Test Condition 2**

ORIGINAL PAGE IS
OF POOR QUALITY
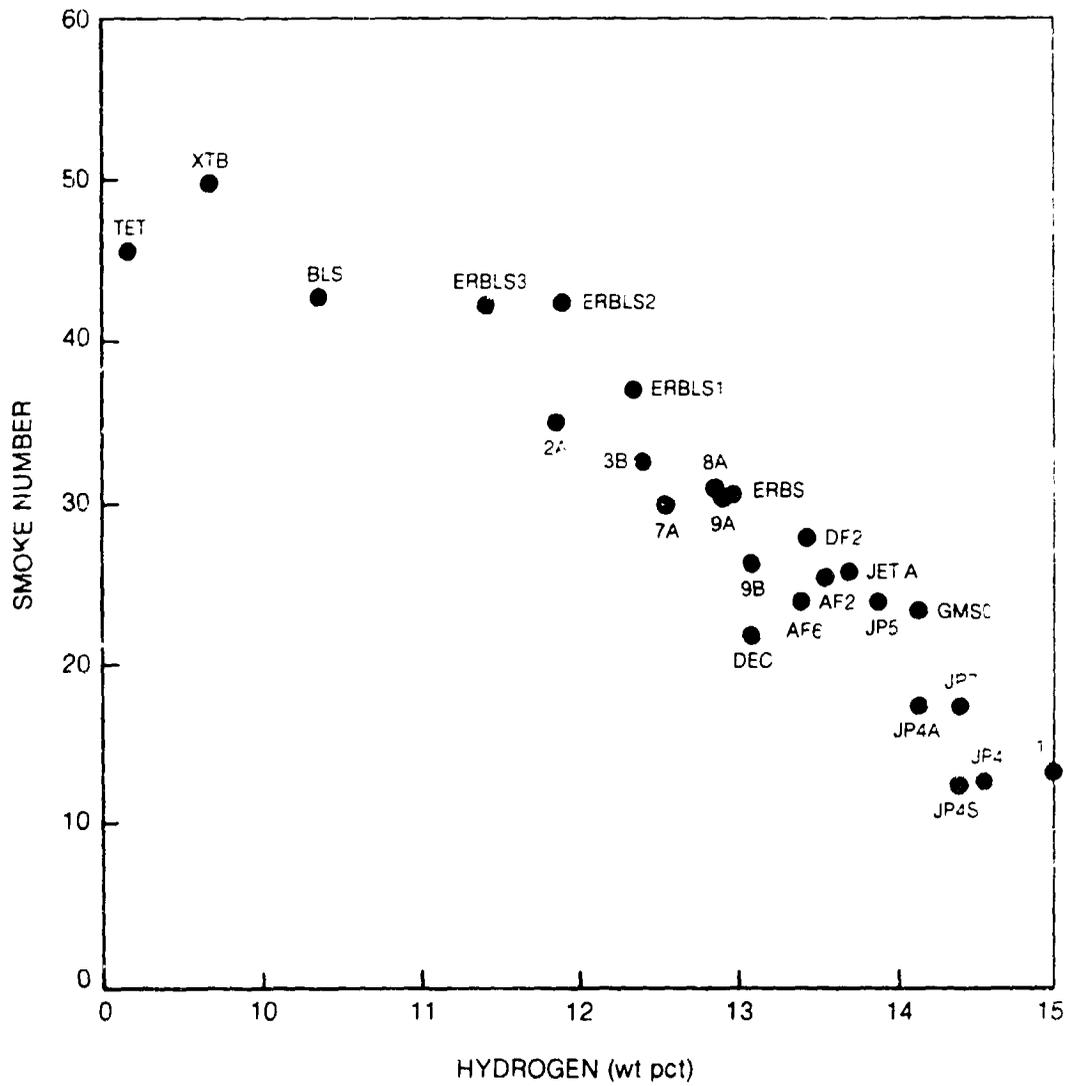
Fig. A-5 Dependence of Smoke Number on Fuel Hydrogen Content
for Test Condition 2

ORIGINAL PAGE IS
OF POOR QUALITY
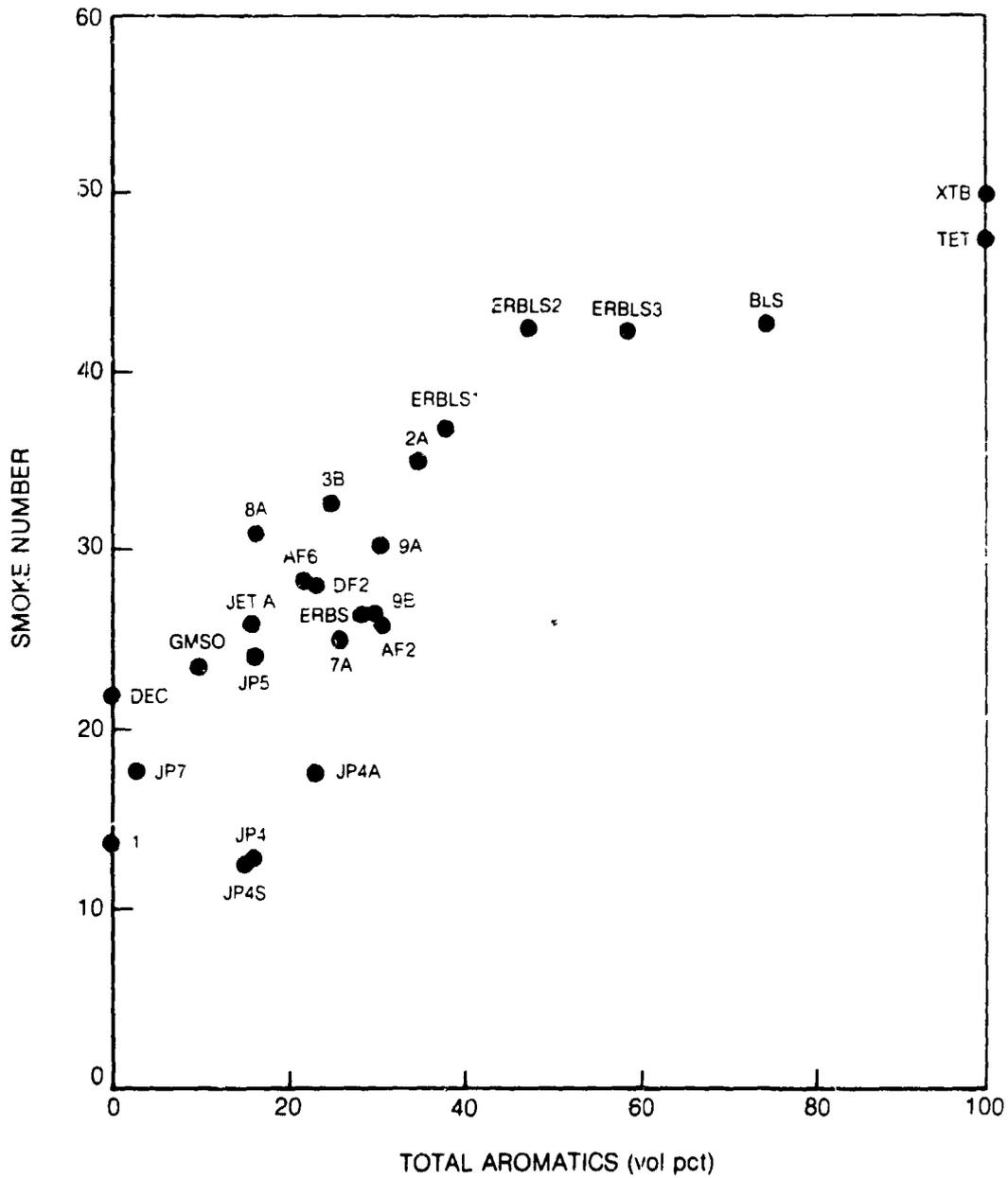
**Fig. A-6 Dependence of Smoke Number on Fuel Total Aromatics
for Test Condition 2**

83—7—29—16

ORIGINAL PAGE IS
OF POOR QUALITY
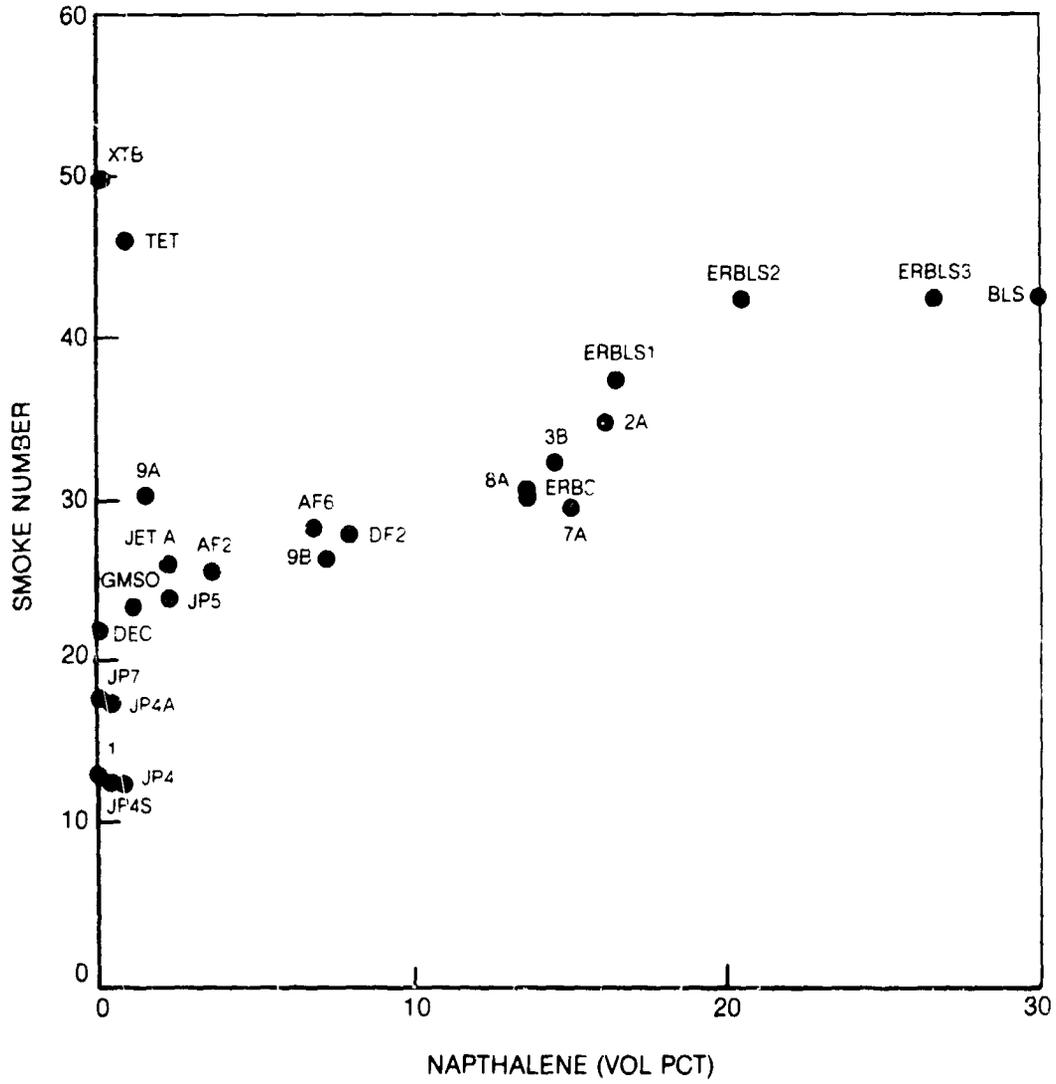
Fig. A-7 Dependence of Smoke Number on Fuel Napthalene Content
for Test Condition 2
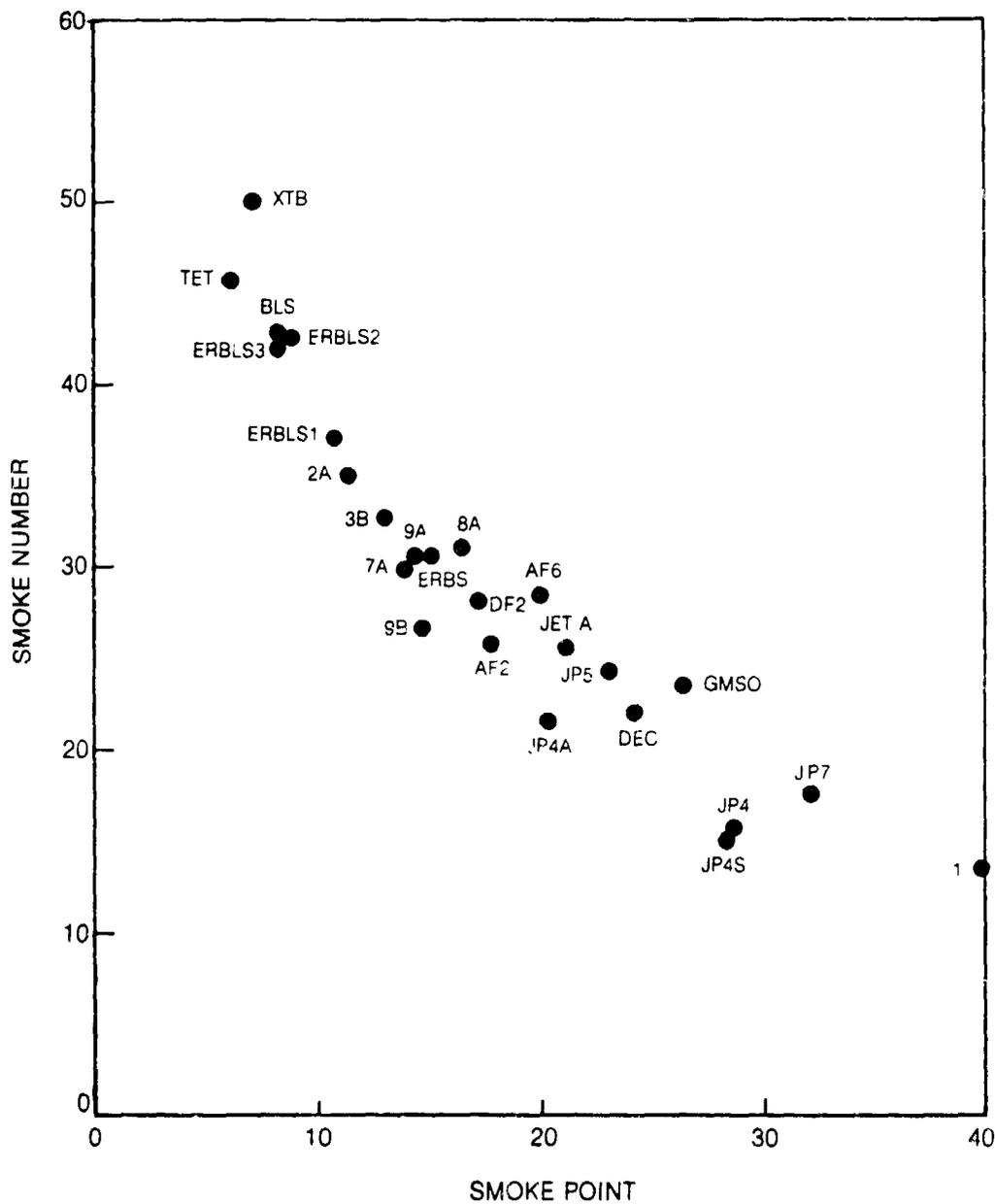
Fig. A-8 Dependence of Smoke Number on Smoke Point for Test Condition 2

83-7-29-18